



24018786

LIBRARY
Michigan State
University

This is to certify that the
dissertation entitled
The Solubility of Nonpolar Gases in
Organic Liquids and Water
presented by
Richard Paul Kennan
has been accepted towards fulfillment
of the requirements for
Ph.D. degree in Physics


Major professor

Date March 9, 1990

**PLACE IN RETURN BOX to remove this checkout from your record.
TO AVOID FINES return on or before date due.**

DATE DUE	DATE DUE	DATE DUE
_____	_____	_____
_____	_____	_____
_____	_____	_____
_____	_____	_____
_____	_____	_____
_____	_____	_____
_____	_____	_____

MSU Is An Affirmative Action/Equal Opportunity Institution

The Solubility of Nonpolar Gases in
Organic Liquids and Water.

By

Richard Paul Kennan

A DISSERTATION

Submitted to

Michigan State University

in partial fulfillment of the requirements
for the degree of

DOCTOR OF PHILOSOPHY

Department of Physics and Astronomy

1990

6059715

ABSTRACT

SOLUBILITY OF NONPOLAR GASES IN ORGANIC LIQUIDS AND WATER.

By

Richard Paul Kennan

We have measured the Ostwald solubility $L(T)$, as a function of temperature in the approximate range 10.0-50.0°C, for ^{133}Xe gas in 45 organic solvents, viz., 16 alkanes, 13 alkanols, 6 carboxylic acids, 4 alkanals, 3 cycloalkanes, and 3 perfluoroalkanes. From our data for each solute-solvent system we determine the following thermodynamic functions of solution: chemical potential $\Delta\mu_2^* = -RT \ln L$, enthalpy $\Delta\bar{h}_2^*$, and entropy $\Delta\bar{s}_2^*$, where $\Delta\mu_2^* = \Delta\bar{h}_2^* - T\Delta\bar{s}_2^*$, all based on the number density scale. The average observed entropy of solvation of Xe is $\Delta\bar{s}_2^* = -4.1 \pm 0.5$ cal/mol K, remarkably independent of solvent. The results are analyzed with scaled-particle theory from which we obtained the effective hard core diameters a_1 , and the cavity energies g_{cav} and enthalpies h_{cav} for all the solvents at 25°C. Thermodynamic perturbation theory is used to find the total enthalpy of solvation for the Xe-alkane systems. We generalize the analysis to evaluate the solvation enthalpy for all of the noble gases in the alkanes. We discuss the role of configurational entropy, as well as molecular dynamics approaches to calculation of free energies of solvation. Finally the results are examined empirically and values are given for the contribution to

chemical potential, enthalpy, and entropy of solvation, of the six functional groups: CH_2 (linear molecules), CH_3 , OH, COOH, CHO, and CH_2 (cyclomolecules).

We have also measured the pressure dependence of the Ostwald (L) and mole-fraction (x_2) solubilities for the nonpolar gases N_2 , Ar, Kr, and Xe in water at 25.0°C. The pressure ranges studied for each gas were approximately: N_2 (44-116 atm), Ar (22-101 atm), Kr (33-81 atm), and Xe (5-48 atm). For N_2 , Ar, and Kr we see clear deviations from Henry's Law, $f_2 = k_H x_2$. The data are analyzed in terms of the Kirkwood-Buff solution theory. The role of solvent -induced (hydrophobic) interactions shall be discussed. For the Kr-water system we shall compare our experimental results to recent computer simulation predictions. We also use statistical mechanics arguments to introduce a new solubility parameter which is appropriate to high pressure solubility measurements. Extensions of our analysis to other gas-liquid data is discussed.

To Mom and Dad

ACKNOWLEDGEMENTS

The experiments described in this thesis were suggested by Professor Gerald L. Pollack. I cannot overemphasize his contribution to this work through his guidance, encouragement, and friendship. I would also like to thank Professors Jules Kovacs, Aaron Galonsky, Dan Stump, and Jerry Cowen for serving on my guidance committee.

I would like to thank Jeff Himm and Gary Holm for their assistance in the laboratory in the early and late stages of this research project, and Charles Scriptor for all of his help with computers. Many of the figures in this thesis were produced with the generous aid of John and Linda Kennan. Thanks are also due to Peggy Andrews for her general assistance.

It would have been impossible to complete this work without the help of my friends both in the department and outside it. For moral support above and beyond the call of duty, I wish to express my deepest gratitude to Carrie Huang, Joel Gales, and Diandra Leslie-Pelecky. On the home front I would like to thank Richard and Nancy Olsen-Harbich for their kind friendship over the years. I also would like to thank the Physics Department's brilliant dramatic

ensemble, the N.R.F.T.C. Players.

Most of all I want to thank my family, especially my parents for whom I have seldom done my filial duty.

The research reported here has been supported under the Navel Medical Research and Development Command.

Table of Contents

Chapter	Page
1. General Introduction and Overview.....	1
2. Introduction: Solubility of Xenon in 45 Organic Solvents.....	3
3. Theoretical Background.....	6
3.1 Phase Equilibria.....	6
3.2 Two Component Systems.....	8
3.3 Ostwald Solubility.....	9
3.4 Solvation Thermodynamics.....	10
3.5 Physical Interpretation.....	13
3.6 Other Concentration Scales.....	17
4. Experimental.....	19
4.1 Outline of Method.....	19
4.2 Radioactive Tracers.....	22
4.3 Solution Components.....	23
4.4 The Experimental Apparatus.....	27
4.5 Volume Determination.....	28
4.6 Data Acquisition.....	33
4.7 Experimental Procedure.....	36
5. Results.....	40
5.1 Thermodynamic Analysis.....	40
5.2 Entropy of Solvation.....	49
5.3 Enthalpy of Solvation.....	54
5.4 Temperature Dependence of L and $\Delta\mu$	56
5.5 Total Entropy and Enthalpy.....	57
5.6 Mole Fraction Scale.....	63
6. Theoretical Analysis.	65
6.1 The Excess Chemical Potential.....	65
6.2 Distribution Functions.....	70
6.3 The Van der Waals Picture of Liquids..	80
6.4 Determination of $\Delta\mu_2^*$	87
6.5 The Scaled Particle Theory.....	93
6.6 Application to Real Liquids.....	101
6.7 Evaluation of the Cavity Terms.....	106
6.8 The Interaction Term.....	134
6.9 Comparison with Experimental Data....	146
7. Empirical Analysis and Predictions.....	159
8. Conclusions.....	171

9. Introduction: Solubility of Inert Gases in Water at Elevated Pressure.....	178
10. Experimental.....	181
11. Results.....	188
12. Pressure and Concentration Dependence.....	194
13. Data Analysis.....	201
14. Number Density Scale.....	211
15. Conclusions.....	219
 Appendix	
A. Derivation of Equation (6.78).....	222
B. Computer Program to Evaluate U_{int}	225
 List of References.....	 229

List of Figures

Figure 1. Schematic of two component solution.....	11
Figure 2. Three phase system of xenon gas in equilibrium with octane and water at 20°C.....	11
Figure 3. Schematic description of the solvation process. First the center of mass of the solute is placed at fixed position \vec{R}_0 , and then the particle is released. The contributions to the chemical potential are indicated next to each arrow.....	16
Figure 4. Idealized solubility apparatus.....	21
Figure 5. Experimental apparatus.....	31
Figure 6. Schematic of detection electronics.....	32
Figure 7. Normalized counting rate vs time for a typical experiment (Figure 2 of reference 18). The letter A indicates the time the valve was opened, and the letter B indicates the time a run might end, about 8 hours after equilibrium has been reached.....	39
Figure 8. $L(T)$ for Xe in six representative organic solvents.....	48
Figure 9. Excess chemical potential, $\Delta\mu_2^*(T)$ for six representative organic solvents (Figure 1 of reference 17).....	50
Figure 10. Radial distribution function, $g(r)$, for a typical gas, liquid, and solid.....	75
Figure 11. Lennard-Jones potential, $U(r)$. Lower diagram shows repulsive portion of $U(r)$ as determined in WCA theory.....	82
Figure 12. Radial distribution functions for (i)Lennard-Jones fluid $g(r)$, (ii) for repulsive portion of L-J potential $g_0(r)$, (iii) for hard spheres $g_{hs}(r)$	83

Figure 13. Definition of a cavity in the SPT.....	94
Figure 14. $g_{cav}(R_{12})/kT$ <u>vs</u> cavity radius R_{12}	100
Figure 15 Effective hard sphere diameter for 45 organic solvents <u>vs</u> number of carbon atoms.....	111
Figure 16. (a) g_{cav} for Xe in 45 organic solvents at 25.0°C. (b) corresponding excess chemical potential, $\Delta\mu_2^* = -RT\ln L$	115
Figure 17. Molecular diameter <u>vs</u> polarizability for several inert gas solutes. Solid line shows extrapolation for noble gases.....	116
Figure 18. Excess chemical potential <u>vs</u> solute polarizability for noble gases in Tetradecane, Decane, and Hexane. Filled in points along ordinate are the SPT predicted values for a hard sphere solute of 2.58Å.....	117
Figure 19. Excess chemical potential <u>vs</u> solute polarizability for noble gases in polar solvents methanol, and ethanol. Filled in points along ordinate are the SPT predicted values for a hard sphere solute of 2.58Å.....	118
Figure 20. (a) h_{cav} for Xe in 45 organic solvents <u>vs</u> number of carbon atoms. (b) corresponding experimental excess enthalpy, Δh_2^*	123
Figure 21. (a) s_{cav} for Xe in 45 organic solvents <u>vs</u> number of carbon atoms. (b) corresponding experimental excess entropy, Δs_2^*	124
Figure 22. Heat of vaporization for 45 organic solvents at 25°C <u>vs</u> number of carbon atoms.....	125
Figure 23. Number Density for 45 organic solvents at 25°C <u>vs</u> number of carbon atoms.....	126
Figure 24. Thermal Expansivity for 45 organic solvents at 25°C <u>vs</u> number of carbon atoms.....	127

Figure 25. Cavity free energy, g_{cav} , vs T for Xe in 6 representative organic solvents.....	133
Figure 26. Lennard-Jones potential with hard sphere cutoff.....	138
Figure 27. Verlet-Weiss and Percus Yevick pair distribution functions for hard sphere fluid. Packing fraction = 0.5.....	139
Figure 28. Calculated and experimental excess enthalpies of solvation for Xe in alkanes.....	147
Figure 29. Calculated and experimental excess enthalpies of solvation for He, Ne, Ar, Kr, and Xe in (a) octane, (b) tetradecane.....	156
Figure 30. Excess chemical potential $\Delta\mu_2^* = -RT \ln L$ vs number of CH ₂ groups at 25°C.....	160
Figure 31. Experimental data for Xe in 37 solvents. Excess chemical potential divided by solvent number density vs number of CH ₂ groups at 25°C.....	163
Figure 32. Experimental data for Xe in 37 solvents. Excess enthalpy divided by solvent number density vs number of CH ₂ groups	164
Figure 33. Experimental data for Xe in 37 solvents. $T\Delta s_2^*$ divided by solvent number density vs number of CH ₂ groups.....	165
Figure 34. g_{int}/ρ_1 vs number of CH ₂ groups for Xe in 37 solvents.....	170
Figure 35. Schematic of experimental setup (a) high pressure equilibration system (b) analysis system.....	182
Figure 36. Solute fugacity vs mole-fraction solubility at 25°C.....	192
Figure 37. Henry's constant vs mole-fraction solubility at 25°C.....	193

Figure 38. $\ln(f_2/x_2) - Pv_2^0/RT$ vs mole-fraction
solubility at 25°C.....203

Figure 39. $\ln(f_2/x_2) - Pv_2^0/RT$ vs mole-fraction
solubility for He and N₂ at 25°C for various
values of v_2^0210

List of Tables

<p>Table I. Solubility data for experiments with ^{133}Xe in 45 organic solvents. First row gives Ostwald solubility and the second row is the excess chemical potential, $\Delta\mu_2^* = -RT\ln L$ (cal/mol).....</p>	42
<p>Table II. Experimental data for excess enthalpy, Δh_2^*, and entropy Δs_2^*, for ^{133}Xe in 45 organic solvents.....</p>	51
<p>Table III Enthalpy and entropy of solution. The second and third columns are the total entropy and enthalpy of solution. The fourth and fifth columns are the entropy and enthalpy evaluated on the mole fraction scale.....</p>	60
<p>Table IV. Heat of vaporization, number density and thermal expansivity for 45 organic solvents.....</p>	108
<p>Table V. SPT calculations for 45 organic solvents. The second column is the effective hard sphere radius. The third column is the packing fraction. The fourth column is cavity free energy for ^{133}Xe.....</p>	112
<p>Table VI. Cavity enthalpy and entropy.....</p>	128
<p>Table VII. Parameters to evaluate interaction energy. Second column is hard sphere cutoff. Third column is the energy integral using the Verlet-Weiss distribution function. Fourth column is the resulting Lennard-Jones energy parameter for the pure organic solvent.....</p>	144
<p>Table VIII. Predicted enthalpy of solvation for ^{133}Xe in alkanes.....</p>	145
<p>Table IX. Excess chemical potential, enthalpy, and entropy for He, Ne, Ar and Kr in the alkanes, including hexane, octane, nonane, dodecane, and tetradecane.....</p>	150

Table X. g_{cav} , h_{cav} , s_{cav} , and u_{int} for He, Ne, Ar, and Kr in the alkanes, including pentane through hexadecane.....	152
Table XI. Empirical energy parameters for Xe solubility in 37 organic solvents.....	166
Table XII Predicted <u>vs</u> experimental values of Ostwald solubility for ¹³³ Xe in selected organic solvents.....	166
Table XIII. Experimental results for solubility of N ₂ , Ar, Kr, and Xe in water at 25.0°C. The second column is the solute partial pressure. The third column is the solute fugacity. The fourth and fifth columns are the mole-fraction and Ostwald solubilities respectively. The sixth column is the new solubility parameter γ . The seventh column is the excess chemical potential of the solute in the liquid. The eighth column is the experimental average value of partial molar volume.....	191
Table XIV. Results of Kirkwood-Buff analysis. The third column gives the partial molar volume of the solute used in Eq.(12.14). The fourth and fifth columns give the results for the KB integral G_{22} and the log of the infinite dilution limit of Henry's constant, $\ln(k_H^0)$	204

1 .Introduction

The phase equilibrium problem is ubiquitous to modern (or any) life. Whether it is the delivery of oxygen from the lung to the blood stream, or an industrial extraction process to remove unwanted hydrocarbons from natural gas, or the removal of a nasty stain from your best sweater; we are constantly confronted with the problem of how a substance is transferred from one medium to another. In general, when two phases are brought into contact there is an exchange of matter until the concentration in each each phase attains a constant value. To understand the physics that determines this equilibrium state is a difficult, but important task.

The goals of the research outlined in this thesis are to understand the solubility of gases in liquids and to predict solubilities in general gas-liquid systems. In pursuit of this goal we have measured the solubility of simple gases in various organic solvents and water. The resulting body of data has been analyzed using current molecular theories based on thermodynamics and statistical mechanics. By studying gas solubility one may be able to build a theoretical and empirical framework that can serve as a basis for more complicated phase equilibrium systems.

The thesis is divided into two parts. The first section

details experiments involving solubility measurements of the radioisotope ^{133}Xe in several homologous series of organic solvents. The solvents are chosen to range from simple nonpolar liquids to more complicated hydrogen bonding liquids. The second section covers experiments on the pressure dependence of gas solubility in water. The solute gases are: N_2 , Ar, Kr, and Xe. These gases are meant to represent a series of prototypical nonreactive solutes. The experimental results are applicable to problems of medical, industrial, and environmental interest. Specific examples will be cited in the introduction to each section.

Gas solubility can also serve as a probe in understanding intermolecular interactions. Due to the advances in computational techniques it has become possible to accurately model pure liquids.^{1,2} The resulting thermodynamic properties obtained are sensitive to the intermolecular potentials chosen. Optimized potential functions are determined by varying parameters until the best results are obtained.³ By extending these 'computer experiments' to dilute liquid mixtures it may be possible to understand the various factors which influence the potentials and place them on a more sound physical basis. Accurate experimental data on well chosen solute-solvent systems would be useful towards this end.

2. Introduction: Solubility of Xenon in 45 Organic Solvents.

This section of my thesis describes experiments which measure the Ostwald solubility (L) as a function of temperature of ^{133}Xe in 45 organic solvents including; alkanes, alkanols, cycloalkanes, alkanals, carboxylic acids, and perfluoroalkanes.

A great deal of progress has been made in understanding the physics of simple liquid-gas systems such as the solubility of an inert gas in its own liquid, or the solubility of one inert gas in the liquid phase of another inert gas, e.g., Ar \rightarrow Kr, Kr \rightarrow Xe, etc.^{4,5} These experiments are prototypical in the sense that they are the simplest gas-liquid systems that one can study.

A logical next step is to look at simple solutes in more complicated solvents (the case of simple solvents with complex solutes isn't experimentally accessible; just try dissolving hexane in liquid nitrogen). To this end we have chosen the inert gas xenon in the several homologous series mentioned above.

Some of the reasons why Xe was chosen as a solute are: All the inert gas elements are monatomic and do not chemically interact with the solvents under conditions of

these experiments. Much is known about interactions and properties of these elements. Xenon has a commercially available radioisotope, ^{133}Xe , whose concentrations in the gas phase can be easily measured.

Liquids are often considered in two groups: water⁶ (and aqueous solutions) and other liquids (mainly organic). We have selected 45 solvents so as to bridge these groups. Most of our solvents are nonpolar molecules, some are medium chain length molecules with a polar head group, and CH_3OH and HCOOH are small polar molecules for which hydrogen bonding is important. The obvious motivation for looking at homologous series is that one can try to spot trends that can be generalized to other systems.

Practical aspects of this work stem from biological and industrial applications. Xenon has several applications which are dependent on its solubility and diffusion. Because Xe is highly soluble in fats and relatively insoluble in aqueous solutions, the isotope ^{133}Xe is widely used in nuclear medicine to study cerebral blood flow, pulmonary function etc. A further application of Xe is as an inhalational anesthetic,⁷ a property associated with Xe solubility in lipids of cell membranes.⁸ Since the mechanism of general anesthesia is not understood some workers in the field believe that Xe is the prototype anesthetic to study.⁹ Also, solubility properties of Xe under pressure are useful for studying decompression sickness and inert gas narcosis, two problems of deep sea

diving.¹⁰ Finally, there are environmental and safety questions associated with the emission of ^{133}Xe and other radioactive inert gases from nuclear reactors.^{11,12}

There is presently a great deal of interest in developing synthetic blood substitutes (now euphemistically referred to as oxygen carriers in the industry). Perfluorocarbons and related compounds form the basis of many new blood substitute candidates because they carry oxygen efficiently and do not induce an immune system response.¹³ Thus understanding gas solubility in simple perfluorocarbons and their analogous hydrocarbons would be quite useful.

While a first principles understanding is beyond the scope of this work, we hope to develop empirical and analytic techniques that will allow the prediction of Xe solubility from knowledge of bulk properties of the solute and solvent. We aim ultimately to generalize, at least qualitatively, the solubility parameters obtained for Xe to solubility of other inert gases.

3 .Theoretical Background

3.1 Phase Equilibria

Chemical potential (μ) is a fundamental quantity in the determination of phase equilibria in multicomponent systems. The most useful definitions for our purposes are:¹⁴

$$\mu_i = \left(\frac{\partial G}{\partial n_i} \right)_{P,T,N'} = \left(\frac{\partial A}{\partial n_i} \right)_{T,V,N'} , \quad (3.1)$$

where G is the Gibb's free energy of the system, A is the Helmholtz free energy, n_i is the number of molecules of type i , T is the absolute temperature, P is the pressure, V is the volume and N' represents all other molecules in the system with the exception of the i^{th} type.

Suppose we have a two phase system, for example a liquid in contact with its own vapor, the condition for equilibrium at constant T and P is:

$$\mu_{\ell}(T,P) = \mu_g(T,P) . \quad (3.2)$$

We shall use the subscript ℓ to denote the liquid phase and g to denote the gas phase. For low pressures we assume the gas phase is ideal, ignoring internal degrees of freedom we have:

$$\mu_g = -kT \ln (\rho_g \Lambda^3) = -kT \ln (P_g \Lambda^3 / kT) \quad , \quad (3.3)$$

where ρ_g is the number density of the gas (molecules/unit volume), k is Boltzmann's constant and Λ is called the thermal wavelength for a particle of mass m ; i.e. $\Lambda = h / (2\pi mkT)^{1/2}$.

The chemical potential for the liquid can likewise be evaluated:

$$\mu_\ell = -kT \ln (\rho_\ell \Lambda^3) + \Delta\mu^* \quad , \quad (3.4)$$

where ρ_ℓ denotes the number density of the liquid and $\Delta\mu^*$ is called the excess chemical potential. It is the contribution to the free energy from intermolecular interactions in the liquid. A more detailed derivation of the above equations is reserved until chapter 6, but for now we shall content ourselves with these results. Equating (3.3) and (3.4) we find:

$$\Delta\mu^* = -kT \ln (\rho_\ell / \rho_g) \quad . \quad (3.5)$$

Thus by knowing the vapor pressure and density of the liquid we can determine its excess chemical potential. Typically, far from the triple point, a liquid is about 1000 times as dense as its vapor. This would lead to an excess chemical potential of about -17 kJ/mole at room temperature. Although

this is a reflection of the strong binding energy in the liquid we must keep in mind that there are also entropic contributions to the chemical potential. These can play a large role as we shall see later.

3.2 Two Component Systems

The relations derived in the previous section can easily be generalized to two component gas-liquid systems. We now imagine a liquid solvent in equilibrium with a gaseous solute (Fig. 1). The condition for equilibrium is that the chemical potential of the dissolved solute equals the chemical potential of the solute in the gas:

$$\mu_2^{\ell} = \mu_2^g \quad . \quad (3.6)$$

Throughout this thesis the subscript 1 and 2 will refer to the solvent and solute respectively, and superscripts g and ℓ will refer, respectively, to the gas and liquid, according to the usual conventions.

The statistical mechanics of solute-solvent mixtures starts with a standard partition function^{15,16} from which one may obtain by standard techniques the following chemical potential for a single solute molecule in the liquid solvent^{14,17}:

$$\mu_2^{\ell} = -kT \ln \langle \exp(-B_0 / kT) \rangle + kT \ln \rho_2^{\ell} \Lambda^3 \quad . \quad (3.7)$$

The key quantity in Eq.(3.7), B_0 , is the binding energy of a single solute molecule to a fixed configuration of the solute-solvent system. The ensemble average of the exponential in Eq.(3.7) is taken over all such configurations. This term is also referred to as the excess chemical potential for the dissolved solute, $\Delta\mu_2^*$. The second term in (3.7) is equivalent to the chemical potential of an ideal gas at density ρ_2^{ℓ} (the number density of solute molecules dissolved in the solvent).

For the chemical potential of a solute molecule in the gas (assumed ideal) one has:

$$\mu_2^g = kT \ln (\rho_2^g \Lambda^3) \quad , \quad (3.8)$$

in which ρ_2^g is the number density of the gaseous solute molecules. Equating (3.7) and (3.8) we find:

$$\Delta\mu_2^* = -kT \ln (\rho_2^{\ell} / \rho_2^g) \quad . \quad (3.9)$$

3.3 Ostwald Solubility

In the experiments described in this thesis we directly measured the Ostwald solubility as a function of temperature $L(T)$ of xenon gas in various organic solvents. Ostwald solubility is an intuitive as well as a theoretically significant measure of solubility. It is defined as the (equilibrium) ratio of the (volume) concentration of dissolved gas molecules in the liquid solvent to their

concentration in the gas phase. If ρ_2^{ℓ} , ρ_2^g are the number densities of solute 2 in the liquid and gas phases respectively, then:

$$L = \rho_2^{\ell} / \rho_2^g \quad . \quad (3.10)$$

At 20°C the Ostwald solubility of Xe is about 0.12 in water⁶ and about 4.4 in n-octane,^{18,19} a common nonpolar solvent (see Fig. 2).

One can immediately see the importance of the Ostwald solubility by substituting Eq. (3.10) into (3.9), which gives:

$$\Delta\mu_2^* = -kT \ln(L) \quad . \quad (3.11)$$

The Ostwald solubility provides a direct measurement of the excess chemical potential.

3.4 Solvation Thermodynamics

We start this section by reviewing standard thermodynamics. The Gibbs free energy for a system can be expressed in terms of its state variables as²⁰:

$$G(T,P,N) = E + PV - TS = H - TS \quad , \quad (3.11a)$$

$$G(T,P,N) = \sum_{i=1}^r n_i \mu_i \quad , \quad (3.11b)$$

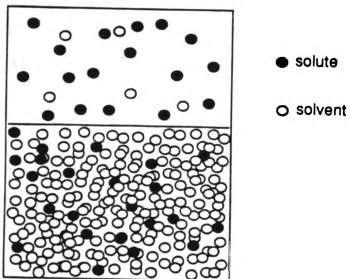


Figure 1. Schematic of two component solution.

[Xe] = 1	gas
[Xe] = 4	octane
[Xe] = 0.1	water

[] = concentration
(dimensionless)

T = 20 °C

Figure 2. Three phase system of xenon gas in equilibrium with octane and water at 20°C.

where E is the energy of the system, S is the entropy, H is the enthalpy ($H=E+PV$), and n_i is the number of molecules of type i (of which there are r different species) whose chemical potential is μ_i . The differential is:

$$dG = -SdT + VdP + \sum_{i=1}^r \mu_i dn_i \quad . \quad (3.12)$$

The most important information we shall be concerned with is the first derivative of the free energy, i.e:

$$S = -\left(\frac{\partial G}{\partial T}\right)_P \quad , \quad (3.13a)$$

we may then evaluate H in terms of G and its temperature derivative by using Eq.(3.11a). The partial molar enthalpy and entropy (h , and s respectively) can be found by differentiating (3.11b):

$$s_i = -\left(\frac{\partial \mu_i}{\partial T}\right) \quad , \quad h_i = \mu_i + Ts_i \quad , \quad (3.13b)$$

where :

$$S = \sum_{i=1}^r n_i s_i \quad , \quad H = \sum_{i=1}^r n_i h_i \quad . \quad (3.13c)$$

Generalizing these, we may find the partial molar enthalpy and entropy of the solvation process by taking the temperature derivative of the excess chemical potential,

$\Delta\mu_2^*$:

$$\Delta s_2^* = - \left(\frac{\partial \Delta \mu_2^*}{\partial T} \right) , \quad \Delta h_2^* = \Delta \mu_2^* + T \Delta s_2^* . \quad (3.14)$$

We call Δh_2^* and Δs_2^* , respectively, the excess partial molar enthalpy and entropy. One may also find the Helmholtz free energy of solvation and the internal energy of solvation. However these differ from G , and H by a factor of Pv_2 (where v_2 is the molar volume of the solute in the solvent) which is usually negligible [see section 3.21 of ref. 14 for a complete discussion].

3.5 Physical Interpretation of the Solvation Process

In section 3.2 we introduced the concept of the excess chemical potential, $\Delta \mu_2^*$. I shall now present a physical interpretation of this quantity developed by Ben-Naim.²¹ For simplicity we consider a two component system at temperature T , and pressure P with N_1 and N_2 representing the number of molecules of solvent and solute respectively, Because the Gibbs free energy is an extensive quantity the mathematical derivative in equation (3.1) can be replaced by:

$$\mu_2 = G(T, P, N_1, N_2 + 1) - G(T, P, N_1, N_2) . \quad (3.15)$$

This statement is valid for a macroscopic system, where the addition of one molecule may be viewed as an infinitesimal change in the variable N_2 . In order to interpret various contributions to the chemical potential Ben-Naim introduced

the concept of the pseudo-chemical potential. It is defined as:

$$\mu_2^{\text{pseudo}} = G(T, P, N_1, N_2 + 1; \vec{R}_0) - G(T, P, N_1, N_2) \quad . \quad (3.16)$$

This corresponds to the chemical potential for placing the solute atom at a fixed position within the solvent. We assume the solvent is homogeneous and macroscopic so the actual position \vec{R}_0 is irrelevant as long as it is within the bulk of the solvent. By explicitly solving both (3.15) and (3.16) from partition functions one can show²¹:

$$\mu_2^{\ell} = \mu_2^{\text{pseudo}} + kT \ln (\rho_2^{\ell} \Lambda^3) \quad . \quad (3.17)$$

Therefore it is immediately apparent that the pseudo-chemical potential is equal to the excess chemical potential, $\Delta\mu_2^*$, defined in Eq. (3.7). We may interpret equation (3.17) as follows. The full chemical potential can be viewed as a two step process for adding an extra particle to the solvent. First, we place the molecule at a fixed position. The change in free energy for this is μ_2^{pseudo} ($= \Delta\mu_2^*$). Next, we release the constraint imposed on the fixed position; this leads to an additional change in free energy, $kT \ln (\rho_2 \Lambda^3)$. For classical systems $\rho_2 \Lambda^3 \ll 1$, thus the free energy resulting from the release of the particle is always negative. This quantity is referred to as the liberation free energy.²¹ An explanation of the

various factors that make up the liberation free energy are as follows. When the particle is released it acquires a translational kinetic energy which leads to a free energy of $kT \ln(\Lambda^3)$. Also, when the particle is released it may now wander throughout the volume of the solvent, which gives rise to a free energy $-kT \ln(V)$. Finally, once the particle is released it is indistinguishable from the other N_2 particles in the solvent. This adds a free energy contribution of $kT \ln(N_2)$. Putting all of these together forms the liberation free energy. The entire discussion is outlined in Figure 3.

The important property of equation (3.17) is that it is generalized for any kind of molecule, whether it be atomic argon or a complex protein, all that is required is that classical statistical mechanics be obeyed. Of course there still is the problem of developing a solid theoretical calculation of $\Delta\mu_2^*$, however we now at least have some feel for what it is we are dealing with.

3.6 Other Concentration Scales

The Ostwald solubility, which has dominated much of our previous discussion, is based on the number density scale. This means that it is dependent on the number density of the solute in both the liquid and gas phase. However, there are many other measures of gas solubility. The most popular alternative is the mole fraction scale. The mole fraction solubility (x_1) is defined as the equilibrium ratio of the

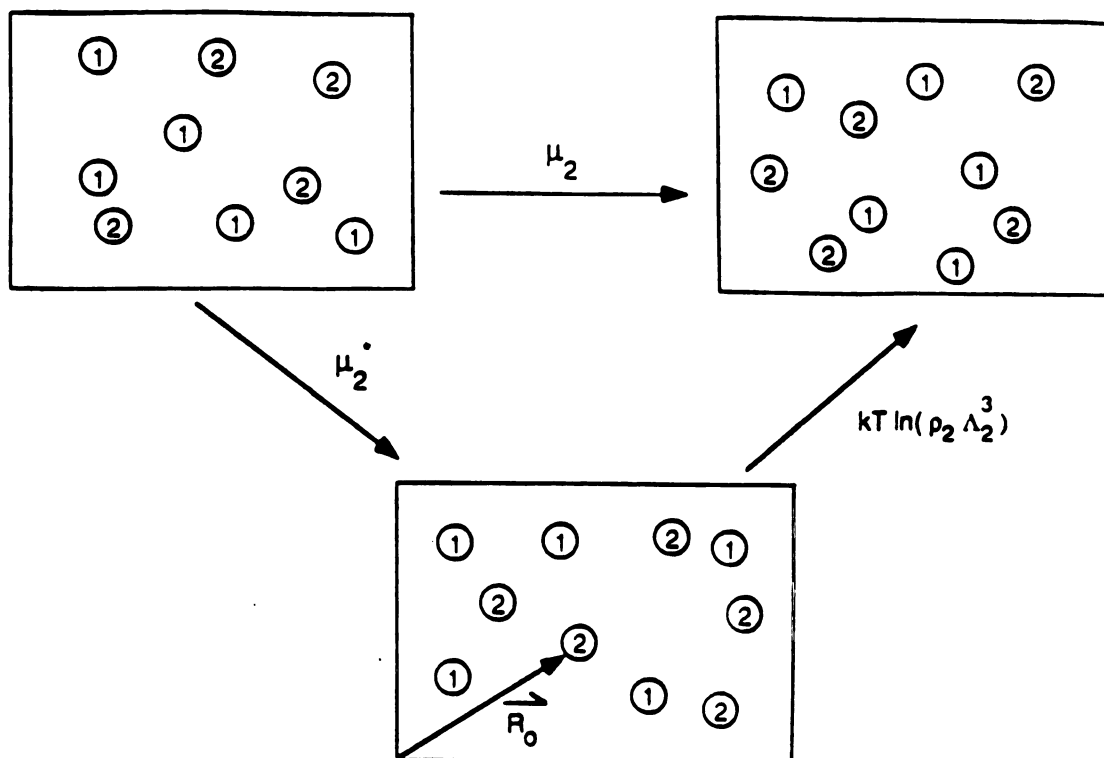


Figure 3. Schematic description of the solvation process. First the center of mass of the solute is placed at fixed position \vec{R}_0 , and then the particle is released. The contributions to the chemical potential are indicated next to each arrow.

number of moles of dissolved solute divided by the total number of moles of solution:

$$x_i = \frac{N_i}{\sum_j N_j} \quad . \quad (3.18)$$

For a two component solution this reduces to:

$$x_2 = N_2 / (N_1 + N_2) \quad , \quad (3.19)$$

where N_2 and N_1 are the number of moles of solute and solvent respectively. Note that unlike the Ostwald solubility this makes no direct reference to the gas phase concentration. If the gas phase is ideal we can relate x_2 to the Ostwald solubility, L ¹⁹:

$$x_2 = 1 \left[\frac{RT}{L P_2 \bar{V}_1} + 1 \right]^{-1} \quad , \quad (3.20)$$

where P_2 is the pressure of the solute gas and \bar{V}_1 is the molar volume of the solvent.

For a dilute solution the chemical potential for component i may be written as²²:

$$\mu_i = \mu_i^\circ + kT \ln(x_2) \quad . \quad (3.21)$$

The quantity μ_i° in equation (3.21) is known as the standard state of the dissolved solute. It is hypothetical in the

sense that we cannot give a physical interpretation of it. For example, one might say that it is the chemical potential of the pure solute (i.e. $x_2=1$), however equation (3.21) only holds in the case of very dilute solutions. Despite this flaw the mole fraction scale is still useful and has many applications.^{20,22} Its strength lies in the fact that it can be used to describe liquid mixtures and electrolyte solutions, where knowledge of the vapor phase is often hard to obtain.

There are of course many other concentration scales that are available,²⁰ but only the number density scale avoids the problem of defining standard states and allows a strict physical interpretation of the associated chemical potential.

4. Experimental

4.1 Outline of Method

For the discussion in this section please refer to Figure 4. Here we have a two compartment chamber separated by a valve. The upper chamber contains the solute gas while the lower chamber contains the liquid solvent and a stirring device. An accurate pressure gauge is connected to the gas volume which will allow us to determine the gas density at any time through its equation of state. The gas volume in the upper chamber is denoted $V_g^{(1)}$, the liquid volume is V_L , and the gas space in the lower chamber is $V_g^{(2)}$. The entire system is immersed in a constant temperature bath. The procedure of the experiment is to fill $V_g^{(1)}$ with a known amount of gas. This is determined by measuring the initial pressure, determine the gas density from it, and multiplying the density by the initial volume:

$$N_{\text{initial}} = \rho_{\text{initial}} \times V_g^{(1)} \quad . \quad (4.1)$$

We then open the valve and start the stirrer. The pressure will drop until equilibrium is reached and the solvent is saturated. We now measure the final pressure and determine the final density, ρ_{final} . (For this idealized system we

neglect the vapor pressure of the solvent. In a real experiment we must take the solvent vapor pressure into account.) The final number of solute particles can be expressed as:

$$N_{\text{final}} = \rho_{\text{final}}^{\text{gas}} * (V_{\text{g}}^{(1)} + V_{\text{g}}^{(2)}) + \rho_{\text{final}}^{\text{dissolved}} * V_{\ell} \quad , \quad (4.2)$$

where the second density is that of the solute which is in the liquid. We now can introduce the Ostwald solubility, which for this system is obviously:

$$L = \frac{\rho_{\text{final}}^{\text{dissolved}}}{\rho_{\text{final}}^{\text{gas}}} \quad . \quad (4.3)$$

We now substitute $L * \rho_{\text{final}}^{\text{gas}}$ for $\rho_{\text{final}}^{\text{dissolved}}$ in equation (4.2). Since the system is closed the number of solute molecules is conserved, thus we can equate (4.2) with (4.1) and solve for L:

$$L = \alpha \frac{V_{\text{g}}^{(1)}}{V_{\ell}} - \frac{V_{\text{g}}^{(1)} + V_{\text{g}}^{(2)}}{V_{\ell}} \quad , \quad (4.4)$$

where α is the ratio of initial to final gas density, (ρ_i/ρ_f) .

To briefly summarize, we have outlined a simple technique in which L is obtained by recording the decrease in pressure during equilibration.

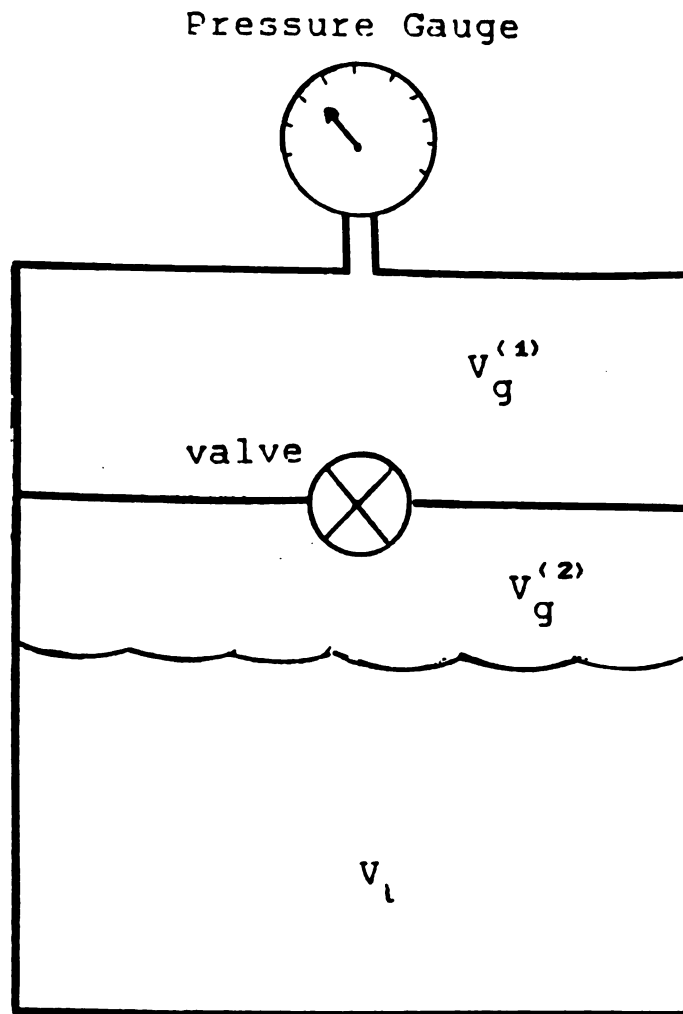


Figure 4. Idealized solubility apparatus.

4.2 Radioactive Tracers

There are several problems which come up when actually measuring the Ostwald solubility as described in the previous section. First of all, one must be sure to measure the pressure drop associated with the solute gas. Two contributions of background gases are, (a) the vapor pressure of the solvent, and (b) any other gases dissolved in the liquid. For dilute solutions the vapor pressure of the solvent does not change significantly from its pure value,¹⁵ so it can be corrected for. The second problem is overcome by carefully degassing the solvent when loading it into the apparatus. This can lead to fairly elaborate and time consuming setup procedures.

Another problem is the necessity of noninvasive pressure measurement. In other words, we do not want to change the system by measuring its pressure. Many of the more accurate pressure gauges and sensors are able to detect changes in pressure through moving parts such as diaphragms or Bourdon tubes.²³ A result of this is often a small change in gas volume which must be accounted for due to our need to know absolute differences in mass (density*volume).

The most difficult problem to overcome is sensitivity over a wide range of gas concentration. As mentioned earlier, gas solubility in various solvents can vary by more than factors of one hundred.^{6,24} The best reasonably priced transducers and gauges have an uncertainty of 0.05 percent of the full scale reading. Therefore a 0.05% error at one

pressure could become a 5% error on another. To get around this one must use a series of pressure sensors for the range appropriate to the system being studied. A related difficulty is that for systems where the Ostwald solubility is low, the observed change in pressure will be small compared to the total pressure (or even the vapor pressure).

This can be overcome by using large liquid volumes, however for some expensive solvents this is not a feasible alternative.

By using radioactive tracers one can avoid all of these problems. Since the tracer is the only gas which is observed, background gases can be ignored. Furthermore, the tracer can be monitored by external detectors, which are truly noninvasive. And finally, since radioactive decay has an uncertainty of $(N_{\text{counts}})^{-0.5}$ one can get desired accuracy over a wide range by simply waiting for enough counts. Since the goal of this experiment is to look at gas solubility over a wide range of solvents, the advantages of using radioactive tracers is apparent.

4.3 Solution Components

The solute gas chosen for our experiments is the radioisotope Xenon-133. Xenon is one of the noble gases. Its atomic radius is 2.23Å, which qualifies it as the largest and most polarizable of the 5 inert gases with stable isotopes, viz., He, Ne, Ar, Kr, and Xe. The next noble gas in this series is radon which has no stable isotopes.

Xenon-133 is a byproduct of ^{235}U fission and is readily available commercially. It is unstable and decays with a half life of 5.245 days.²⁵ Because of its high solubility in fats and low solubility in aqueous solutions, ^{133}Xe is used extensively in nuclear medicine to study cerebral blood flow pulmonary function, etc.¹⁸ The decay process for ^{133}Xe is as follows: the isotope first decays by beta emission to an excited state of ^{133}Cs , this nuclear excited state then decays with a half life of 6.3×10^{-9} sec by emitting an 81 keV gamma ray. The beta rays are rapidly attenuated, but the gamma ray intensity can readily be quantitatively measured to determine ^{133}Xe concentration.

Xenon-133 was purchased from the Medi-Physics Company (Plainfield, N.J.) in 20 millicurie (mCi) aliquots (this is a recommended human dosage for cerebral blood flow studies). A typical amount of ^{133}Xe used during a run was of the order of 100 μCi . In practice, one aliquot usually supplied enough xenon for a month (≈ 10 runs). The corresponding partial pressure of the tracer is approximately 1 picoatmosphere (10^{-12} atm), therefore it's safe to say that our results correspond to the limit of infinite dilution. The tracer was usually mixed with air at 1 atm. In order to make sure the air did not effect our results control experiments were done in which ^{133}Xe was mixed with naturally occurring nonradioactive xenon at a total pressure of 1 atm. No difference was observed. The solvents studied were an extension of previous work involving n-alkanes and

n-alkanols²⁶ (the prefix n- means that the molecule is a straight chain). They include cycloalkanes, alkanals, carboxylic acids, and perfluoroalkanes.

N-alkanes can be described as straight chains of singly bonded carbon atoms which are saturated with hydrogen:



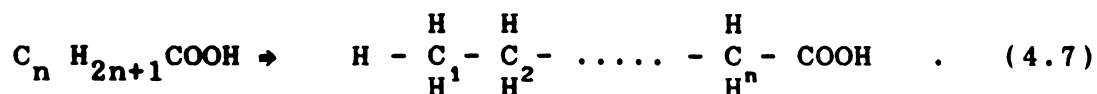
They are composed of n-2 acyl groups (CH₂) and two methyl groups (CH₃). We studied the alkanes ranging from pentane (C₅) to eicosane (C₂₀). The alkanes were purchased from Humphrey Chemical Co. (New Haven, Conn.), and were all at least 99% pure.

N-alkanols differ from n-alkanes in the addition of a hydroxyl (OH) group to a terminal carbon:



Ethanol was obtained from Aaper Alcohol and Chemical Co, while the other alkanols were from Aldrich Chemical (Milwaukee, Wis.). Purities were: 99.9% (methanol), 99+% (propanol and butanol), 99% (pentanol, octanol, decanol, and undecanol), 98% (hexanol, heptanol, and dodecanol), 97% (nonanol and tetradecanol), and 200 proof ethanol.

Carboxylic acids are formed by replacing the terminal hydrogen with a carboxyl group (COOH):



Alkanals, also known as aldehydes, have a terminal CHO group ($C_n H_{2n+1} CHO$). Cycloalkanes ($C_n H_{2n}$) are similiar to alkanes except that the carbon atoms form a closed ring; as a consequence they have no methyl groups. These solvents were also obtained from Aldrich Chemical. Their purities were the highest reasonably available: formic acid (95%-99%, remainder water), acetic acid (>99%), propanoic acid (>99%), n-butanoic acid acid (>99%), n-pentanoic acid (>99%), n-heptanoic acid (>99%), propanal (>99%), n-butanal (>99%), n-pentanal (99%) , n-heptanal (95%), cyclopentane (78%; 99.6% saturated C_5 hydrocarbons), cyclohexane (>99%), and cyclooctane (>99%).

Perfluoroalkanes are alkanes with fluorine substituted for hydrogen ($C_n F_{2n+2}$). They were obtained from SCM Specialty Chemicals (Gainesville, FL). Their purities were also the highest reasonably available: perfluorohexane (99%, of which 85% is n- $C_6 F_{10}$), perfluoroheptane (97%-99%, mixed isomers), and perfluorooctane(90% mixed isomers). Other perfluoroalkanes were either prohibitively expensive or not available.

4.4 The Experimental Apparatus

A diagram of the apparatus is shown in Figure 5. The design is similiar to that used in previous work,²⁶ except

the upper and lower portions are now held together by an indium sealed brass flange instead of a threaded brass connection. The apparatus can be disassembled at the flange for cleaning and loading. The upper portion of the apparatus consists of two valves and a brass gas volume. The lower portion is a pyrex flask which is joined to a glass-to-metal seal. The brass flange is soldered to this seal. A small matching groove is cut on both faces of the flange and is filled with 0.040" diameter indium wire. The top and bottom are connected by six screws which press the indium to form a reliable seal. The indium can be reused many times by reforming the wire in a hydraulic press.

The lower volume contains a glass encased stir bar in order to mix the solvent. Most commercial stir bars are coated with Teflon because it is non-reactive. We found it necessary to remove this coating because xenon is very soluble in Teflon. The stir bar is then encased in glass to protect it from potentially corrosive solvents.

A ball valve separates the upper and lower volume. The advantage to using a ball valve is that its volume is well defined. In other words, once the valve is opened the volume that is exposed is that of the hole in the ball regardless of how much you open it. The second valve, a Hoke valve, is for loading the gas. This does not have any critical volume requirements because it remains sealed throughout the entire run.

During a run the apparatus is immersed in a fluid bath

in order to regulate temperature. The bath was controlled to $\pm 0.1^\circ\text{C}$ by a Lauda/Brinkman K-2/RD circulator. The bath fluid was a 4:1 mixture of water:ethylene glycol in order to prevent freeze-up of the circulator cooling coils.

We used Pb shielding ≈ 1 cm to reduce background radiation and to isolate the volume $V_g^{(1)}$ from the rest of the apparatus. This is important because we want the detector to measure the concentration in the gas phase only. Any scattered gamma emissions from ^{133}Xe in the liquid which reach the detector will lead to errors. One cm of Pb attenuates 81keV gamma rays by a factor of $10^{6.27}$. We checked the shielding by putting ^{133}Xe in V_{rest} with the apparatus in the bath and the shielding in place. No counts were observed above background.

4.5 Volume Determination

One of the most important criteria for determining solubility by the method outlined in section 4.1 is the accurate determination of volumes. The relevant volumes for the apparatus are indicated in Figure 5. Of these seven volumes five are the same for every run, namely, $V_g^{(1)}$, V_{rest} , V_{sb} , V_{hb} , and V_{ee} . The remaining two, $V_g^{(2)}$ and V_ℓ , are determined at the start of each new run. Each volume is described below:

$$V_g^{(1)} = \text{initial gas volume ,}$$

$$V_g^{(2)} = \text{the rest of the gas volume ,}$$

$$\begin{aligned}
 V_{\text{rest}} &= \text{total volume excluding } V_g^{(1)} , \\
 V_\ell &= \text{volume of the liquid} , \\
 V_{\text{hb}} &= \text{volume of hole in ball valve} , \\
 V_{\text{sb}} &= \text{volume of stir bar} , \\
 V_{\text{ee}} &= \text{volume below the ball valve} .
 \end{aligned}$$

They are related by:

$$V_{\text{rest}} = V_{\text{ee}} + V_{\text{hb}} \quad (4.8)$$

$$V_g^{(2)} = V_{\text{rest}} - V_{\text{sb}} - V_\ell . \quad (4.9)$$

To determine V_{ee} (ee stands for everything else), we weigh the apparatus before and after filling V_{ee} with water at a known temperature. We make a buoyancy correction for the weight of air displaced by the water. If m_{obs} is the observed mass, then the true mass, m_{true} , is:

$$m_{\text{true}} = m_{\text{obs}} / \left(1 - \frac{\rho_{\text{air}, T}}{\rho_{\text{H}_2\text{O}, T}} \right) , \quad (4.10)$$

where $\rho_{x, T}$ is the density of x at temperature T. One can then determine V_{ee} by:

$$V_{\text{ee}} = m_{\text{true}} / \rho_{\text{H}_2\text{O}, T} . \quad (4.11)$$

The volume of the hole in the ball was calculated from measurements made on the disassembled valve. We can then

find V_{rest} from (4.8). The volume of the glass encased stir bar, V_{sb} , was found by measuring the water it displaced in a graduated cylinder.

Once V_{rest} was known, we were able to find $V_g^{(1)}$ by performing a dilution run. This consists of loading ^{133}Xe in $V_g^{(1)}$ with V_{rest} evacuated. Once we determine the concentration of gas in $V_g^{(1)}$, c_o (normalized to correct for radioactive decay), we open the main valve and allow the gas to expand into $V_g^{(2)}$. After several hours the system equilibrates and we note the final normalized concentration, c_f . Since the amount of xenon is conserved (subject to radioactive decay) we have:

$$c_o V_g^{(1)} = c_f (V_g^{(1)} + V_{rest}) \quad , \quad (4.12)$$

which in turn gives:

$$V_g^{(1)} = V_{rest} * \alpha / (1 - \alpha) \quad , \quad (4.13)$$

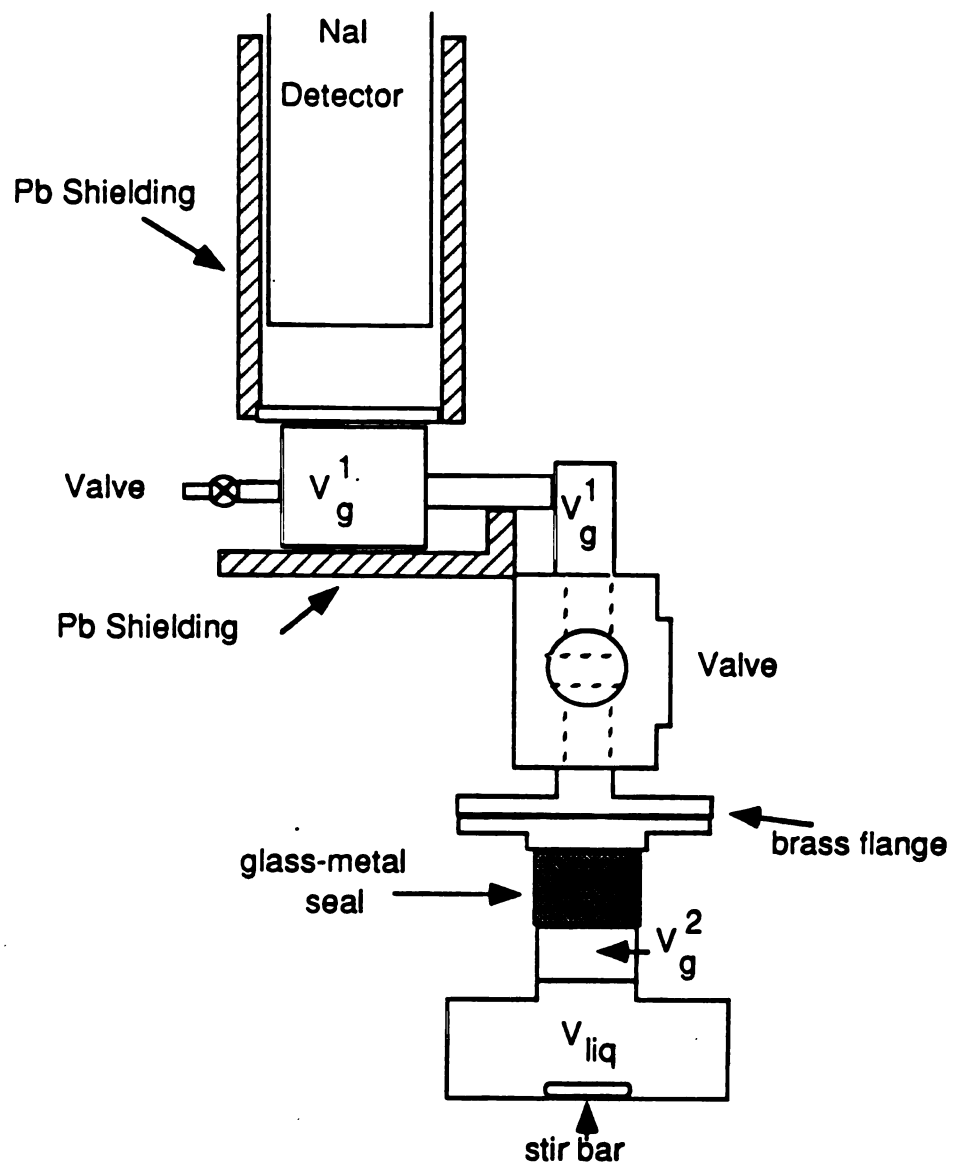


Figure 5. Experimental apparatus.

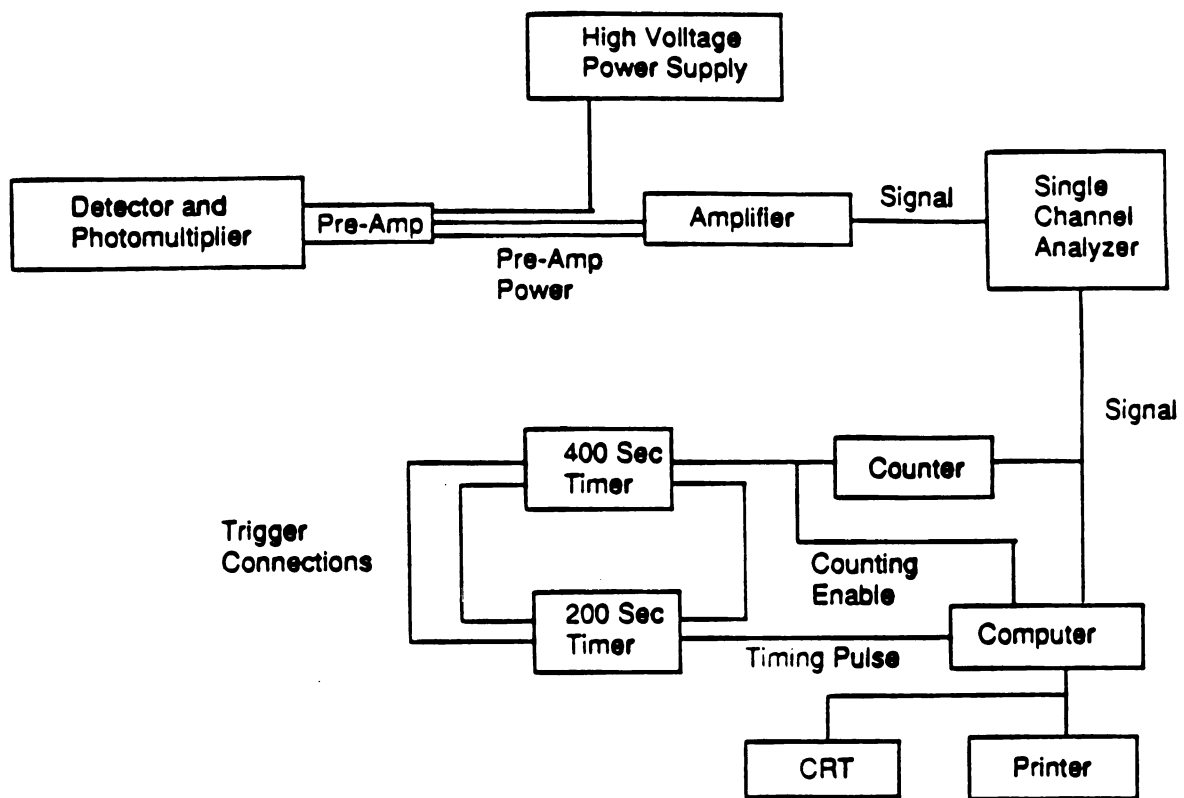


Figure 6. Schematic of detection electronics.

where $\alpha = (c_o / c_f)$. For the apparatus used in these measurements $V_{rest} \approx 250\text{cm}^3$, and $V_g^{(1)} \approx 50\text{cm}^3$.

4.6 Data Acquisition

The electronics are shown in Figure (6). Gamma ray intensity is monitored by a well -counter NaI(Tl) scintillation crystal connected to a photomultiplier (Harshaw Chemical Company, type 7SF8). A high voltage power supply (Power Designs, Inc., model 1570) supplies 1100 volts for the photomultiplier via the preamp (Ortec model 276). Signals from the photomultiplier go through the base preamplifier and a Nimbin mounted amplifier (Ortec Model 485), then through a single channel analyzer (SCA, Ortec Model 406A), and finally into a microcomputer counter (Micro Development Tool 1000). The SCA is set with a suitably wide window (10-90keV) so as to permit passage of ^{133}Xe signals while keeping the system stable and the background low. The window was set by feeding signals of known amplitudes into the amplifier and observing the output on a multichannel analyzer (Northern Electronics model NS633). The resulting output was then compared to a ^{133}Xe spectrum. Two timers (Ortec Model 719) are supplied a 0.1 sec timing pulse by the computer.

The computer is programmed to take data and print out the results. It counts the number of decays in a 400 sec interval and then waits an additional 200 sec before counting again (the time intervals are somewhat arbitrary

and are based on historical reasons). A result is printed every ten minutes with averages printed every hour.

Two corrections are made to the raw data. Because the electronics are not perfect, a pulse into the detector is not recorded if it follows an earlier pulse too closely, i.e., the detector has a 'dead time'. The dead time can be measured by sending signals of known frequency into the electronics and observing the output. In this way, we determined the dead time for our system to be about $\tau \approx 3.33 \times 10^{-6}$ sec.

In order to calculate the dead time correction we must exploit the random nature of the radioactive decay process. The probability of k events in a time interval, given a mean rate of μ events in that interval, is described by a Poisson distribution²⁸:

$$P(k) = \frac{\mu^k}{k! e^{-\mu}} \quad . \quad (4.14)$$

We now take the dead time, τ , to be our unit of time. Thus μ becomes the mean number of events in time τ . The probability that a single signal occurs within time τ of an earlier signal is given by:

$$P(1) = \mu e^{-\mu} \quad . \quad (4.15)$$

Since μ is small (typically of order 10^{-3}) we can expand the exponential. To first order this reduces to:

$$P(1) = \mu \quad . \quad (4.16)$$

The actual counting rate is then approximated by:

$$N_{\text{act}} = N_{\text{obs}} (1 + P(1)) = N_{\text{obs}} (1 + \mu) \quad , \quad (4.17)$$

where N_{obs} is the observed number of counts over period T . We approximate μ by using the observed counting rate multiplied by the dead time:

$$\mu = (N_{\text{obs}} / T) * \tau \quad . \quad (4.18)$$

Plugging into (4.17) we have:

$$N_{\text{act}} = N_{\text{obs}} (1 + (N_{\text{obs}} / T) * \tau) \quad . \quad (4.19)$$

We have programmed the computer to make this correction using the parameters : $T=400\text{sec}$, and $\tau=3.33 \times 10^{-6}\text{sec}$.

The second correction we make is to subtract off background counts. We measure background radiation over periods of several hours with the evacuated apparatus and shielding in place. Background is subtracted after the dead time correction is made. Typical background rates are about 1500 counts/400 sec. During an actual run counting rates vary from 250,000 counts/400 sec (at the beginning) to 50,000 counts/400 sec (at the end).

4.7 Experimental Procedure

I shall now outline the experimental procedure to determine the Ostwald solubility of ^{133}Xe in an arbitrary solvent. Referring to Figure (5) may be useful.

The solvents are generally used as purchased, we do not degas them. Control experiments were done on degassed solvents and have shown the dissolved gases do not effect xenon solubility²⁶ (if we equilibrated the solvent with 1 atm of air, the gas concentration would amount to about 0.01 mole/liter).

With the ball valve closed and the apparatus disassembled, air is evacuated from volume $V_g^{(1)}$ through the loading valve (Hoke bellows valve). A trace amount of ^{133}Xe is allowed to expand into $V_g^{(1)}$, and then air is let in to bring the total pressure to 1 atm. The loading valve is then closed.

The glass portion of the apparatus is loaded with about 200 ml of solvent, and is weighed (we make the usual buoyancy correction). Using known densities^{29,30} we calculate the liquid volume. The perfluoroalkanes and cyclopentane were mixed isomers, so we measured the density ourselves using a standard volumetric method. This allows us to calculate gas volume $V_g^{(2)}$ using (4.9). After putting in the stirring bar, the apparatus is assembled (see Section 4.5). The apparatus is then mounted rigidly in the temperature bath so the detector geometry does not change in

the course of the run.

With the main valve closed, we start the computer and begin taking data. During a run the initial counting rate, c_i , is measured hourly for six to eight hours. Each value is corrected for decay, and the mean value is calculated. Once the gas is uniformly distributed in $V_g^{(1)}$, as indicated by a steady counting rate, we open the main valve and start the stirrer. The solubility can then be calculated from a generalization of equation (4.4):

$$L = \frac{c_i}{c_f} e^{-\lambda \Delta t} \frac{V_g^{(1)}}{V_\ell} \frac{V_g^{(1)} + V_g^{(2)}}{V_\ell}, \quad (4.20)$$

where λ is the decay constant for ^{133}Xe ($\lambda = 0.9177 \times 10^{-4} \text{ min}^{-1}$) and Δt is the time elapsed between measurement of c_i and c_f . We calculate the Ostwald solubility each hour until L reaches a constant value. Time to equilibrium is typically 12 hours. We wait an additional 8 to 12 hours to insure equilibrium has been reached (see Figure 7).

In order to obtain $L(T)$ in these experiments one needs to know the densities $\rho(T)$ at each temperature at which $L(T)$ is measured. The idea is that after charging the apparatus with solute and solvent and then measuring L at some initial temperature, say 25°C , one can measure L at a different temperature by just changing the temperature and waiting for the new solute-solvent equilibrium. Once the bath temperature is changed we recalculate equation (4.20) using

the new liquid and gas volumes, V_{ℓ} and $V_g^{(2)}$. This procedure works because the masses of solute and solvent are fixed in the sealed apparatus. Thus, in a typical determination of $L(T)$ we measured solubility sequentially at temperatures of 20,30,40,50,10 and, finally, again 20°C (the temperatures we cycle through depends on the solvent of course). We went through a cycle like this two times independently for each solvent.

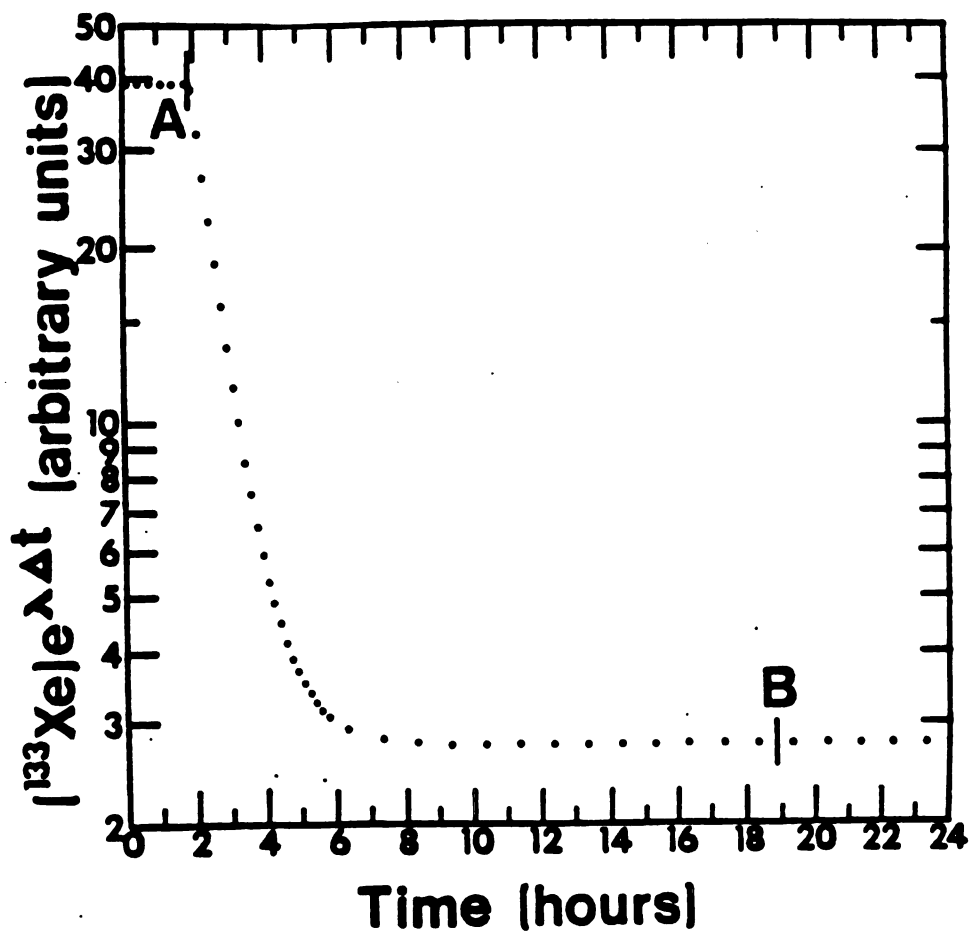


Figure 7. Normalized counting rate vs time for a typical experiment (Figure 2 of reference 18). The letter A indicates the time the valve was opened, and the letter B indicates the time a run might end, about 8 hours after equilibrium has been reached.

5. Results

5.1 Thermodynamic Analysis

Table I gives the results of our experiments for 45 solvents. These include: 16 alkanes, 13 alkanols, 6 carboxylic acids, 4 alkanals, 3 cycloalkanes, and 3 perfluoroalkanes. The first row for each solvent gives the measured value of $L(T)$ at each temperature. The second row gives the corresponding chemical potential, $\Delta\mu_2^*$ (cal/mole), which is calculated from $L(T)$ by equation (3.11):

$$\Delta\mu_2^* = -RT \ln L .$$

The data given at each temperature are each averages of at least 2 separate runs. Typical uncertainties for $\delta L/L$ are about 0.015. The uncertainty $\delta(\Delta\mu_2^*) = -RT(\delta L/L)$ varies from ± 6 cal/mole at 278.15K to ± 10 cal/mole at 323.15K.

Figure 8 shows the Ostwald solubility plotted as a function of temperature (C) for six representative solvents, one for each homologous series. They are: n-hexane, n-hexanol, cyclohexane, n-heptanoic acid, n-heptanal, and n-perfluorohexane. Each of these solvents has a similar backbone with different terminal groups attached (or hydrogens replaced by fluorines). Figure 9 is a plot of the

corresponding chemical potential versus temperature. For the solvents illustrated the largest solubility occurs in hexane, this corresponds to the most negative free energy, while the lowest solubility occurs in perfluorohexane, which has the highest free energy. From these figures we can see the general tendency in the $\text{Xe}_{\text{solute}} - \text{organic}_{\text{solvent}}$ system for $L(T)$ to decrease with temperature, while $\Delta\mu_2^*(T)$ increases with temperature.

From equation (3.11) it is clear that the sign of $\Delta\mu_2^*$ is negative if L is greater than one, as is the case for 44 of these solvents (HCOOH excluded). For all such solvents a positive free energy is required to remove a solute molecule from a fixed position in the solvent to a fixed position in the gas. Conversely for those in which L is less than one, a positive free energy is required to place a solute at fixed position in the liquid.

Over the temperature range we used, the experimental data for $\Delta\mu_2^*(T)$ can be fitted well by a straight line of the form $\Delta\mu_2^*(T) = a + bT$. Since the partial molar entropy is proportional to the temperature derivative of the chemical potential, $s_2^* = -(\partial\mu_2^*/\partial T)_p$, one can write:^{6,24}

$$-RT \ln(L) = \Delta\mu_2^*(T) = \Delta h_2^* - T\Delta s_2^* \quad , \quad (5.1)$$

Table I. Solubility data for experiments with ^{133}Xe in 45 organic solvents. First row gives the Ostwald solubility, $L(T)$, and the second row gives the excess chemical potential $\Delta\mu_2^* = -RT \ln L$. Temperature is in degrees celsius.

Temperature	10	20	30	40	50
alkanes					
n-carbon					
5	$L(T) = 6.41$	5.48			
	$\Delta\mu_2^*(T) = -1045$	-991			
6	$L(T) = 5.91$	5.07	4.55		
	$\Delta\mu_2^*(T) = -999$	-945	-913		
7	$L(T) = 5.41$	4.67	4.13	3.75	3.37
	$\Delta\mu_2^*(T) = -950$	-898	-854	-822	-780
8	$L(T) = 4.99$	4.36	3.90	3.47	3.31
	$\Delta\mu_2^*(T) = -904$	-858	-820	-774	-769
9	$L(T) = 4.70$	4.14	3.70	3.32	2.99
	$\Delta\mu_2^*(T) = -871$	-828	-788	-747	-703
10	$L(T) = 4.42$	3.92	3.52	3.14	2.84
	$\Delta\mu_2^*(T) = -836$	-796	-758	-712	-670
11	$L(T) = 4.18$	3.72	3.35	3.00	2.71
	$\Delta\mu_2^*(T) = -805$	-765	-728	-684	-640
12	$L(T) = 4.03$	3.59	3.22	2.90	2.64
	$\Delta\mu_2^*(T) = -784$	-744	-704	-662	-623
13	$L(T) = 3.88$	3.44	3.09	2.80	2.53
	$\Delta\mu_2^*(T) = -763$	-720	-679	-641	-596
14	$L(T) = 3.76$	3.35	3.02	2.72	2.49
	$\Delta\mu_2^*(T) = -745$	-704	-666	-623	-586
15	$L(T) =$	3.24	2.92	2.64	2.41
	$\Delta\mu_2^*(T) =$	-685	-645	-604	-565

Table I cont.....

16	L(T) =	3.14	2.85	2.57	2.35
	$\Delta\mu_2^*(T)$ =	-667	-631	-587	-549
17	L(T) =		2.76	2.51	2.30
	$\Delta\mu_2^*(T)$ =		-612	-573	-535
18	L(T) =		2.71	2.47	2.25
	$\Delta\mu_2^*(T)$ =		-601	-563	-521
19	L(T) =			2.42	2.21
	$\Delta\mu_2^*(T)$ =			-550	-509
20	L(T) =			2.36	2.17
	$\Delta\mu_2^*(T)$ =			-534	-498

Table I cont.....

Temperature	10	20	30	40	50
alkanols					
n-carbon					
1	L(T) = 2.46	2.20	1.98	1.79	
	$\Delta\mu_2^*(T) = -507.4$	-460.4	-411.5	-362.3	
2	L(T) = 2.79	2.47	2.22	2.02	1.85
	$\Delta\mu_2^*(T) = -577.9$	-527.9	-481.5	-436.0	-395.4
3	L(T) = 3.02	2.65	2.38	2.16	1.98
	$\Delta\mu_2^*(T) = -621.3$	-567.7	-521.3	-482.2	-439.0
4	L(T) = 3.04	2.68	2.40	2.17	1.98
	$\Delta\mu_2^*(T) = -625.8$	-574.7	-527.4	-482.2	-439.0
5	L(T) = 2.97	2.62	2.36	2.13	1.95
	$\Delta\mu_2^*(T) = -613.3$	-561.3	-516.5	-467.0	-419.6
6	L(T) = 2.97	2.62	2.34	2.12	1.92
	$\Delta\mu_2^*(T) = -611.9$	-559.1	-512.7	-467.0	-419.6
7	L(T) = 2.91	2.57	2.31	2.09	1.91
	$\Delta\mu_2^*(T) = -601.6$	-594.4	-503.3	-457.5	-413.5
8	L(T) = 2.86	2.52	2.25	2.05	1.88
	$\Delta\mu_2^*(T) = -590.7$	-537.3	-489.6	-445.8	-404.4
9	L(T) = 2.79	2.49	2.24		
	$\Delta\mu_2^*(T) = -577.5$	-530.5	-484.5		
10	L(T) = 2.74	2.43	2.20	2.00	1.83
	$\Delta\mu_2^*(T) = -567.8$	-518.4	-475.5	-432.0	-388.4
11	L(T) =	2.34	2.11	1.92	1.76
	$\Delta\mu_2^*(T) =$	-496.2	-449.8	-406.3	-363.8
12	L(T) =		2.12	1.94	1.78
	$\Delta\mu_2^*(T) =$		-453.5	-410.8	-369.6
14	L(T) =			1.91	1.72
	$\Delta\mu_2^*(T) =$			-404.0	-364.8

Table I cont.....

Temperature	10	20	30	40	50
carboxylic acids					
n-carbon					
1	L(T) = 0.474 $\Delta\mu_2^*(T) = 420.1$	0.456 458.1	0.437 498.7	0.420 539.8	0.414 566.3
2	L(T) = $\Delta\mu_2^*(T) =$	1.71 -312.0	1.58 -275.2	1.47 -239.7	1.37 -204.3
3	L(T) = 2.97 $\Delta\mu_2^*(T) = -611.7$	2.66 -570.0	2.41 -530.0	2.21 -493.2	2.04 -456.6
4	L(T) = 3.22 $\Delta\mu_2^*(T) = -658.7$	2.89 -618.9	2.61 -577.0	2.37 -537.5	2.16 -494.8
5	L(T) = 3.20 $\Delta\mu_2^*(T) = -653.9$	2.84 -607.4	2.56 -567.2	2.31 -521.3	2.11 -478.6
7	L(T) = 3.12 $\Delta\mu_2^*(T) = -639.5$	2.78 -594.9	2.50 -553.0	2.27 -511.0	2.07 -468.1
alkanals					
3	L(T) = 3.09 $\Delta\mu_2^*(T) = -634.9$	2.80 -600.0	2.55 -564.4		
4	L(T) = 3.47 $\Delta\mu_2^*(T) = -700.0$	3.12 -662.5	2.83 -625.6	2.56 -585.7	2.40 -560.9
5	L(T) = 3.50 $\Delta\mu_2^*(T) = -705.2$	3.15 -668.8	2.84 -628.4	2.59 -592.4	2.40 -560.0
7	L(T) = 3.32 $\Delta\mu_2^*(T) = -675.7$	2.98 -636.3	2.70 -598.4	2.47 -561.9	2.26 -524.2

Table I. cont....

Temperature	5	10	15	20	25
n-carbon perfluoroalkanes					
6	L(T) = 2.48	2.39	2.30	2.20	2.11
	$\Delta\mu_2^*(T) = -501.8$	-489.8	-477.9	-459.3	-442.4
7	L(T) = 2.23	2.16	2.09	2.01	1.95
	$\Delta\mu_2^*(T) = -443.3$	-433.8	-423.2	-406.7	-396.3
8	L(T) = 2.15	2.06	2.00	1.92	1.85
	$\Delta\mu_2^*(T) = -422.1$	-408.0	-396.3	-379.7	-365.8
n-carbon perfluoroalkane					
7	L(T) = 1.87	1.76	1.67		
	$\Delta\mu_2^*(T) = -378.0$	-350.4	-327.8		
8	L(T) = 1.79	1.67	1.59		
	$\Delta\mu_2^*(T) = -349.4$	-318.0	-296.6		

Table I cont.....

Temperature	5	10	15	20	25
n-carbon cycloalkanes					
5	L(T) = 6.88	6.49	6.04	5.75	5.33
	$\Delta\mu_2^*(T) = -1066$	-1053	-1030	-1019	-991.8
6	L(T) =		5.28	5.00	4.70
	$\Delta\mu_2^*(T) =$		-952.2	-937.3	-916.8
8	L(T) =		4.26	4.02	3.79
	$\Delta\mu_2^*(T) =$		-829.4	-809.9	-789.7
Temperature					
	30	40	50		
n-carbon cycloalkanes					
5	L(T) = 5.04				
	$\Delta\mu_2^*(T) = -974.8$				
6	L(T) = 4.46	3.98	3.58		
	$\Delta\mu_2^*(T) = -900.1$	-859.7	-818.5		
8	L(T) = 3.58	3.21	2.91		
	$\Delta\mu_2^*(T) = -768.8$	-725.3	-686.2		

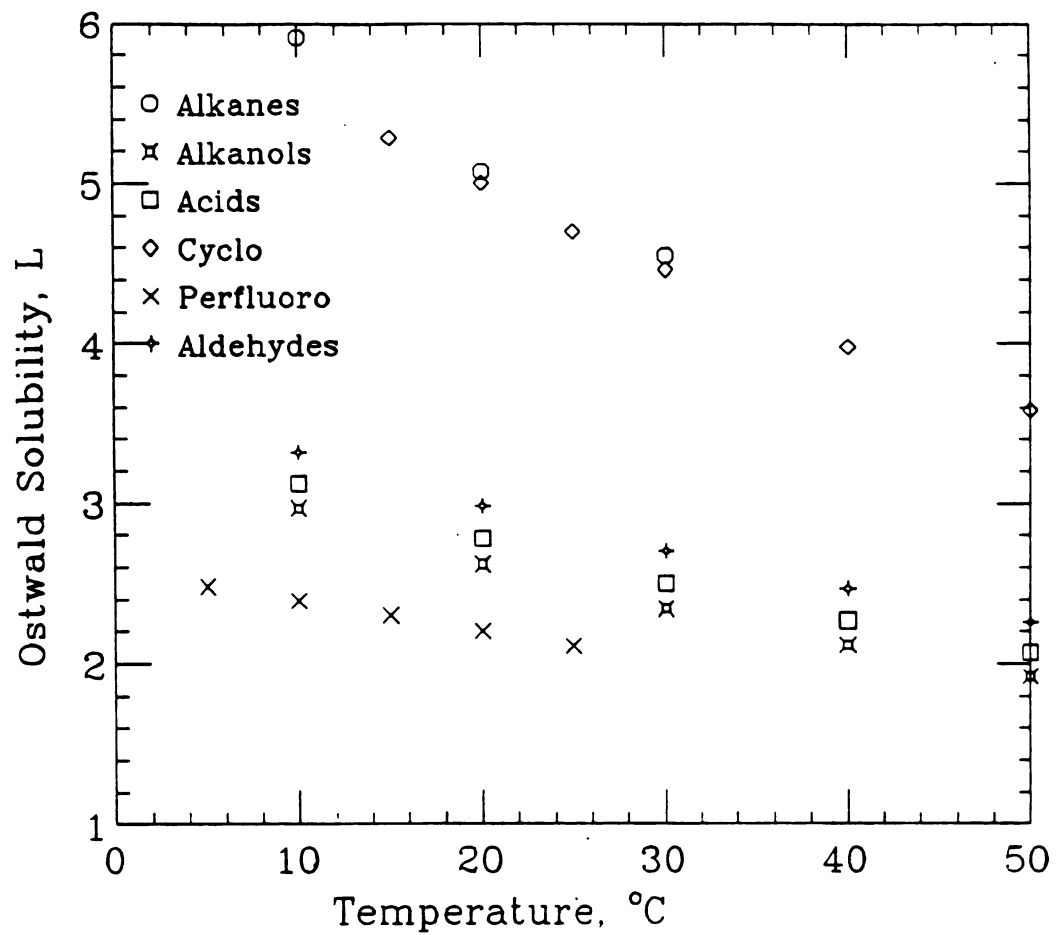


Figure 8. $L(T)$ for Xe in six representative organic solvents.

i.e., the slope of $\Delta\mu_2^*(T)$ is the negative average entropy of solvation ($\Delta\bar{s}_2^*$) over the temperature interval, and the intercept at $T=0$ (T is the absolute temperature) is the average enthalpy of solvation ($\Delta\bar{h}_2^*$). One might at first think that this interpretation ignores the effect of a strong temperature dependence of the enthalpy having a strong temperature dependence which could then be seen in $\Delta\mu_2^*(T)$, however this is not correct since³¹:

$$\left(\frac{\partial H}{\partial T}\right)_{p,N} = T\left(\frac{\partial S}{\partial T}\right)_{p,N} \quad (5.2)$$

Any temperature dependent contribution from the enthalpy to the free energy is cancelled by a temperature dependent contribution from the entropy (provided we take the derivatives under the proper conditions). This does not mean that $\partial\Delta h_2^*/\partial T$ is meaningless, in fact this quantity is the specific heat of solvation, Δc_p^* .¹⁴ This quantity turns out to be very small, but it may be of interest in more detailed studies in the future. The tabulated values of $\Delta\bar{h}_2^*$, and $\Delta\bar{s}_2^*$ for the 45 solvents studied can be found in Table II.

5.2 Entropy of Solvation

In viewing Figure 9 one can see the slopes of the straight line fits are all quite similar. This means that the solvation entropies all fall close together. This

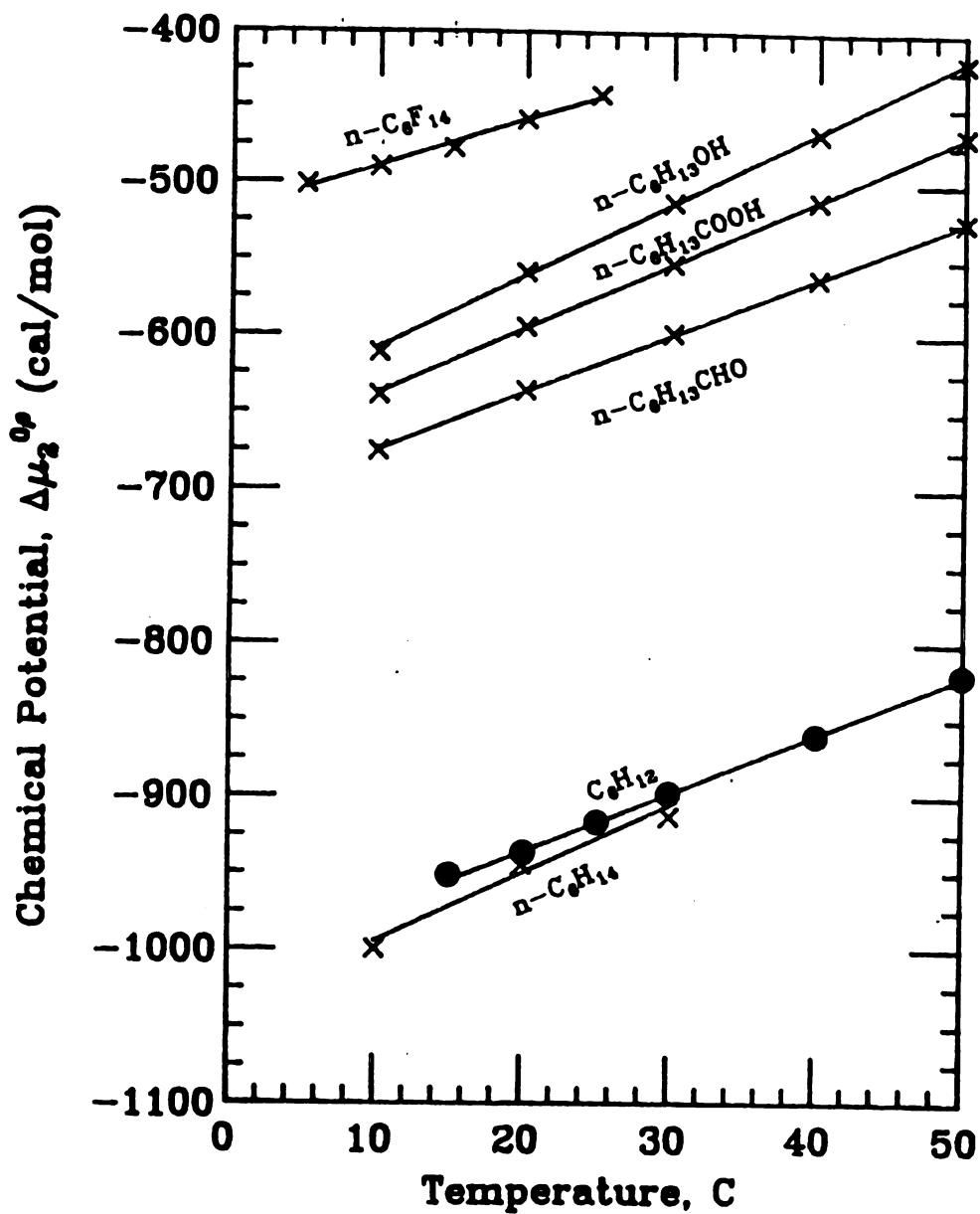


Figure 9. Excess chemical potential, $\Delta\mu_2^*(T)$ for six representative organic solvents (Figure 1 of reference 17).

Table II. Experimental data for excess enthalpy and entropy for ^{133}Xe in 45 organic solvents.

alkanes

n-C	$\Delta\bar{h}_2^*$ ($\frac{\text{cal}}{\text{mol}}$)	$\Delta\bar{s}_2^*$ ($\frac{\text{cal}}{\text{mol}\cdot\text{K}}$)
5	-2582	-5.429
6	-2264	-4.482
7	-2109	-4.121
8	-2109	-4.260
9	-2044	-4.145
10	-2007	-4.128
11	-1958	-4.069
12	-1922	-4.017
13	-1924	-4.104
14	-1879	-4.005
15	-1869	-4.038
16	-1819	-3.928
17	-1769	-3.820
18	-1807	-3.979
19	-1762	-3.875
20	-1727	-3.808

cycloalkanes

n-C	$\Delta\bar{h}_2^*$ ($\frac{\text{cal}}{\text{mol}}$)	$\Delta\bar{s}_2^*$ ($\frac{\text{cal}}{\text{mol}\cdot\text{K}}$)
5	-2120	-3.77
6	-2065	-3.85
8	-2022	-4.14

Table II. cont.....

alkanols

n-C	Δh_2^* ($\frac{\text{cal}}{\text{mol}}$)	Δs_2^* ($\frac{\text{cal}}{\text{molK}}$)
1	-1880	-4.84
2	-1869	-4.57
3	-1910	-4.57
4	-1943	-4.66
5	-1924	-4.64
6	-1959	-4.77
7	-1922	-4.67
8	-1900	-4.64
9	-1890	-4.65
10	-1826	-4.45
11	-1790	-4.41
12	-1720	-4.20
14	-1630	-3.90

Table II. cont....

carboxylic acids

n-C	$\Delta \bar{h}_2^*$ ($\frac{\text{cal}}{\text{mol}}$)	$\Delta \bar{s}_2^*$ ($\frac{\text{cal}}{\text{molK}}$)
1	-640.2	-3.75
2	-1366	-3.60
3	-1702	-3.86
4	-1819	-4.10
5	-1885	-4.35
7	-1844	-4.26

alkanals (aldehydes)

n-C	$\Delta \bar{h}_2^*$ ($\frac{\text{cal}}{\text{mol}}$)	$\Delta \bar{s}_2^*$ ($\frac{\text{cal}}{\text{molK}}$)
3	-1632	-3.52
4	-1710	-3.57
5	-1743	-3.67
7	-1742	-3.77

perfluoroalkanes

n-C	$\Delta \bar{h}_2^*$ ($\frac{\text{cal}}{\text{mol}}$)	$\Delta \bar{s}_2^*$ ($\frac{\text{cal}}{\text{molK}}$)
6	-1335	-2.99
7	-1188	-2.67
8	-1221	-2.87

observation is further supported on Table II which indicates that the values of $\Delta\bar{s}_2^{-*}$ are all negative and commensurate in magnitude. The average value of the solvation entropy over all our solvents is, $(\Delta\bar{s}_2^{-*})_{\text{ave}} = -4.1 \pm 0.5$ cal/mol K .

The entropy is associated with the process of taking the solute from fixed position in the gas and placing it at fixed position in the solvent. The negative entropy can be thought of as solvent ordering during this process. We can conclude from our data that the amount of ordering is more or less independent of the solvent used. This isn't too surprising since our solvents were generally large floppy molecules compared to the solute. We shall see later that the solvation entropy is much more dependent on the solute particle. It is interesting to compare our results to Xe solubility in water. For the Xe \rightarrow H₂O system, the corresponding $\Delta\bar{s}_2^{-*}$, averaged from 10-40°C is about -18 cal/mol K , calculated from the data of Benson and Krause.³²

This is indicative of a high degree of solvent ordering upon hydration. This ordering can be associated with the high polarizability of Xe, hydrogen bonding, dipole-dipole interactions, and the small relative size of H₂O molecules.⁹

These combined effects can lead to ice-like structures surrounding the solute^{9,32}, and thus decreases the entropy of the liquid.

5.3 Enthalpy (Energy) of Solvation

Before analyzing the enthalpy a brief reminder, for the

systems we are looking at the excess enthalpy of solvation is essentially the same as the excess energy of solvation since PV is small in a liquid. If we assume the gas phase is ideal then the solvation enthalpy, $\Delta\bar{h}_2^*$, can be thought of as the energy required to take the solute from infinity and put it at a fixed position in the liquid.

One can see from Figure 9 and Table II that for all the solvents, except HCOOH (formic acid), the solvation process is enthalpically dominated, i.e. $\Delta\bar{h}_2^*/T\Delta\bar{s}_2^* > 1$. For these solvents (excluding HCOOH) we find $\Delta\bar{h}_2^*/T\Delta\bar{s}_2^* = 1.5 \pm 0.15$, also remarkably constant. The average value of enthalpy for the same solvents is $\Delta\bar{h}_2^* = -1840 \pm 250$ cal/mole. Values for enthalpy are spread more widely than for entropy as one can see from Figure 9. The alkanes and cycloalkanes tended to have a large negative enthalpy, while the perfluoroalkanes and the small polar molecules (such as acetic and formic acids) have enthalpies of comparatively small magnitude. All values of enthalpy were negative. This demonstrates a net attraction between the solute and the solvent.

Solubility of Xe and other noninteracting gases in water is entropically dominated. Using the $\text{Xe} \rightarrow \text{H}_2\text{O}$ data from Benson and Krause³² we find that $\Delta\bar{h}_2^* = -4050$ cal/mole, averaged from 10-40°C, which leads to $\Delta\bar{h}_2^*/T\Delta\bar{s}_2^* = 0.75$. Even though the enthalpic contribution is larger in water than in the organics it is overwhelmed by the entropy caused by solvent organization. It shouldn't really be surprising that the enthalpy in water is high since water has a permanent

dipole moment, but the interactions between other water molecules are also very strong. This competition is reflected in the solvation entropy and keeps the solubility of nonpolar gases in water low. A simple way to think of it is that water likes the solute, but it likes itself a lot better and reorganizes to keep as many hydrogen bonds intact as possible.

5.4 Temperature Dependence of $L(T)$ and $\Delta\mu_2^*(T)$

It is clear from our earlier discussions that the temperature dependence of the chemical potential is determined by the entropy. Thus we attribute the positive slope of the curves of Figure 9 to a negative entropy. We now ask: What determines the temperature dependence of the solubility itself, $L(T)$. To illustrate this clearly we start with the now familiar relation (equation 5.1):

$$\Delta\mu_2^*(T) = -RT \ln(L) = \Delta\bar{h}_2^* - T\Delta\bar{s}_2^* .$$

Solving for $L(T)$ we have:

$$L(T) = \exp \left(-\frac{\Delta\bar{h}_2^*}{RT} + \frac{\Delta\bar{s}_2^*}{R} \right) . \quad (5.3)$$

Assuming $\Delta\bar{h}_2^*$ and $\Delta\bar{s}_2^*$ are essentially constant in the temperature range of interest we differentiate (5.3) with respect to temperature:

$$\frac{dL}{dT} = L \frac{\Delta \bar{h}_2^*}{R T^2} \quad (5.4)$$

One can also show:³³

$$L(T) = L(T_0) \exp \left(\frac{-\Delta \bar{h}_2^* (T - T_0)}{R T T_0} \right) \quad (5.5)$$

where T is the temperature of interest and T_0 is a chosen reference temperature. This leads us to the surprising result (at least for me it was) that the temperature dependence of the Ostwald solubility is due to the enthalpy, while the temperature dependence of the chemical potential is due to the entropy. We conclude that the experimentally observed decrease in gas solubility with increasing temperature (see Figure 8) is associated with negative enthalpies of solvation.

5.5 Total Entropy and Enthalpy

Up to this point we have focused on the entropy and enthalpy associated with the excess chemical potential, $\Delta \mu_2^*$. This is the chemical potential for the fictional process of placing the solute at fixed position in the solvent. Its value in constructing a physical model of solvation has been discussed earlier. We would now like to look at the total entropy and enthalpy for the entire (real) solvation process. Our starting point is the chemical potential for

the solute and the equilibrium condition (equations 3.6-3.8):

$$\begin{aligned}\mu_2^g &= kT \ln (\rho_2^g \Lambda^3) \\ \mu_2^l &= kT \ln (\rho_2^l \Lambda^3) + \Delta\mu_2^* \\ \mu_2^g &= \mu_2^l \quad .\end{aligned}$$

Taking the temperature derivative at constant pressure and composition we calculate the total entropy:

$$\Delta s_2^{\text{tot}} = - \frac{\partial}{\partial T} \left(\mu_2^l - \mu_2^g \right)_P = \left(s_2^l - s_2^g \right) \quad , \quad (5.6)$$

where:

$$s_2^g = -k \ln (\rho_2^g \Lambda^3) - kT \left(\frac{1}{\rho_2^g} \frac{\partial \rho_2^g}{\partial T} \right)_P \quad (5.7)$$

$$s_2^l = -k \ln (\rho_2^l \Lambda^3) - kT \left(\frac{1}{\rho_2^l} \frac{\partial \rho_2^l}{\partial T} \right)_P + \Delta s_2^* \quad (5.8)$$

For fixed particle number we can write the derivatives of density as negative derivatives of volume. This allows us to substitute the isobaric expansivity, $\alpha = (1/V)(\partial V/\partial T)_P$, into (5.7) and (5.8). For dilute solutions we assume the expansivity of the liquid mixture is the same as that of the pure liquid, α_l . The gas expansivity, α_g , is easily derived from the ideal gas equation of state:

$$\alpha_g = 1 / T \quad . \quad (5.9)$$

Putting all this together, the relationship between the total entropy, Δs_2^{tot} , and the solvation entropy, Δs_2^* is :

$$\Delta s_2^{\text{tot}} = \Delta s_2^* - k \ln(L) - k + kT\alpha_\ell \quad . \quad (5.10)$$

We can now find the total enthalpy through equations (2.6) and (2.13b):

$$\Delta \mu_2^{\text{tot}} = 0 = \Delta h_2^{\text{tot}} - T\Delta s_2^{\text{tot}} \quad . \quad (5.11)$$

Therefore:

$$\Delta h_2^{\text{tot}} = T\Delta s_2^* - kT\ln(L) - kT + kT^2\alpha_\ell \quad , \quad (5.12)$$

which is equivalent to:

$$\Delta h_2^{\text{tot}} = \Delta h_2^* + kT - kT^2\alpha_\ell \quad . \quad (5.13)$$

Table III shows Δh_2^{tot} and Δs_2^{tot} for the 45 solvents used.

Table III. Enthalpy and entropy of solution. The second and third columns are the total entropy and enthalpy of solution. The fourth and fifth columns are the entropy and enthalpy evaluated on the mole-fraction scale.

alkanes

n-C	$\Delta\bar{h}_2^{-t} \left(\frac{\text{cal}}{\text{mol}} \right)$	$\Delta\bar{s}_2^{-t} \left(\frac{\text{cal}}{\text{molK}} \right)$	$\Delta\bar{h}_2^{-o} \left(\frac{\text{cal}}{\text{mol}} \right)$	$\Delta\bar{s}_2^{-o} \left(\frac{\text{cal}}{\text{molK}} \right)$
5	-2899	-9.72	-2818	-16.90
6	-2615	-8.77	-2691	-16.37
7	-2478	-8.31	-2415	-15.36
8	-2493	-8.36	-2429	-15.34
9	-2440	-8.18	-2378	-15.09
10	-2410	-8.08	-2351	-14.93
11	-2379	-7.98	-2308	-14.74
12	-2348	-7.88	-2278	-14.56
13	-2350	-7.88	-2278	-14.51
14	-2307	-7.74	-2239	-14.30
15	-2301	-7.72	-2233	-14.23
16	-2253	-7.76	-2180	-14.00
17	-2206	-7.40	-2154	-13.68
18	-2246	-7.54	-2191	-13.91

cycloalkanes

n-C	$\Delta\bar{h}_2^{-t} \left(\frac{\text{cal}}{\text{mol}} \right)$	$\Delta\bar{s}_2^{-t} \left(\frac{\text{cal}}{\text{molK}} \right)$	$\Delta\bar{h}_2^{-o} \left(\frac{\text{cal}}{\text{mol}} \right)$	$\Delta\bar{s}_2^{-o} \left(\frac{\text{cal}}{\text{molK}} \right)$
5	-2478	-8.31	-2385	-15.68
6	-2437	-8.17	-2263	-15.34
8	-2440	-8.18	-2417	-15.84

Table III cont...

alkanols

n-C	$\Delta h_2^{-t} \left(\frac{\text{cal}}{\text{mol}} \right)$	$\Delta S_2^{-t} \left(\frac{\text{cal}}{\text{molK}} \right)$	$\Delta h_2^{-o} \left(\frac{\text{cal}}{\text{mol}} \right)$	$\Delta S_2^{-o} \left(\frac{\text{cal}}{\text{molK}} \right)$
1	-2263	-7.59	-2250	-18.82
2	-2268	-7.61	-2257	-17.87
3	-2325	-7.80	-2300	-17.39
4	-2372	-7.96	-2345	-17.13
5	-2361	-7.92	-2331	-16.79
6	-2397	-8.04	-2364	-16.64
7	-2359	-7.91	-2317	-16.26
8	-2342	-7.86	-2304	-16.05
9	-2343	-7.86	-2310	-15.90
10	-2272	-7.62	-2234	-15.50
11	-2239	-7.51	-2210	-15.35

carboxylic acids

n-C	$\Delta h_2^{-t} \left(\frac{\text{cal}}{\text{mol}} \right)$	$\Delta S_2^{-t} \left(\frac{\text{cal}}{\text{molK}} \right)$	$\Delta h_2^{-o} \left(\frac{\text{cal}}{\text{mol}} \right)$	$\Delta S_2^{-o} \left(\frac{\text{cal}}{\text{molK}} \right)$
1	-1052	-3.53	-1051	-17.99
2	-1780	-5.97	-1780	-17.02
3	-2101	-7.05	-2088	-16.67
4	-2223	-7.46	-2204	-16.49
5	-2301	-7.72	-2287	-16.48
7	-2276	-7.63	-2239	-15.84

Table III cont...

alkanals (aldehydes)

n-C	$\Delta\bar{h}_2^{-t} \left(\frac{\text{cal}}{\text{mol}} \right)$	$\Delta\bar{S}_2^{-t} \left(\frac{\text{cal}}{\text{molK}} \right)$	$\Delta\bar{h}_2^{-o} \left(\frac{\text{cal}}{\text{mol}} \right)$	$\Delta\bar{S}_2^{-o} \left(\frac{\text{cal}}{\text{molK}} \right)$
3	-1966	-6.60	-1946	-16.13
4	-2071	-6.95	-2039	-15.83
5	-2115	-7.09	-2076	-15.61
7	-2152	-7.22	-2137	-15.38

perfluoroalkanes

n-C	$\Delta\bar{h}_2^{-t} \left(\frac{\text{cal}}{\text{mol}} \right)$	$\Delta\bar{S}_2^{-t} \left(\frac{\text{cal}}{\text{molK}} \right)$	$\Delta\bar{h}_2^{-o} \left(\frac{\text{cal}}{\text{mol}} \right)$	$\Delta\bar{S}_2^{-o} \left(\frac{\text{cal}}{\text{molK}} \right)$
6	-1632	-5.48	-1606	-13.5
7	-1515	-5.08	-1487	-13.0
8	-1565	-5.25	-1536	-13.1

Expansivity data was obtained from standard sources^{35,36} (we measured the expansivity for the perfluoroalkanes and cyclopentane using our temperature dependent density data, $\rho(T)$). Although the solvation enthalpy, Δh_2^* is not accessible to direct measurement, the total solvation enthalpy, Δh_2^{tot} , is. This is the heat of solution at constant pressure. The heat of solution has been measured for various gases in water using calorimetric techniques, and general agreement is found with solubility derived values.³⁴ No such measurements have been made to date on our system.

5.6 Mole Fraction Scale

The standard approach to solubility is to calculate chemical potential on the mole fraction scale $\Delta\mu_2^{\circ}$ (see discussion in section 3.6) :

$$\Delta\mu_2^{\circ} = -RT \ln x_2 \quad .$$

The corresponding enthalpy ($\Delta\bar{h}_2^{\circ}$) and entropy ($\Delta\bar{s}_2^{\circ}$) are obtained by writing $\Delta\mu_2^{\circ} = \Delta\bar{h}_2^{\circ} - T\Delta\bar{s}_2^{\circ}$ and proceeding in a manner analogous to what we have used. The tabulated enthalpies and entropies can be found in Table III. Note that the enthalpy on the mole fraction scale ($\Delta\bar{h}_2^{\circ}$) is very close to the total enthalpy of solvation ($\Delta\bar{h}_2^{\text{tot}}$). This fact has strengthened confidence in the mole fraction scale, but also note the entropy ($\Delta\bar{s}_2^{\circ}$) is not the same as the total

entropy ($\Delta\bar{s}_2^{-tot}$) or the entropy of solvation ($\Delta\bar{s}_2^{-*}$). In fact the mole fraction entropy has no straightforward interpretation (and, in my opinion, is often misused).

6. Theoretical Analysis

6.1 The Excess Chemical Potential, $\Delta\mu_2^*$.

Now that we have experimentally determined the excess chemical potential, also referred to as the free energy of solvation, our task is to predict it from as close to first principles as possible. This goal will constitute the bulk of this chapter.

The chemical potential is derived from the partition function. In order to keep things clear we will first work out the case for a single component, N particle, atomic liquid in the canonical ensemble (all results are generalizable to the grand canonical ensemble). The classical partition function is:

$$Q(V,T) = \frac{1}{N! h^{3N}} \int d\vec{r}^N \int d\vec{p}^N \exp[-\beta\mathcal{K}(\vec{r}^N, \vec{p}^N)] \quad , \quad (6.1)$$

where \mathcal{K} is the hamiltonian of the system, h^{3N} (h is Planck's constant) accounts for quantum corrections to the differential volume elements in phase space, $N!$ corrects for the indistinguishability of the particles, β is the Boltzmann factor ($1/kT$), and (\vec{r}^N, \vec{p}^N) is a point in the $6N$

dimensional phase space that describes the system.¹⁶ An important simplification that arises in the classical approximation is the separation of potential and kinetic terms to characterize the liquid state.³⁵ This allows us to write the Hamiltonian as:

$$\mathcal{H}(\vec{r}^N, \vec{p}^N) = K(\vec{p}^N) + U(\vec{r}^N) \quad , \quad (6.2)$$

where $K(\vec{p}^N)$ is the kinetic energy of the classical degrees of freedom, $K(\vec{p}^N) = \sum_{i=1}^N (p_i^2/2m)$, and $U(\vec{r}^N)$ is the potential energy. We can now write the partition function as:

$$Q(V, T) = \left[\frac{1}{N! h^{3N}} \int d\vec{r}^N \int d\vec{p}^N \exp[-\beta K(\vec{p}^N)] \right] \times \left[\frac{1}{V^N} \int d\vec{r}^N \exp[-\beta U(\vec{r}^N)] \right] \quad . \quad (6.3)$$

In writing equation 6.3 we have used the fact that $\int d\vec{r}^N / V^N = 1$ (note that we now have two integrals over $d\vec{r}^N$). The first bracketed term is the partition function for an N particle ideal gas, Q_{ideal} . The second term is referred to as the configurational partition function, Q_{con} .¹⁶ Evaluation of the ideal partition function is straightforward:³⁶

$$Q_{ideal} = \frac{\Lambda^{-3N}}{N!} V^N \quad , \quad (6.4)$$

Λ denotes the de Broglie wavelength, $\Lambda = (2\pi\beta h^2/m)^{1/2}$. The Helmholtz free energy, $A(N, V, T)$, is:

$$A = -kT \ln Q(V, T) \quad . \quad (6.5)$$

For our partition function this is equivalent to:

$$A = -kT \ln Q_{\text{ideal}} - kT \ln Q_{\text{con}} = A_{\text{ideal}} + \Delta A^* \quad , \quad (6.6)$$

where A_{ideal} is the free energy for an ideal gas and ΔA^* is the excess free energy. The corresponding chemical potentials are found by differentiating with respect to N , it therefore becomes obvious that the chemical potential can be expressed as:

$$\mu = \mu_{\text{ideal}} + \Delta\mu^* \quad , \quad (6.7)$$

where $\mu_{\text{ideal}} = -kT \ln(\rho_2 \Lambda^3)$. To derive an expression for the excess chemical potential we use identity (3.15):

$$\begin{aligned} \Delta\mu^* &= \Delta A^*(N+1, V, T) - \Delta A^*(N, V, T) \\ &= kT \ln \left(\frac{V Q_{\text{con}}(N, V, T)}{Q_{\text{con}}(N+1, V, T)} \right) \quad . \end{aligned} \quad (6.8)$$

The ratio $Q_{\text{con}}(N+1, V, T)/Q_{\text{con}}(N, V, T)$ is given by:

$$\frac{Q_{\text{con}}(N+1, V, T)}{Q_{\text{con}}(N, V, T)} = \frac{\int \exp[-\beta U_{N+1}(\vec{r}^{N+1})] d\vec{r}^{N+1}}{\int \exp[-\beta U_N(\vec{r}^N)] d\vec{r}^N} . \quad (6.9)$$

If the potential energy is pair decomposable we may write the potential energy of the N+1 particle system as:

$$U_{N+1}(\vec{r}^{N+1}) = U_N(\vec{r}^N) + \phi_0 , \quad (6.10)$$

where ϕ_0 is the binding energy of the $(N+1)^{\text{st}}$ particle with all the others in configuration \vec{r}^N . Equation (6.9) becomes:

$$\frac{Q_{\text{con}}(N+1, V, T)}{Q_{\text{con}}(N, V, T)} = \frac{\int \exp[-\beta \phi_0] \exp[-\beta U_N(\vec{r}^N)] d\vec{r}^{N+1}}{\int \exp[-\beta U_N(\vec{r}^N)] d\vec{r}^N} . \quad (6.11)$$

In a system with translational invariance, the point \vec{r}^{N+1} may be taken as the origin for the remaining N position vectors. This allows us to integrate over \vec{r}^{N+1} , which yields a factor of V. Equation (6.11) reduces to:

$$\begin{aligned} \frac{Q_{\text{con}}(N+1, V, T)}{Q_{\text{con}}(N, V, T)} &= \frac{V \int \exp[-\beta \phi_0] \exp[-\beta U_N(\vec{r}^N)] d\vec{r}^N}{\int \exp[-\beta U_N(\vec{r}^N)] d\vec{r}^N} \\ &= V \langle \exp(-\beta \phi_0) \rangle , \end{aligned} \quad (6.12)$$

where the angular brackets denote a canonical ensemble average over the N particle system. Substitution of (6.12)

in (6.8) gives:

$$\Delta\mu^* = -kT \ln \langle \exp(-\beta\phi_0) \rangle . \quad (6.13)$$

For a two component system we can write the partition function for a simple structureless solute (2) dissolved in a fluid (1) :

$$Q = Q_1^{\text{ideal}} Q_2^{\text{ideal}} V^{-(N_1+N_2)} \times \int d\vec{r}^{N_1} \int d\vec{r}^{N_2} \exp \left[-\beta (U_{11}(\vec{r}^{N_1}) + U_{12}(\vec{r}^{N_1}, \vec{r}^{N_2}) + U_{22}(\vec{r}^{N_2})) \right]. \quad (6.14)$$

For dilute solutions the contribution from solute-solute interactions, U_{22} is negligible.¹⁴ Following the same steps as before one can show that the free energy for adding the (N_2+1) th particle is:

$$\Delta\mu_2^* = -kT \ln \langle \exp(-\beta B_0) \rangle , \quad (6.15)$$

where B_0 is the binding energy of the added solute to a fixed configuration of the solute-solvent system, i.e:

$$U_{12}^{N_2+1}(\vec{r}^{N_2+1}) = U_{12}^{N_2}(\vec{r}^{N_2}) + B_0 , \quad (6.16)$$

and the ensemble average is taken over all coordinates of the (N_1+N_2) particles.

Now we can appreciate an important simplification that occurs by using an inert structureless solute like Xe as a

probe. If we used a more complicated molecule with internal degrees of freedom (such as vibrational and rotational) it is conceivable that the potential energy would be a function of the solute conformation (shape), we would have to perform a double ensemble average: one over all spatial configurations of the (N_1+N_2) molecules and a second over all possible configurations of the solute molecule itself, i.e:

$$\Delta\mu_2^* = -kT \ln \langle \exp(-\beta B_0(P_2)) \rangle_{P_2}, \quad (6.17)$$

P_2 represents the internal coordinates of the solute molecule.¹⁴ A clear example where this would be necessary is the solvation of a polymer in water. By using an inert gas probe we can focus on free energy changes due to the liquid solvent and not have to worry about contributions from the solute.

6.2 Distribution Functions

An alternative approach to describing the liquid state that has proven to be quite powerful is the distribution function method. I shall present a brief overview of the technique, a more complete discussion is given in reference 36. As in the last section I shall work in the limit of an atomic liquid to keep the development simple,, but the results are readily generalizable.

The phase space probability distribution function in a

classical system is defined as:

$$f(\vec{r}^N, \vec{p}^N) = \exp[-\beta\mathcal{H}(\vec{r}^N, \vec{p}^N)] / \int d\vec{r}^N \int d\vec{p}^N \exp[-\beta\mathcal{H}(\vec{r}^N, \vec{p}^N)]. \quad (6.18)$$

The probability of a state (\vec{r}^N, \vec{p}^N) is simply $f(\vec{r}^N, \vec{p}^N) d\vec{r}^N d\vec{p}^N$. We have shown earlier that the Hamiltonian factors into kinetic and potential terms. Therefore we can write the total phase space distribution function as a momentum probability distribution, $\phi(\vec{p}^N)$, and a configurational probability distribution, $P(\vec{r}^N)$. The latter will be important in this discussion. The configurational probability distribution tells the probability for observing the system at configuration space point \vec{r}^N , it is defined as:

$$P(\vec{r}^N) = \exp[-\beta U(\vec{r}^N)] / \int d\vec{r}^N \exp[-\beta U(\vec{r}^N)]. \quad (6.19)$$

Note the denominator is equal to $(V^N \times Q_{\text{con}})$.

We can determine distribution functions for a small number of particles by integrating over all coordinates except those pertaining to the particles of interest. The joint probability distribution for finding a labelled particle 1 at \vec{r}_1 and a labelled particle 2 at \vec{r}_2 is:

$$P^{(2/N)}(\vec{r}_1, \vec{r}_2) = \int d\vec{r}_3 \int d\vec{r}_4 \dots \int d\vec{r}_N P(\vec{r}^N). \quad (6.20)$$

Since we cannot label identical particles, a more meaningful

quantity is the reduced probability distribution function, $\rho^{(2/N)}(\vec{r}_1, \vec{r}_2)$. It is defined as the probability distribution for finding any pair of particles at \vec{r}_1 and \vec{r}_2 :

$$\rho^{(2/N)}(\vec{r}_1, \vec{r}_2) = N(N-1) P^{(2/N)}(\vec{r}_1, \vec{r}_2) \quad . \quad (6.21)$$

The factor of $N(N-1)$ refers to the fact that there are N ways of choosing the first particle and $(N-1)$ ways of choosing the second. Similarly, the n -particle distribution function is defined as:

$$\rho^{(n/N)}(\vec{r}^n) = \frac{N!}{(N-n)!} \left[\frac{\int d\vec{r}^{N-n} \exp[-\beta U(\vec{r}^N)]}{\int d\vec{r}^N \exp[-\beta U(\vec{r}^N)]} \right] \quad . \quad (6.22)$$

For an homogeneous fluid, the single particle distribution function is simply the bulk density:

$$\rho^{(1/N)}(\vec{r}_1) = \rho = N/V \quad . \quad (6.23)$$

In the special case of an ideal gas, $U(\vec{r}^N)=0$ and $Q_{con} = 1$. Thus the n -particle distribution function becomes:

$$\rho^{(n/N)}(\vec{r}_n) = \rho^n \frac{N!}{N^n(N-n)} = \rho^n(1 + O(n/N)) \quad . \quad (6.24)$$

For example the pair distribution function for an ideal gas is:

$$\rho^{(2/N)}(\vec{r}_1, \vec{r}_2) = \rho^2(1 - 1/N) \approx \rho^2, \quad (6.25)$$

where the last equality depends on N being large; which it is for any macroscopic system. We now introduce yet another distribution function, $g(\vec{r}_1, \vec{r}_2)$:

$$g(\vec{r}_1, \vec{r}_2) = \rho^{(2/N)} / \rho^2, \quad (6.26)$$

which is the fractional deviation of the two particle distribution from the ideal gas limit. It is essentially a measure of how much the system deviates from complete randomness.³⁵ If the system is isotropic as well as homogeneous, the pair distribution function $g(\vec{r}_1, \vec{r}_2)$ is a function only of the separation between the two particles, $r_{12} = |\vec{r}_1 - \vec{r}_2|$; it is then referred to as the radial distribution function and simply written as $g(r)$.¹⁶ From our definition of $g(r)$ one may write the following:

$$\rho g(r) = \rho(\rho^{(2/N)}(0, \vec{r}) / \rho^2) = \rho^{(2/N)} / \rho. \quad (6.27)$$

Since we have already seen $\rho^{(1/N)}(\vec{r}_1) = \rho$, equation (6.27) can be interpreted as follows; $\rho g(r)$ is equivalent to the conditional probability density that a particle will be found at \vec{r} given that another is at the origin. This is based on the well known theorem of statistics: If A and B are random variables with joint probability distribution

$P(A \cap B)$, then the conditional probability distribution, $P(A|B)$, that A occurs if B also occurs is³⁷:

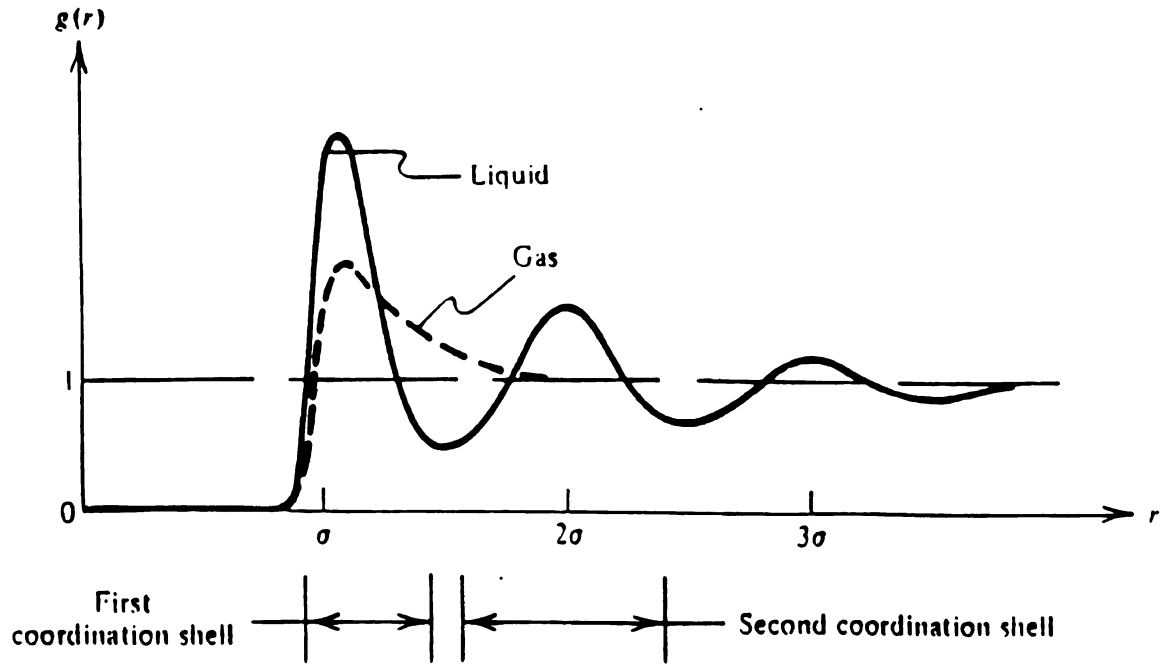
$$P(A|B) = P(A \cap B) / P(B) , \quad (6.28)$$

where $P(B)$ is the probability distribution for B. Our definition of $\rho g(r)$ can also be stated as follows; $\rho g(r)$ gives the average density of particles a distance r from a particle at the origin. The average number of particles in volume element dV at distance r is thus:

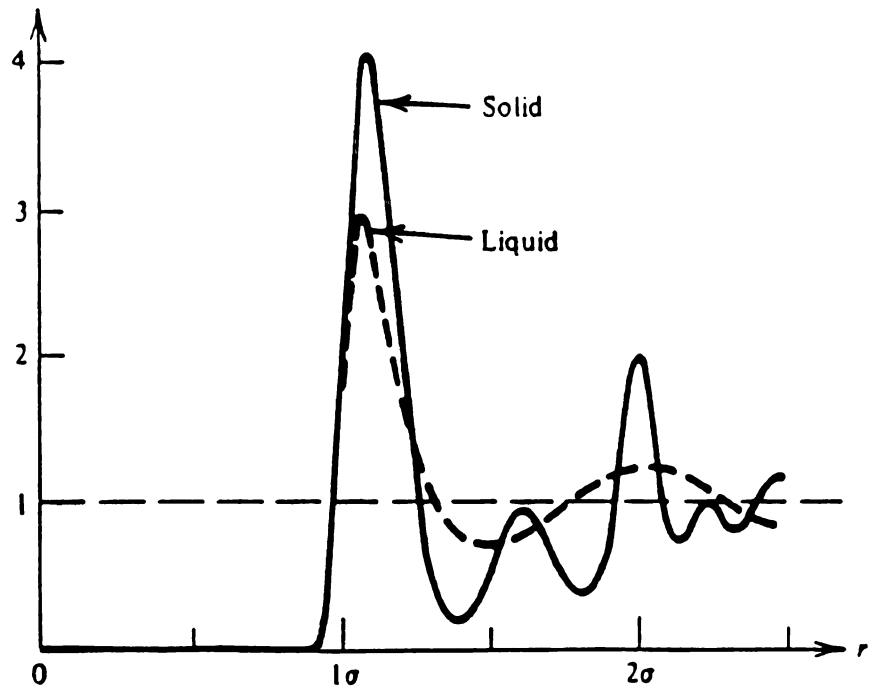
$$dN(r) = \rho g(r) dV . \quad (6.29)$$

Figure 10 shows $g(r)$ for an atomic solid, liquid and gas.

The radial distribution function plays an important role in the physics of liquids. There are two main reasons for this. First, the radial distribution function is directly measurable by scattering experiments (although it can be difficult to interpret results for complex molecular



The radial distribution function for a simple fluid.



Radial distribution functions for liquid and solid argon at the triple point ($\sigma = 3.4 \text{ \AA}$).

Figure 10. Radial distribution function, $g(r)$, for a typical gas, liquid, and solid.

liquids). Secondly, if the particles interact through pairwise additive forces, thermodynamic properties of the fluid can be written in terms of integrals over $g(r)$.

The two thermodynamic functions we shall require in our analysis are the excess internal energy of solvation, u_{int} , and the excess free energy of solvation, $\Delta\mu^*$. I shall now present brief explanations of how these quantities are determined from $g(r)$. Detailed derivations can be found in reference 36.

The internal energy of an atomic fluid can be written as:

$$E = \frac{3}{2} NkT + \bar{U} \quad , \quad (6.30)$$

where the first term is the mean kinetic energy (same as for an ideal gas), and the second term is the mean potential energy. Using our definition of $\rho g(r)$ we can easily find \bar{U} . Consider a tagged particle at the origin. If we assume the intermolecular interactions, $u(r)$, are pairwise additive we can express the potential energy between the tagged particle and all other particles at distances between r and $r+dr$ as:

$$dU = u(r)dN(r) = u(r)\rho g(r)dV = u(r)\rho g(r)4\pi r^2 dr \quad (6.31)$$

The total potential energy of the liquid is found by integrating over r , and multiplying by $N/2$. The factor of N arises since any particle could be the tagged particle, and

the factor of two compensates for double counting of pair interactions. The average potential energy per particle is therefore:

$$\bar{u} = \frac{\bar{U}}{N} = 2\pi\rho \int_0^{\infty} u(r)g(r)r^2 dr \quad . \quad (6.31)$$

For the case of a dilute solution (we use the conventional subscript notation in which 1 refers to the solvent and 2 refers to the solute), the excess internal energy (excluding kinetic energy) of the solute is:

$$du_{int} = u_{12}(r_{12})\rho_1 g_{12}(r_{12})4\pi r_{12}^2 dr_{12} \quad , \quad (6.32)$$

In Eq. (6.32) the function $g_{12}(r_{12})$ is the solvent-solute pair correlation function and $\rho_1 g_{12}(r)$ is the number density of solvent molecules a distance r from the tagged solute. The excess internal energy for this solute molecule is found by integrating over r_{12} :

$$u_{int} = 4\pi\rho_1 \int_0^{\infty} g_{12}(r)u_{12}(r)r^2 dr \quad . \quad (6.33)$$

This is sometimes called the excess internal energy of solvation. Note that for a pure liquid, for which $u_{int}^{(1,2)}$ goes into $u_{int}^{(1,1)}$, the excess solvation energy is twice the average excess energy per particle, \bar{u} . This is because the average energy in equation (6.31) is the potential energy to assemble the whole liquid, while the solvation energy in

equation (6.33) is the potential energy to bring one extra particle into a pre-assembled system.

In order to calculate the excess free energy of solvation we must introduce the idea, due to Onsager³⁸ and Kirkwood,³⁹ of a coupling parameter ξ which can vary from $\xi=0$ to $\xi=1$. We imagine the following process: we would like to introduce a new particle into the system by turning on its interaction with the other particles in the system. When $\xi=0$ the new particle does not interact with the system at all, and when $\xi=1$ we have the full intermolecular interaction $u_{12}(r_{12})$. This can be expressed as:

$$u_{12}(\xi, r_{12}) = \xi u_{12}(r_{12}) \quad . \quad (6.34)$$

To find the excess chemical potential we use equation (6.8):

$$\Delta\mu^* = \Delta A^*(N+1, V, T) - \Delta A^*(N, V, T) \quad .$$

Since the Helmholtz free energy is related to work in thermodynamics we can conclude that the excess chemical potential is the isothermal, reversible work that has to be done on the system against intermolecular forces in order to add one more molecule to the system under conditions of constant volume and temperature.⁴⁰ In other words $\Delta\mu^*$ is the work done on the system in going from the initial state with N molecules coupled with each other and 1 molecule not

coupled ($\xi=0$) to a final state with $N+1$ molecules fully coupled ($\xi=1$). Following the same steps as before we choose the new molecule to be at the origin. For an arbitrary intermediate value of ξ we can write the radial distribution function about the central molecule as $g(r,\xi)$. The potential energy of interaction of the central molecule is $\xi u(r)$. This means that $u(r)d\xi$ is the work that is done on the system by this one interaction if ξ is increased by $d\xi$. The work done on the system when ξ increases by $d\xi$, due to all the molecules between r and $r+dr$ is:

$$du(r,\xi) = u(r)d\xi \rho g(r,\xi) 4\pi r^2 dr \quad (6.33)$$

The total work, $\Delta\mu^*$, is the integral of (6.33) over r and over ξ from $\xi=0$ to $\xi=1$:

$$\Delta\mu^* = 4\pi\rho \int_0^1 \int_0^\infty u(r)g(r,\xi)r^2 dr d\xi \quad (6.34)$$

For a two component system the solvation free energy is:

$$\Delta\mu_2^* = 4\pi\rho_1 \int_0^1 \int_0^\infty u_{12}(r)g_{12}(r,\xi)r^2 dr d\xi \quad (6.35)$$

A generalized form of this statement is:

$$\Delta\mu_2^* = \int_0^1 U(\xi)d\xi \quad (6.36)$$

where $U(\xi)$ is the spatially averaged coupling energy of the solute to the rest of the system with the interaction potential reduced from its full strength by a factor of ξ .⁴¹

6.3 The Van der Waals Picture of Liquids

One of the fundamental problems in developing a theory of liquids is that there is no idealized model comparable to the ideal gas or the harmonic solid; both of which can be treated exactly.^{31,42} These provide a reference system from which one can base perturbation expansions or at least get an intuitive feel for the physical situation, in order to develop more sophisticated theories.

The van der Waals picture of liquids has helped a great deal to overcome this problem. The basic idea is to look at the different roles of strong short-ranged repulsive intermolecular forces and longer-ranged attractive forces in determining the structure and dynamics of a dense fluid. Though the concept was first utilized by van der Waals in his treatment of nonideal gases, there have been many other contributors to our current understanding.⁴³ The renaissance of this idea was spurred by the discovery from computer simulations that a system of infinitely hard spheres (essentially billiard balls, albeit tiny ones) undergoes a first order fluid-solid phase transition that can be related to freezing and melting of real materials.^{44,45}

The van der Waals picture asserts that the relative arrangements and motions of molecules in a liquid are

determined primarily by packing effects produced by the short-ranged repulsive interactions. Attractive forces, since they vary relatively slowly, play a minor role in structure and to first order can be treated as a mean field which exerts no intermolecular force but provides the cohesive energy that holds the system together at fixed density and temperature.

As an example we shall briefly look at a Lennard-Jones fluid, which is defined by the intermolecular potential, $u(r)$ (see Figure 11):

$$u(r) = 4\epsilon \left[(\sigma/r)^{12} - (\sigma/r)^6 \right] , \quad (6.37)$$

the collision diameter, σ , is the separation of two particles where $u(r)=0$, and ϵ is the depth of the potential well at the minimum in $u(r)$. The properties of the Lennard-Jones fluid are well known from computer simulations,⁴⁶ and it serves as an excellent model of atomic liquids like argon.⁴⁷ The repulsive $(1/r)^{12}$ term arises from electron cloud overlap and Pauli exclusion, and the attractive $(1/r)^6$ term accounts for induced dipole - induced dipole interactions. To examine the role of repulsive and

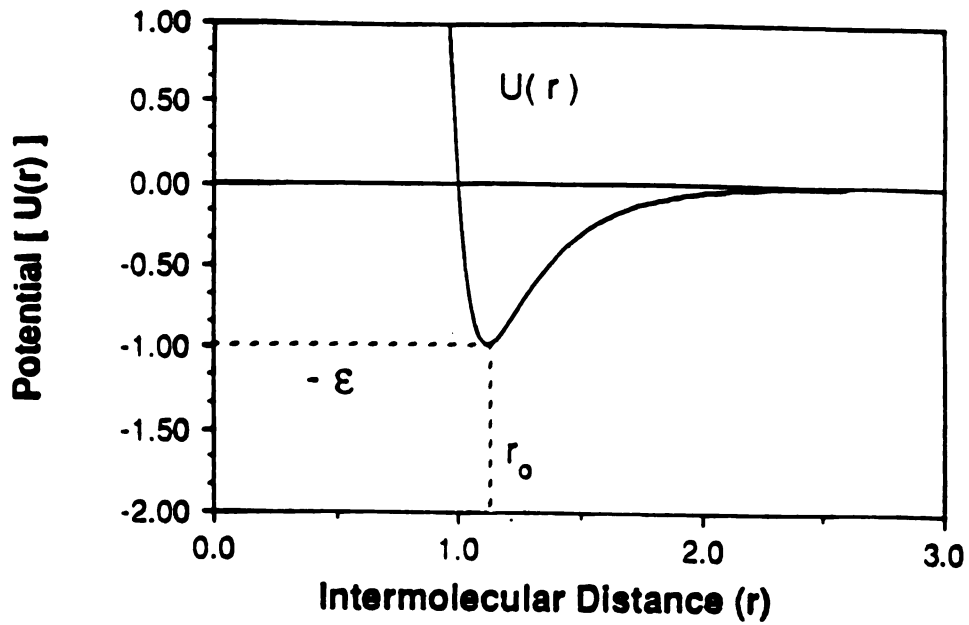
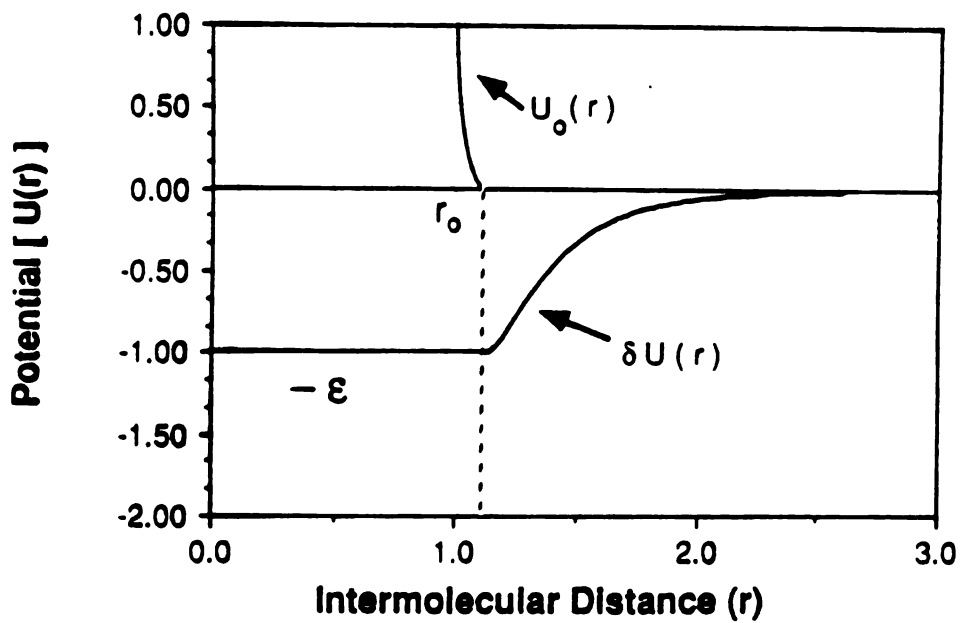


Figure 11. Lennard-Jones potential, $U(r)$. Lower diagram shows repulsive portion of $U(r)$ as determined in WCA theory.



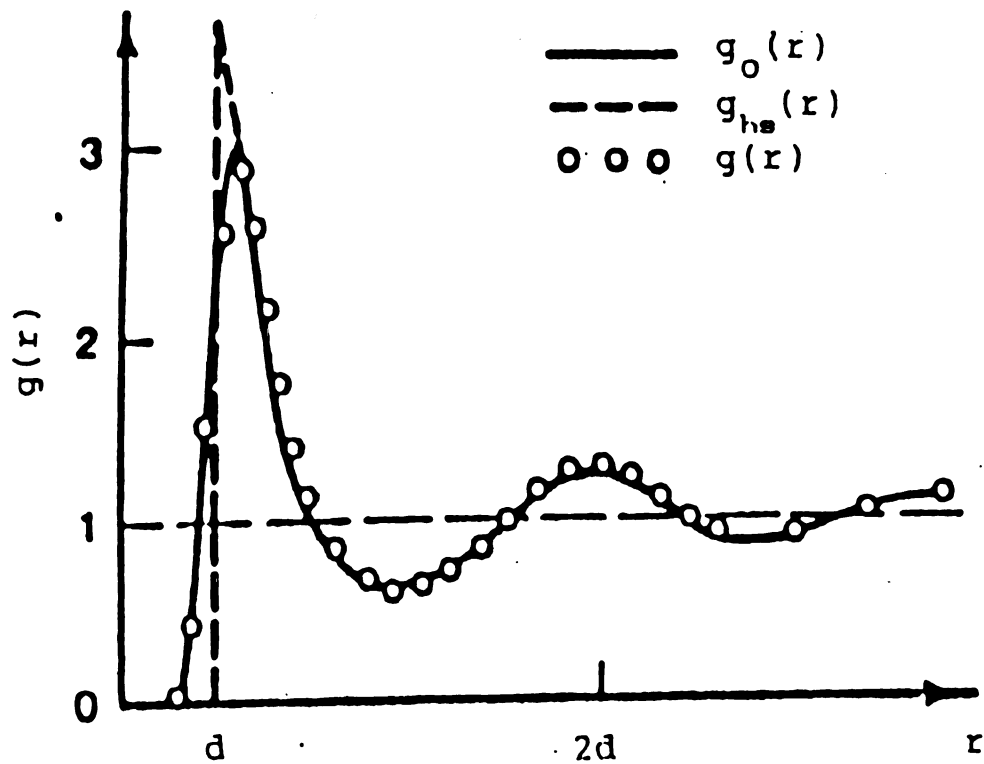


Figure 12. Radial distribution functions for (i) Lennard-Jones fluid $g(r)$, (ii) for repulsive portion of L-J potential $g_0(r)$, (iii) for hard spheres $g_{hs}(r)$.

attractive interactions in determining liquid structure tests were done to compare $g(r)$, the radial distribution function for the full potential $u(r)$, to $g_0(r)$, the radial distribution function that one would obtain from only the repulsive forces (at the same temperature and density). The potential used to determine $g_0(r)$ is (Figure 11):

$$\begin{aligned} u_0(r) &= u(r) + \epsilon & r \leq r_0 \\ u_0(r) &= 0 & r > r_0 \end{aligned} \quad (6.38)$$

In Eq.(6.38) r_0 is the point at which the minimum of $u(r)$ occurs; i.e. $r_0 = 2^{1/6}\sigma$. Figure 12 shows the strong correlation between $g(r)$ and $g_0(r)$ as determined from computer simulations and analytic theory.⁴⁸

To take this experiment one step further it was found that there exists a hard sphere system for which the radial distribution function, $g_{hs}(r)$, is closely related to the actual distribution function, $g(r)$ (Figure 12).⁴⁹ The hard sphere fluid is characterized by the sphere diameter, d , which appears in the hard sphere potential (Figure 11):

$$\begin{aligned} u_{hs} &= \infty & r \leq d \\ u_{hs} &= 0 & r > d \end{aligned} \quad (6.39)$$

The effective hard sphere diameter is chosen to most closely reproduce the structural features of the real fluid.

The fact that the attractive forces play a minor role in

structure was rationalized by Verlet.⁵⁰ In order to understand his argument a few new points must be introduced.

The local particle density is defined as:

$$\rho(\vec{r}) = \sum_{i=1}^N \delta(\vec{r} - \vec{r}_i) \quad , \quad (6.40)$$

where $\delta(x-x_i)$ is the Kronecker delta function. The average density at point \vec{r} is simply $\langle \rho(\vec{r}) \rangle$, which for a homogeneous system is the bulk density, ρ . The Fourier transform of (6.40) is:

$$\begin{aligned} \rho_{\vec{k}} &= \int \exp(-i\vec{k} \cdot \vec{r}) \rho(\vec{r}) d\vec{r} \\ &= \sum_{i=1}^N \exp(-i\vec{k} \cdot \vec{r}_i) \quad , \end{aligned} \quad (6.41)$$

with an autocorrelation function defined as:

$$S(\vec{k}) = \frac{1}{N} \langle \rho_{\vec{k}} \rho_{-\vec{k}} \rangle \quad . \quad (6.42)$$

The function $S(\vec{k})$ is called the static structure factor. For a homogeneous fluid it can be related to the Fourier transform of $g(\vec{r})$ ³⁵:

$$S(\vec{k}) = 1 + \rho \int \exp(-i\vec{k} \cdot \vec{r}) g(\vec{r}) d\vec{r} \quad . \quad (6.43)$$

$S(\vec{k})$ can be experimentally determined from scattering

experiments on the liquid. One can then perform an inverse Fourier transform to determine $g(\vec{r})$.¹⁶

One can show that the limit of $S(\vec{k})$ for $k \rightarrow 0$ is³⁵:

$$S(0) = \rho k T \chi_T = \chi_T / \chi_T^0, \quad (6.44)$$

where χ_T is the isothermal compressibility of the liquid:

$$\chi_T = \frac{1}{\rho} \left(\frac{\partial \rho}{\partial T} \right)_{N, T}, \quad (6.45)$$

and χ_T^0 is the isothermal compressibility for an ideal gas:

$$\chi_T^0 = 1/\rho k T. \quad (6.46)$$

If we apply an external field to the fluid with potential $\phi(\vec{r})$, one can show that this leads to a Fourier transformed density response, $\delta\rho_k$ ³⁵:

$$\delta\rho_k = -S(\vec{k})\phi(\vec{k})\rho/kT, \quad (6.47)$$

where $\phi(\vec{k})$ is the Fourier transform of $\phi(\vec{r})$. Equation (6.47) is a form of the more general fluctuation-dissipation theorem.

Verlet's argument can now be summarized. Equation (6.47) shows that the structure factor determines the density response of a system due to a weak, external field. If the external potential is associated with the potential

of a test particle at the origin, the long-range part of that potential gives rise to a long wavelength response in density. In the long wavelength limit ($k \rightarrow 0$), the response is proportional to $S(0)$ by equation (6.47). By equation (6.44) we see that $S(0)$ is proportional to the compressibility. For typical liquids, the compressibility is very small ($\chi_T / \chi_T^0 \approx 0.02$ near the triple point). Therefore, the density change caused by a long wavelength perturbation is not significant. This phenomenon is referred to as 'repulsive-force screening'.⁵¹ At lower densities, such as in the critical region, the compressibility (and hence $S(0)$) becomes large. This can lead to large density fluctuations. In this regime attractive forces become very important and the van der Waals model is no longer valid.

6.4 Determination of $\Delta\mu_2^*$: 'Hard' and 'Soft' Contributions

The success of the van der Waals model in predicting structure has led to the development of thermodynamic perturbation theories. The idea is to split the excess chemical potential into two parts: a reference term due to the 'hard' repulsive interactions, and a perturbation term due to the 'soft' attractive interactions:

$$\Delta\mu_2^* = \Delta\mu_{\text{hard}} + \Delta\mu_{\text{soft}} \quad (6.48)$$

To treat the 'soft' part of the potential we perform energy

averages using the structural information obtained from the 'hard' part of the potential (this is analogous to quantum mechanical perturbation theory where we compute the expectation value of the energy by employing the wave function of the unperturbed hamiltonian). In this section we shall investigate the validity of equation (6.48).

As we saw in the previous section the intermolecular potential can be written as:

$$u(r) = u_h(r) + u_s(r) \quad , \quad (6.49)$$

where the subscripts h and s refer to the 'hard' and 'soft' parts of the potential. This simple division assumes the solute-solvent pair potential is a function of separation r only. The excess chemical potential is:

$$\Delta\mu_2^* = -kT \ln \langle \exp(-\beta B_o) \rangle = -kT \ln \langle \exp(-\beta B_h - \beta B_s) \rangle \quad , \quad (6.50)$$

where B_h and B_s are the hard and soft contributions to the binding energy of the solute to all the solvent molecules in a specific configuration. If B_h and B_s were independent random variables one could then write:

$$\begin{aligned} \Delta\mu_2^* &= -kT \ln \left[\langle \exp(-\beta B_h) \rangle \langle \exp(-\beta B_s) \rangle \right] \\ &= -kT \ln \langle \exp(-\beta B_h) \rangle - kT \ln \langle \exp(-\beta B_s) \rangle \quad , \quad (6.51) \end{aligned}$$

and therefore $\Delta\mu_2^*$ could be split into two factors. The

point is that B_h and B_s are generally not independent random variables so equation (6.51) is invalid.

A proper interpretation can be obtained by writing the average in equation (6.50) as ¹⁴:

$$\begin{aligned}
 & \langle \exp(-\beta B_h - \beta B_s) \rangle \\
 &= \frac{\int d\vec{r}^M \exp[-\beta U(\vec{r}^M) - \beta B_h] \exp(-\beta B_s)}{\int d\vec{r}^M \exp[-\beta U(\vec{r}^M)]} \\
 &= \frac{\int d\vec{r}^M \exp[-\beta U(\vec{r}^M) - \beta B_h]}{\int d\vec{r}^M \exp[-\beta U(\vec{r}^M)]} \frac{\int d\vec{r}^M \exp[-\beta U(\vec{r}^M) - \beta B_h] \exp(-\beta B_s)}{\int d\vec{r}^M \exp[-\beta U(\vec{r}^M) - \beta B_h]} \\
 &= \langle \exp(-\beta B_h) \rangle \langle \exp(-\beta B_s) \rangle_h \quad . \quad (6.52)
 \end{aligned}$$

where the subscript h on the second average refers to a conditional average. This means the second average is taken assuming that a hard solute particle already exists in the liquid. The excess chemical potential is then:

$$\begin{aligned}
 \Delta\mu_2^* &= -kT \ln \langle \exp(-\beta B_h) \rangle - kT \ln \langle \exp(-\beta B_s) \rangle_h \\
 &= \Delta\mu_h^* + \Delta\mu_{s/h}^* \quad . \quad (6.53)
 \end{aligned}$$

The first term, $\Delta\mu_h^*$, is the free energy to add a single, hard solute molecule at a fixed position. The second term $\Delta\mu_{s/h}^*$ is the conditional free energy to couple the soft part of the solute-solvent interaction given that the hard part of the potential has already been coupled. This is perhaps

better understood using the coupling parameter approach. As we saw earlier the excess chemical potential can be found by utilizing a coupling parameter to turn on the potential and essentially grow the particle in the liquid. Since this process is carried out reversibly it does not matter what path we take to couple the particle. One possible way is to turn on the hard part of the potential first and then turn on the soft part, this is exactly what we have done in equation (6.53). (As you may have guessed one could just as well perform the calculation in the opposite order and couple the attractive forces first and then calculate the conditional averages for the repulsive potential.)

The idea of breaking up the solvation process has been utilized by many researchers in developing simple models to predict solubility. The solvation process is normally modeled by the following physical process: (1) One makes in the solvent a cavity just large enough to fit a solute molecule. The free energy associated with this process is called g_{cav} . For this part of the process the solute is considered to be a hard sphere. (2) One now allows the solvent and solute to interact with the soft potential; the associated free energy is g_{int} ^{52,53}:

$$\Delta\mu_2^* = g_{cav} + g_{int} \quad (6.54)$$

From our previous discussion it is obvious that the cavity free energy is equivalent to $\Delta\mu_h^*$ and the interaction free

energy is equivalent to $\Delta\mu_{e/h}^*$.

Equation (6.54) provides the basis for most successful analytic theories to date on solubility (the term successful implies both accuracy and flexibility). We shall now adopt a model, due to Reiss et al.⁵⁴ and Pierroti,⁵⁵ in order to analyze our data. The primary assumption made by these authors is: Since there is no analytic expression for g_{cav} in a real liquid one exploits the van der Waals model and calculates g_{cav} for an effective hard sphere system whose radii are chosen to best reproduce features of the pure solute and solvent. Although our solute (Xe) qualifies as spherical, the organic solvents certainly are not. One must regard this approximation as, in some sense, averaging over spatial configurations of the solvent.

If we combine our experimental expression for $\Delta\mu_2^*$ with equation (6.54) we have:

$$\Delta\mu_2^* = -RT\ln L = g_{cav} + g_{int} \quad (6.54a)$$

Equation (6.54a) can be interpreted in thermodynamic as well as in statistical mechanical terms. If one calls v_2 the partial molar volume of solute atoms in the solvent, v_2^g the molar volume of solute gas, and ϕ_2 the volume fraction of solution occupied by solute, then we have $L = (\phi_2 v_2^g / v_2)$.

Substituting for L in equation (6.54a) gives:

$$g_{cav} + g_{int} + RT\ln\phi_2 - RT\ln(v_2/v_2^g) = 0 \quad (6.54b)$$

Equation (6.54b) has the following thermodynamic interpretation ³: The free energy for transferring at equilibrium one mole of solute gas into the solution is the zero sum of four terms. The first two terms are for the physical process already described. The third term may be interpreted as the free energy change associated with the entropy of mixing $-R \ln \phi_2$ (entropy increase, free energy decrease) in a real solution. Finally the fourth term is the free energy required for isothermal and reversible compression of the solute from its volume in the gas to its volume in solution (entropy decrease, free energy increase).

The idea that entropy of mixing depends on volume fraction in real solutions is supported by the work of Flory,⁵⁶ Huggins,⁵⁷ and Longuet-Higgins.⁵⁸

6.5 The Scaled Particle Theory for Hard Spheres

We now must calculate the free energy for introducing a hard sphere solute with diameter a_2 into a hard sphere fluid with solvent diameter a_1 . At present there exists no exact theory even for this simple system, although it can be solved numerically⁵⁹. However the scaled particle theory (SPT) has proven to be a very good approximation. Details of this theory are quite lengthy (see refs 60,61) so only a brief outline will be given below.

The basic idea of the SPT is to calculate the reversible work to produce a cavity at fixed position in a fluid of hard spheres. A cavity is defined as a sphere of radius, r , from which the centers of all fluid particles are excluded. It is apparent from Figure 13 that a cavity of radius, r , in a fluid of spheres of diameter, a_1 , is produced by the introduction of a hard spherical solute of diameter, a_2 , such that:

$$r = \frac{a_1 + a_2}{2} \quad (6.55)$$

The equivalence of these two processes allows us to conclude that the free energy to create a cavity in the fluid is the same as that to introduce an appropriately chosen hard sphere solute.

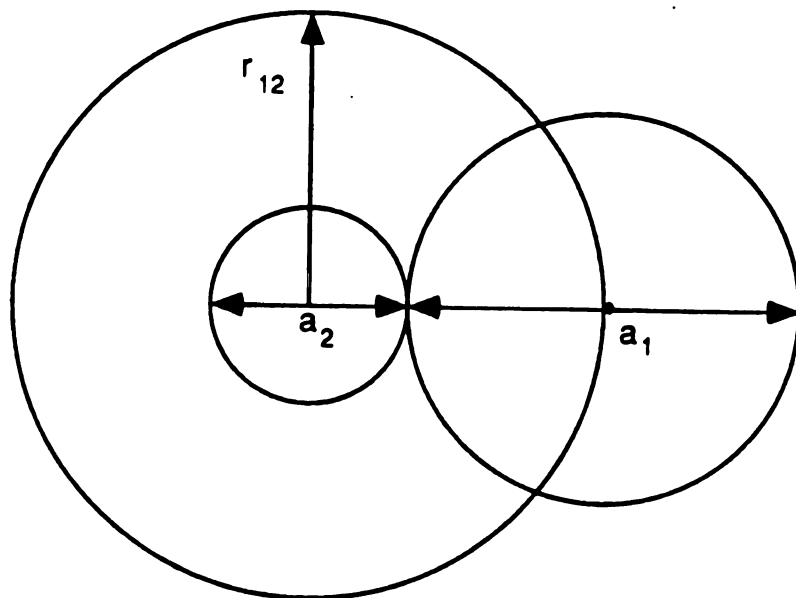


Figure 13. Definition of a cavity in the SPT.

We can see from Figure 13 that for $r=a_1/2$ the diameter of the solute molecule goes to zero. Thus, a cavity with $r = a_1/2$ corresponds to a point solute. If the cavity is smaller than $a_1/2$ only one solvent center can occupy it at any time. The corresponding probability of finding the center of a molecule in the cavity is:

$$p_1(r) = \frac{4}{3} \pi r^3 \rho \quad , \quad r \leq a_1/2 \quad (6.56)$$

where ρ is the number density concentration of solvent molecules. The probability that the cavity is empty is therefore:

$$p_0(r) = 1 - p_1(r) = 1 - \frac{4}{3} \pi r^3 \rho \quad , \quad r \leq a_1/2 \quad (6.57)$$

The reversible work theorem is a general theorem of statistical mechanics which states that the probability of observing a fluctuation in a system is equal to the reversible work required to produce the fluctuation divided by kT .⁶² Thus the probability of finding in the solvent a cavity of radius r that is empty is:

$$p_0(r) = \exp(-W(r)/kT) \quad . \quad (6.58)$$

Since we imagine a process of emptying the cavity at constant N, V, T , we may identify $W(r)$ may with the change in Helmholtz free energy for the process and write:

$$p_0(r) = \exp(-\Delta A(r)/kT) \quad . \quad (6.59)$$

Substituting (6.57) in (6.59) we find:

$$\Delta A(r) = -kT \ln \left(1 - \frac{4}{3} \pi r^3 \rho \right) \quad . \quad r \leq a_1/2 \quad (6.60)$$

In the limit of a macroscopic cavity the free energy is just the thermodynamic work of compression:

$$\Delta A(r) = PV = P \frac{4}{3} \pi r^3 \quad , \quad r \gg a_1 \quad (6.61)$$

where P is the macroscopic pressure in the liquid. We now have two exact results for the cavity free energy. In order to bridge the gap between these two limits we introduce a new function, $p_0(r+dr)$, the probability that a cavity of radius $r+dr$ is found empty. This may be written as:

$$p_0(r+dr) = p_0(r)p_0(dr/r) \quad , \quad (6.62)$$

where $p_0(r)$ was defined earlier and $p_0(dr/r)$ is the conditional probability that a spherical shell of width dr will be empty given that the sphere of radius r already is empty.

If we expand $p_0(r+dr)$ to first order in dr , we obtain:

$$p_o(r+dr) = p_o(r) + \frac{dp_o(r)}{dr} dr \quad . \quad (6.63)$$

Equating (6.62) with (6.63) gives:

$$\begin{aligned} p_o(r)p_o(dr/r) &= p_o(r) + \frac{dp_o(r)}{dr} dr \\ p_o(dr/r) - 1 &= \frac{d \ln p_o(r)}{dr} dr \quad . \end{aligned} \quad (6.65)$$

We now introduce the auxiliary function, $G(r)$, defined by:

$$\rho 4\pi r^2 G(r) dr = 1 - p_o(dr/r) \quad . \quad (6.66)$$

Substituting into (6.65) we have:

$$\frac{d \ln p_o(r)}{dr} = -\rho 4\pi r^2 G(r) \quad , \quad (6.67)$$

which upon integration, yields:

$$\ln p_o(r) - \ln p_o(r=0) = -\rho \int_0^r 4\pi \lambda^2 G(\lambda) d\lambda \quad . \quad (6.68)$$

Since $p_o(0) = 1$, equation (6.68) reduces to:

$$\ln p_o(r) = -\rho \int_0^r 4\pi \lambda^2 G(\lambda) d\lambda \quad , \quad (6.69)$$

or, using equation (6.59):

$$\Delta A(r) = kT\rho \int_0^r 4\pi\lambda^2 G(\lambda) d\lambda \quad . \quad (6.70)$$

The work required to create a cavity of radius, r , is a scaling process, in that we build up the cavity from $\lambda=0$ to $\lambda=r$. This is the same as building up a hard sphere particle at a fixed position in the fluid, hence the name Scaled Particle Theory.

To find $\Delta A(r)$ Reiss et al⁶⁰ used statistical considerations to suggest a simple analytic form for $G(r)$:

$$G(r) = A + (B/r) + (C/r^2) \quad . \quad (6.71)$$

The coefficients A , B , C , are determined by using the limiting forms of $G(r)$:

$$\begin{aligned} G(r) &= (1 - \frac{4}{3} \pi r^3 \rho)^{-1} & r \leq a_1/2 \\ G(r) &= P/kT\rho & r \gg a_1 \end{aligned} \quad , \quad (6.72)$$

along with the assumption that $\Delta A(r)$ and its first two radial derivatives are continuous at $a_1/2$. The result is:

$$\Delta A(r) = K_0 + K_1 r + K_2 r^2 + K_3 r^3 \quad ,$$

in which the coefficients are:

$$\begin{aligned}
K_0 &= kT\{ -\ell n(1-y) + \frac{9}{2} [y/(1-y)]^2 \} - (\pi P a_1^3/6) \\
K_1 &= -(kT/a_1)\{ [6y/(1-y)] + 18[y/(1-y)]^2 \} + \pi P a_1^2 \\
K_2 &= (kT/a_1^2)\{ [12y/(1-y)] + 18[y/(1-y)]^2 \} - 2\pi P a_1 \\
K_3 &= \frac{4}{3} \pi P \quad . \quad (6.73)
\end{aligned}$$

In Eq. (6.73), $y = \pi a_1^3 \rho / 6$, is called the packing fraction of the hard sphere solvent (it is the fraction of space occupied by the fluid). The solvation free energy, $\Delta A(r)$, is for a constant T,V,N system, however this is the same as the Gibbs free energy in a T,P,N system provided the average volume $\langle V \rangle$ in the latter is equal to the exact volume V in the former system.¹⁴ We can therefore equate $\Delta A(r)$ with the cavity energy, g_{cav} , defined in the previous section. Figure 14 shows g_{cav}/kT as a function of the reduced cavity radius $R' = a_{12}/a_2$ for a hard sphere solvent with packing fraction $y = 0.5$. The open circles are those described by equation (6.73) while the closed circles are described by the exact relation (6.60). The cavity free energy increases monotonically as a function of cavity radius and is always positive.

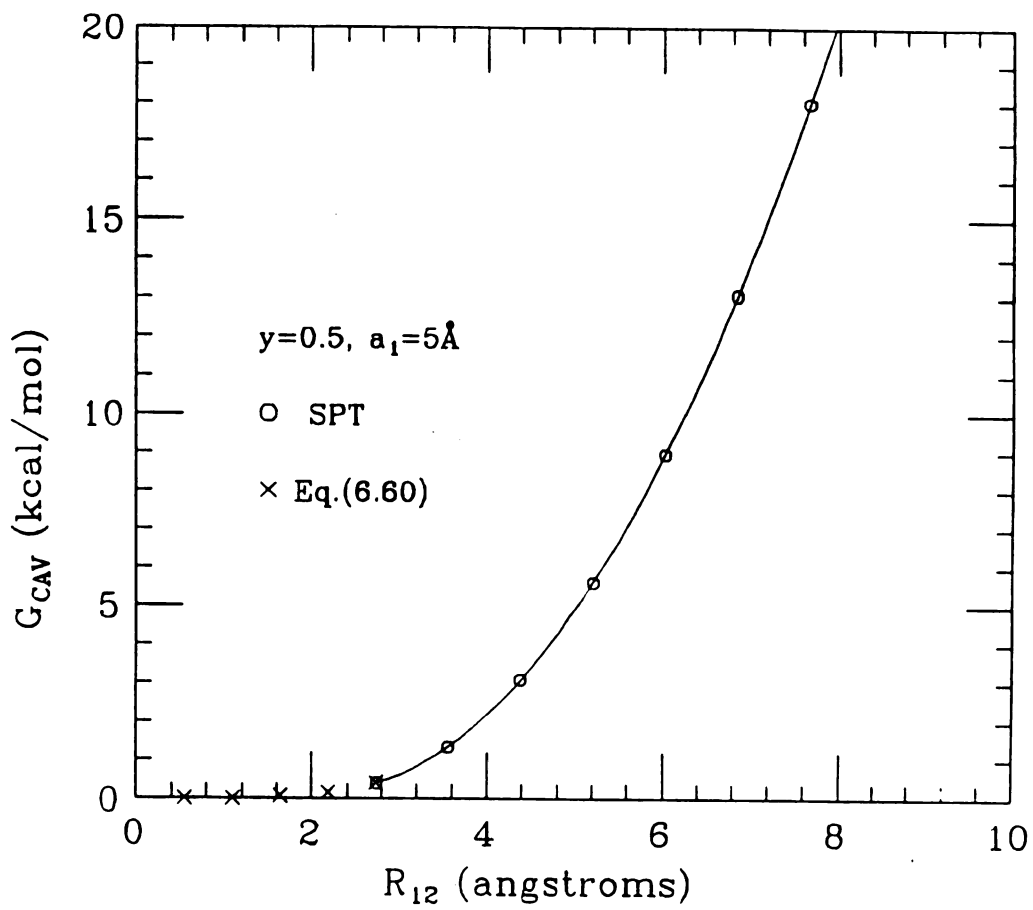


Figure 14. $g_{cav}(R_{12})/kT$ vs cavity radius R_{12} .

To summarize, the free energy required to create a cavity large enough to accommodate a hard sphere of diameter a_2 in a hard sphere fluid with particle diameter a_1 and number density ρ_1 is, by rearranging terms in Eq. (6.73):

$$g_{\text{cav}} = kT \left\{ [6y/(1-y)] [2(r_{12}/a_1)^2 - (r_{12}/a_1)] \right. \\ \left. + [18y^2/(1-y)^2] [(r_{12}/a_1)^2 - (r_{12}/a_1) + 1/4] - \ln(1-y) \right\} \\ + \pi \rho_1 a^3 \left[\frac{4}{3} (r_{12}/a_1)^3 - 2(r_{12}/a_1) + (r_{12}/a_1) - \frac{1}{6} \right] \quad , \quad (6.74)$$

with $r_{12} = (a_1 + a_2)/2$, and $y = \pi a_1^3 \rho_1 / 6$. The total excess chemical potential is defined by equation (6.54):

$$\Delta\mu_2^* = g_{\text{cav}} + g_{\text{int}} \quad . \quad (6.54)$$

An aside for experts: The SPT also leads to an equation of state for the hard sphere fluid which is exact up to the third virial coefficient, which agrees over the entire range of fluid density with the equations of state obtained through machine computation, and which is identical to the equation of state obtained by exact solution of the Percus-Yevick equation.^{63,35}

6.6 Application to Real Liquids

The SPT is extended to the study of real liquids by: (a) using the actual liquid density of the solvent and (b) using

a simple model and the heat of vaporization to determine the optimal hard sphere diameter a_1 of the solvent. This model essentially examines the solvation process for the solvent in its own liquid. The excess chemical potential per mole for a single component gas-liquid system is given by equation (3.5):

$$\Delta\mu^* = -RT \ln (\rho_\ell / \rho_g) ,$$

where ρ_ℓ and ρ_g are the molar densities of the liquid and gas respectively. Assuming the gas phase is ideal, we have:

$$\Delta\mu^* = -RT \ln (\rho_\ell RT / P_g) , \quad (6.75)$$

where P_g is the vapor pressure of the liquid. We now apply our model to this system and equate the excess chemical potential to that of cavity formation plus attractive interaction:

$$\Delta\mu^* = -RT \ln (\rho_\ell RT / P_g) = g_{cav} + g_{int} . \quad (6.76)$$

It follows from equation (6.76) that:

$$\Delta\bar{h}^* = h_{cav} + h_{int}, \quad \Delta\bar{s}^* = s_{cav} + s_{int} . \quad (6.77)$$

The excess molar enthalpy, $\Delta\bar{h}^*$, can be related to the molar heat of vaporization, ΔH_v as follows:

$$\begin{aligned}
 -\Delta H_v (1 - P v_\ell / RT) &= \Delta \bar{h}^* + RT - RT^2 \alpha_\ell \\
 &= h_{cav} + h_{int} - RT + RT^2 \alpha_\ell \cong -\Delta H_v
 \end{aligned}
 \tag{6.78}$$

where the heat of vaporization is defined as, $\Delta H_v = (H_{gas} - H_{liquid})$, α_ℓ is the coefficient of thermal expansion for the pure liquid, and v_ℓ is the molar volume of the liquid. We assume, as usual, that $P v_\ell / RT \ll 1$, so we can neglect it (see appendix # for a detailed derivation of 6.78).

We shall now look at the interaction term. The molar energy of vaporization of a normal liquid is approximately given by:^{36,64}

$$\Delta U_v \cong -2\pi N_A \rho \int_0^\infty u(r) g(r) r^2 dr ,
 \tag{6.79}$$

where $u(r)$ is the pairwise additive intermolecular potential, $g(r)$ is the radial distribution function (see Eq.(6.31)), and N_A is Avogadro's number. On the other hand, the molar energy of interaction can be derived from equation (6.33):

$$u_{int} = 4\pi N_A \rho \int_0^\infty u(r) g(r) r^2 dr .
 \tag{6.80}$$

Hence, it follows that for such a liquid:

$$\Delta U_v = -u_{int} / 2 .
 \tag{6.81}$$

Now we invoke the thermodynamic relation:

$$H = E + PV = K + U + PV \quad , \quad (6.82)$$

where E is the total internal energy, and K is the kinetic energy. We may then reexpress the heat of vaporization as:

$$\begin{aligned} \Delta H_v = H_g - H_\ell &= (K_g - K_\ell) + (U_g - U_\ell) + P(V_g - V_\ell) \\ &\approx RT + \Delta U_v \quad . \end{aligned} \quad (6.83)$$

We have assumed that $V_g \gg V_\ell$, $K_g \approx K_\ell$, and the gas is ideal. Plugging (6.81) in (6.83) we find:

$$h_{int} = 2RT - 2\Delta H_v \quad . \quad (6.84)$$

Once again we use the fact that, in a liquid, the PV term is negligible, hence $u_{int} = h_{int}$.

Finally, by introducing equation (6.84) into (6.78) we get the following relation for the standard molar enthalpy of vaporization:

$$\Delta H_v = h_{cav} + \alpha_\ell RT^2 + RT \quad . \quad (6.85)$$

This is a general equation which should be satisfied by any theory which predicts cavity terms. Now we can use this to determine the effective hard sphere diameter in the SPT. The enthalpy of cavity formation is found using standard

thermodynamics: i.e. $h_{\text{cav}} = -T^2(\partial(g_{\text{cav}}/T)/\partial T)_P$ ⁵⁵:

$$h_{\text{cav}} = \alpha_{\ell} RT^2 (y/z) [(6/z) + (9y/z^2) + 1] , \quad (6.86)$$

where $z=(1-y)$, y is the packing fraction, and α_{ℓ} is the thermal expansivity of the liquid. We have also assumed that $(1/v)(\partial v/\partial T) = -(1/y)(\partial y/\partial T)$. Putting this result in (6.85) we find, finally:

$$\Delta H_v = RT + \alpha_{\ell} RT^2 \left(\frac{(1+2y)^2}{(1-y)^3} \right) . \quad (6.87)$$

The SPT is related to real fluids by using the heat of vaporization, density, and thermal expansivity to find an effective hard sphere diameter for the fluid. It is by no means a first principles theory since it uses the experimentally measured values for these variables (there is no theory to date that can predict the density of even atomic liquids let alone molecular liquids). However, the SPT is consistent with our current goal of being able to predict solubility by knowing only bulk properties of the solute and solvent. Other techniques exist to determine the effective hard sphere diameter of the solvent, a_1 , but they require a detailed knowledge of the intermolecular potential and lots of computer simulation (or very simple molecular structure).^{43,49} This option was not presently available to us.

6.7 Evaluation of the Cavity Term:

Table IV lists the heat of vaporization, number density, and thermal expansivity for each of the solvents studied. Since our experiments were generally done in a range of 5-50°C we have chosen an intermediate temperature of 25.0°C to evaluate a_1 . In theory, a_1 should be temperature independent. In order to evaluate the number density we require the mass density^{29,30,65} and the molecular weight, i.e.; $\rho_M(\text{mol/cm}^3) = \rho_M(\text{g/cm}^3)/\text{M.W.}(\text{g/mol})$.

Table V and Figure 15 show the calculated values of a_1 for the solvents at 25.0°C, we have not included nonadecane, eicosane, dodecanol, and tetradecanol because they are normally solids at this temperature. The values of a_1 were calculated from solving equation (6.87) for y and using the known density to solve for a_1 by the relation; $a_1 = (6y/\pi\rho_1)^{1/3}$. The points on Figure 15 vary monotonically in each homologous series with number of carbons but they bear no simple relation to actual chain lengths. In alkanes, for example, the C-C bond length is about 1.5Å. Of the hydrocarbon solvents we studied, the more polar molecules tend to have a larger effective radius than their nonpolar analogues. One can obtain values of a_1 other ways besides the one we use here. For example, one can use gas viscosity,^{66,67} or second virial coefficient data.^{68,69} However, for all but a few of the short alkanes (and for those molecules the agreement with our values of a_1 is

good⁵⁵) the results are limited by lack of available data.

In order to evaluate g_{cav} we use Eq. (6.74). For the cavity radius we have $r_{12} = (a_1 + a_2) / 2$. For Xe we took the hard core molecular diameter to be $a_2 = 3.973\text{\AA}$; this is the potential parameter σ (or $2^{1/6} r_0$) in the Lennard-Jones (6-12) potential for Xe.⁷³

The calculated values of g_{cav} are in Table V and Figure 16a. All the values of g_{cav} are positive and range from 2.5 to 9.4 kcal/mole. This shows that for a hard sphere fluid it always takes a positive amount of work to make a cavity. The fact that g_{cav} is positive means that its contribution will always tend to lower solubility ($L = e^{-\Delta\mu/RT}$), therefore, systems with low solubility are dominated by repulsive interactions (as intuitively expected). In contrast, the experimental quantities $\Delta\mu_2^*$ for these solvents, with the exception of formic acid, are negative and in the range from about -0.4 to -1.0 kcal/mole. Since, by equation (6.54), $\Delta\mu_2^*$ is just the sum of g_{cav} and g_{int} these results imply that g_{int} must be negative and its magnitude must be a few to several kcal/mole. This isn't surprising since one would

Table IV. Heat of Vaporization, number density, and thermal expansivity for organic solvents at 25.0°C.

alkanes

n-C	$\Delta H_v \left(\frac{\text{kcal}}{\text{mole}} \right)$	$\rho_n \left(\times 10^{21} / \text{cc} \right)$	$\alpha_f \left(10^{-3} / \text{C} \right)$
5	6.39	5.19	1.558
6	7.54	4.5788	1.368
7	8.74	4.0852	1.266
8	9.92	3.6851	1.183
9	11.10	3.3535	1.114
10	12.28	3.0740	1.071
11	13.46	2.8399	0.9704
12	14.64	2.6378	0.9417
13	15.83	2.4613	0.9432
14	17.01	2.3083	0.9300
15	18.20	2.1706	0.9097
16	19.22	2.0524	0.8986
17	20.6	1.9409	0.879
18	21.7	1.8434	0.8661

cycloalkanes

n-C	$\Delta H_v \left(\frac{\text{kcal}}{\text{mole}} \right)$	$\rho_n \left(\times 10^{21} / \text{cc} \right)$	$\alpha_f \left(10^{-3} / \text{C} \right)$
5	6.85	6.1644	1.3298
6	7.90	5.5400	1.2475
8	10.36	4.4702	0.98805

Table IV. cont.....

alkanols

n-C	ΔH_v ($\frac{\text{kcal}}{\text{mole}}$)	ρ_n ($\times 10^3 / \text{cc}$)	α_f ($10^{-3} / \text{C}$)
1	8.94	14.79	1.189
2	10.18	10.267	1.093
3	11.51	8.0178	1.006
4	12.50	6.5509	0.9265
5	13.61	5.5443	0.8804
6	15.00	4.8128	0.8720
7	16.20	4.2446	0.8828
8	17.00	3.8043	0.8491
9	18.60	3.4444	0.7875
10	19.82	3.1453	0.8283
11	21.00	2.8988	0.8105

carboxylic acids

n-C	ΔH_v ($\frac{\text{kcal}}{\text{mole}}$)	ρ_n ($\times 10^3 / \text{cc}$)	α_f ($10^{-3} / \text{C}$)
1	11.03	15.891	1.0249
2	12.49	10.475	1.0114
3	13.7	8.0341	1.0974
4	15.20	6.5163	1.0693
5	16.56	5.5117	0.99941
7	18.1	4.2244	0.91035

Table IV. cont.....

alkanals (aldehydes)

n-C	$\Delta H_v \left(\frac{\text{kcal}}{\text{mole}} \right)$	$\rho_n \left(\times 10^{21} / \text{cc} \right)$	$\alpha_f \left(10^{-3} / \text{c} \right)$
3	7.09	8.2083	1.4619
4	8.05	6.6543	1.3084
5	9.17	5.6298	1.2474
7	11.40	4.2907	1.0333

perfluoroalkanes

n-C	$\Delta H_v \left(\frac{\text{kcal}}{\text{mole}} \right)$	$\rho_n \left(\times 10^{21} / \text{cc} \right)$	$\alpha_f \left(10^{-3} / \text{c} \right)$
6	7.606	2.9844	1.6698
7	8.69	2.6978	1.5047
8	9.77	2.4216	1.4119

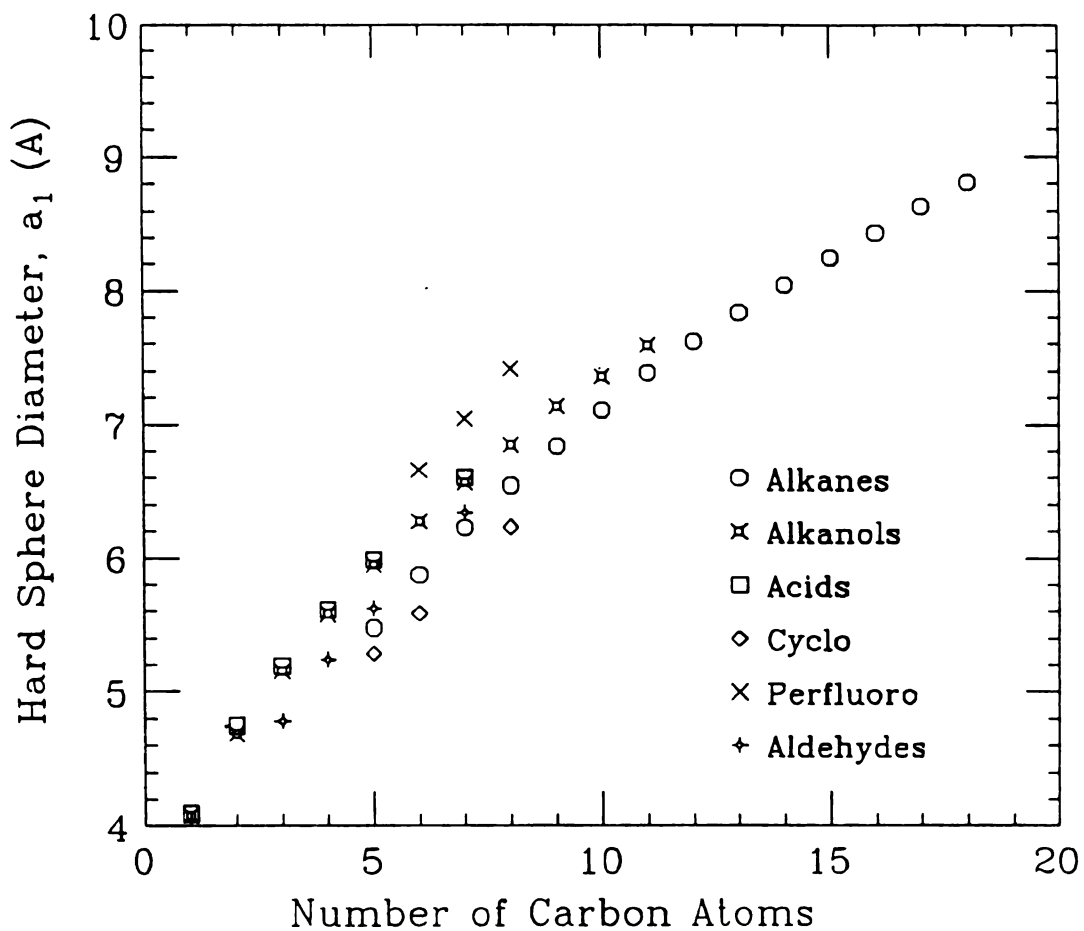


Figure 15 Effective hard sphere diameter for 45 organic solvents vs number of carbon atoms.

Table V. SPT calculations for organic solvents. The second column is the effective hard sphere radius. The third column is the packing fraction. The fourth is the cavity free energy for ^{133}Xe .

alkanes

n-C	a_1 (Å)	γ	g_{cav} (cal/mol)
5	5.476	0.44614	3052
6	5.877	0.48656	3396
7	6.226	0.51611	3645
8	6.543	0.54055	3861
9	6.838	0.56143	4052
10	7.108	0.57791	4191
11	7.386	0.59925	4463
12	7.623	0.61176	4577
13	7.836	0.62006	4613
14	8.044	0.62914	4682
15	8.251	0.63838	4765
16	8.436	0.64516	4805
17	8.635	0.65423	4907
18	8.813	0.66075	4958

cycloalkanes

n-C	a_1 (Å)	γ	g_{cav} (cal/mol)
5	5.286	0.47681	3766
6	5.582	0.50450	4019
8	6.233	0.56678	4775

Table V. cont....

alkanols

n-C	a_1 (Å)	γ	g_{cav} (cal/mol)
1	4.082	0.52668	7366
2	4.686	0.55305	6854
3	5.156	0.57554	6703
4	5.580	0.59588	6667
5	5.948	0.61083	6595
6	6.274	0.62238	6508
7	6.567	0.62929	6327
8	6.843	0.63822	6274
9	7.134	0.65467	6521
10	7.358	0.65612	6279
11	7.591	0.66382	6289

carboxylic acids

n-C	a_1 (Å)	γ	g_{cav} (cal/mol)
1	4.092	0.57015	9429
2	4.746	0.58623	8143
3	5.189	0.58790	7131
4	5.610	0.60244	6872
5	5.986	0.61891	6854
7	6.606	0.63774	6601

Table V. cont....

alkanals (aldehydes)

n-C	a_1 (Å)	γ	g_{cav} (cal/mol)
3	4.780	0.46945	4210
4	5.239	0.50109	4337
5	5.623	0.52417	4414
7	6.342	0.57316	4821

perfluoroalkanes

n-C	a_1 (Å)	γ	g_{cav} (cal/mol)
6	6.662	0.46209	2520
7	7.045	0.49389	2740
8	7.417	0.51733	2876

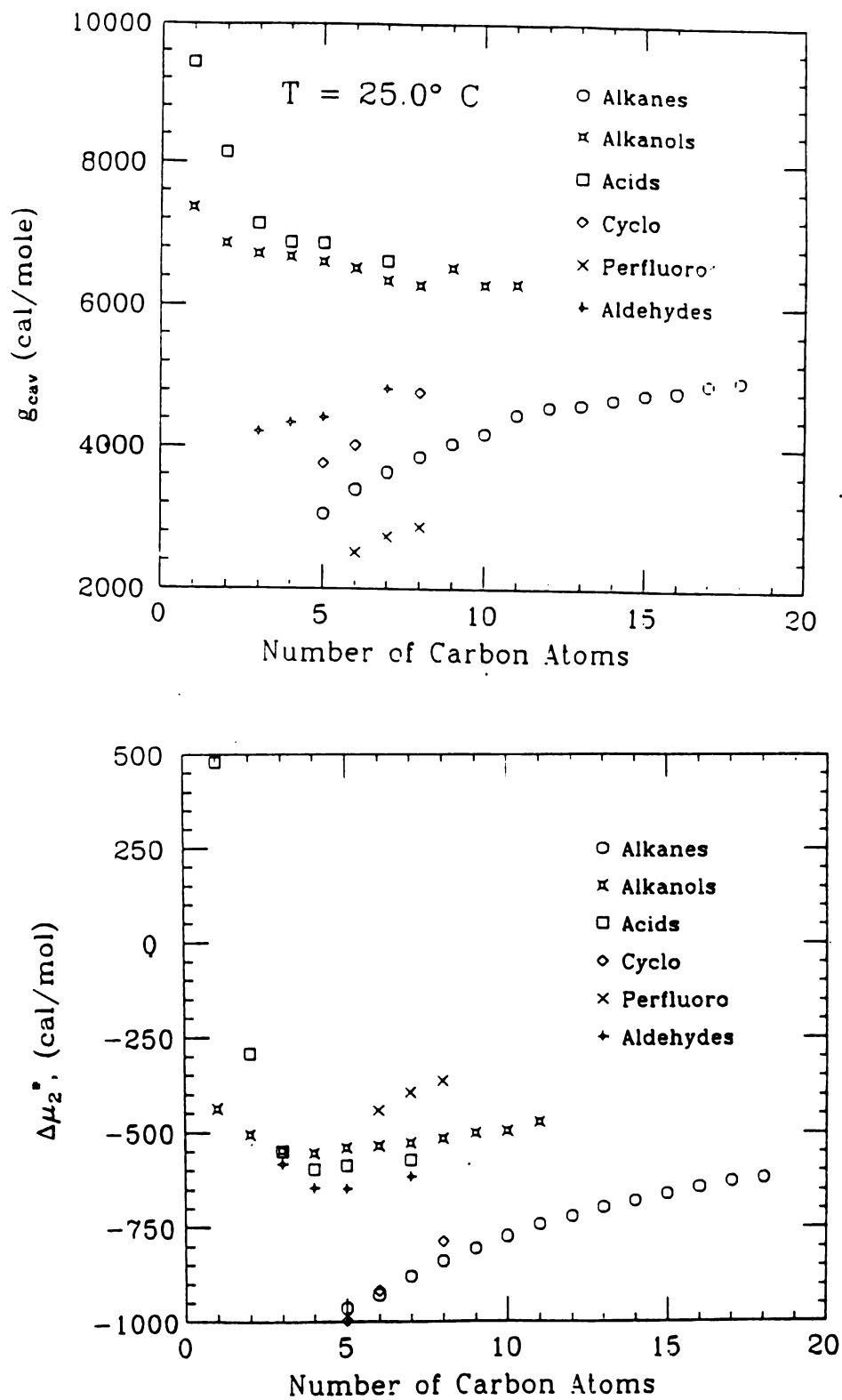


Figure 16. (a) g_{cav} for Xe in 45 organic solvents at 25.0°C. (b) corresponding excess chemical potential, $\Delta\mu_2^* = -RT \ln L$.

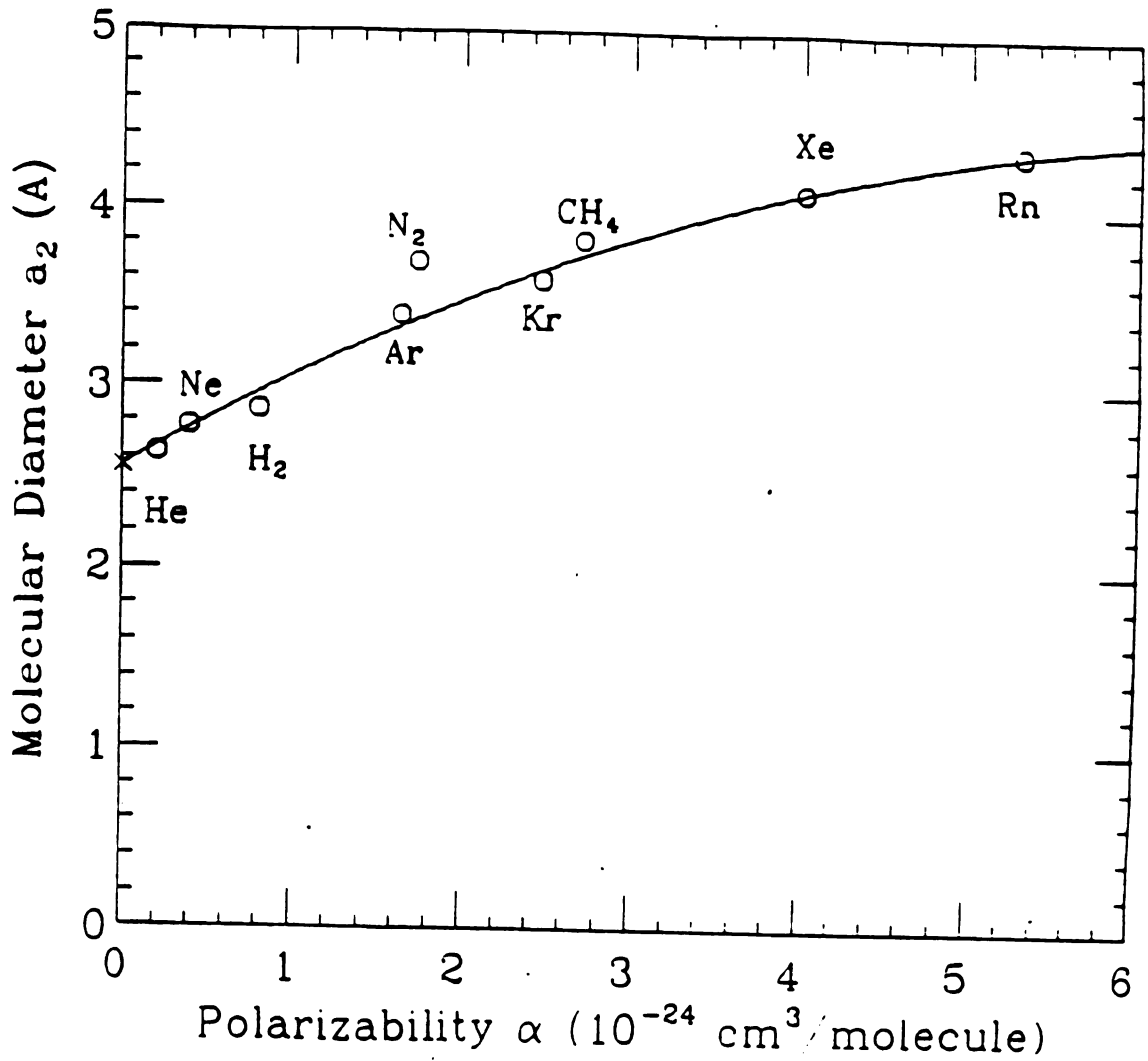


Figure 17. Molecular diameter vs polarizability for several inert gas solutes. Solid line shows extrapolation for noble gases.

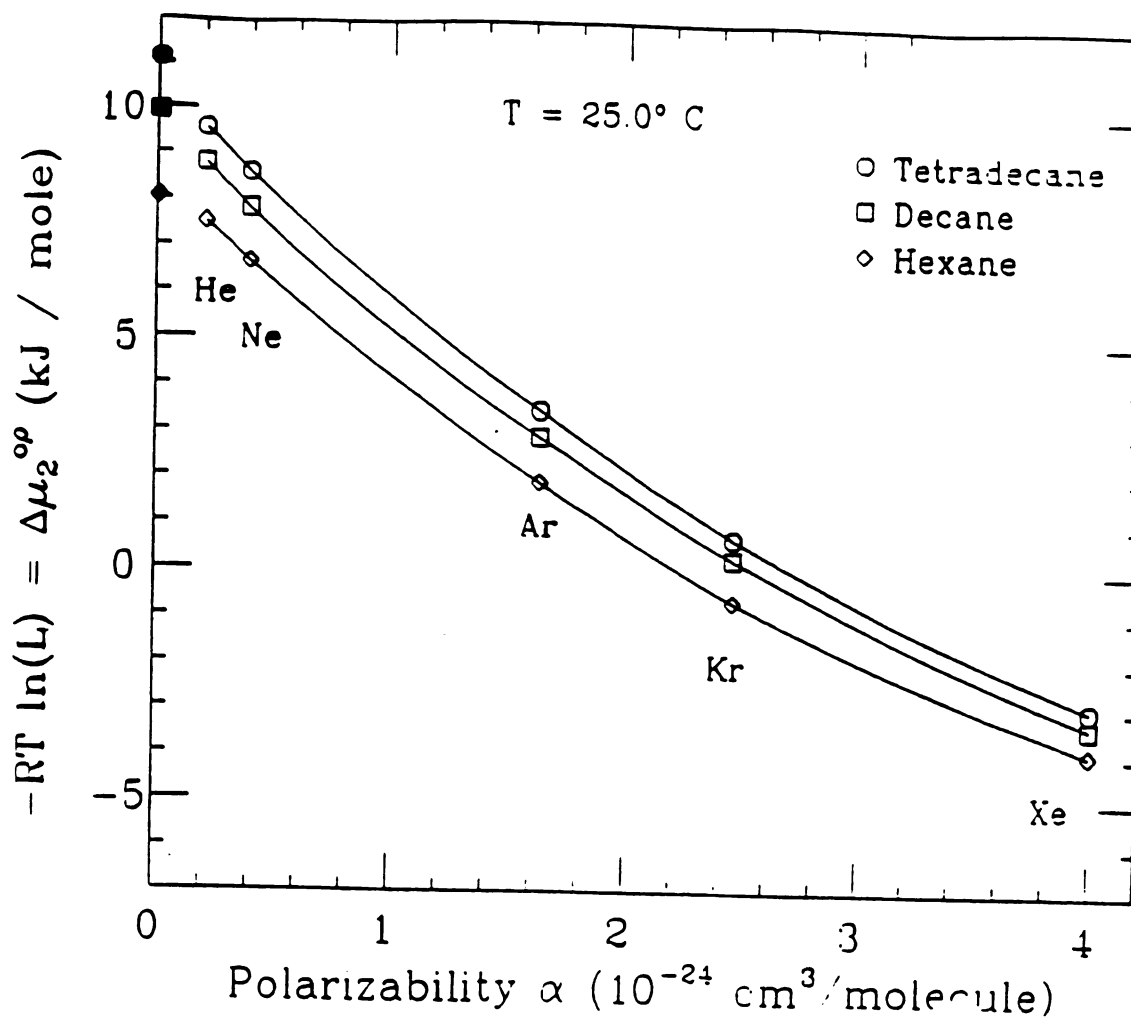


Figure 18. Excess chemical potential vs solute polarizability for noble gases in Tetradecane, Decane, and Hexane. Filled in points along ordinate are the SPT predicted values for a hard sphere solute of 2.58Å.

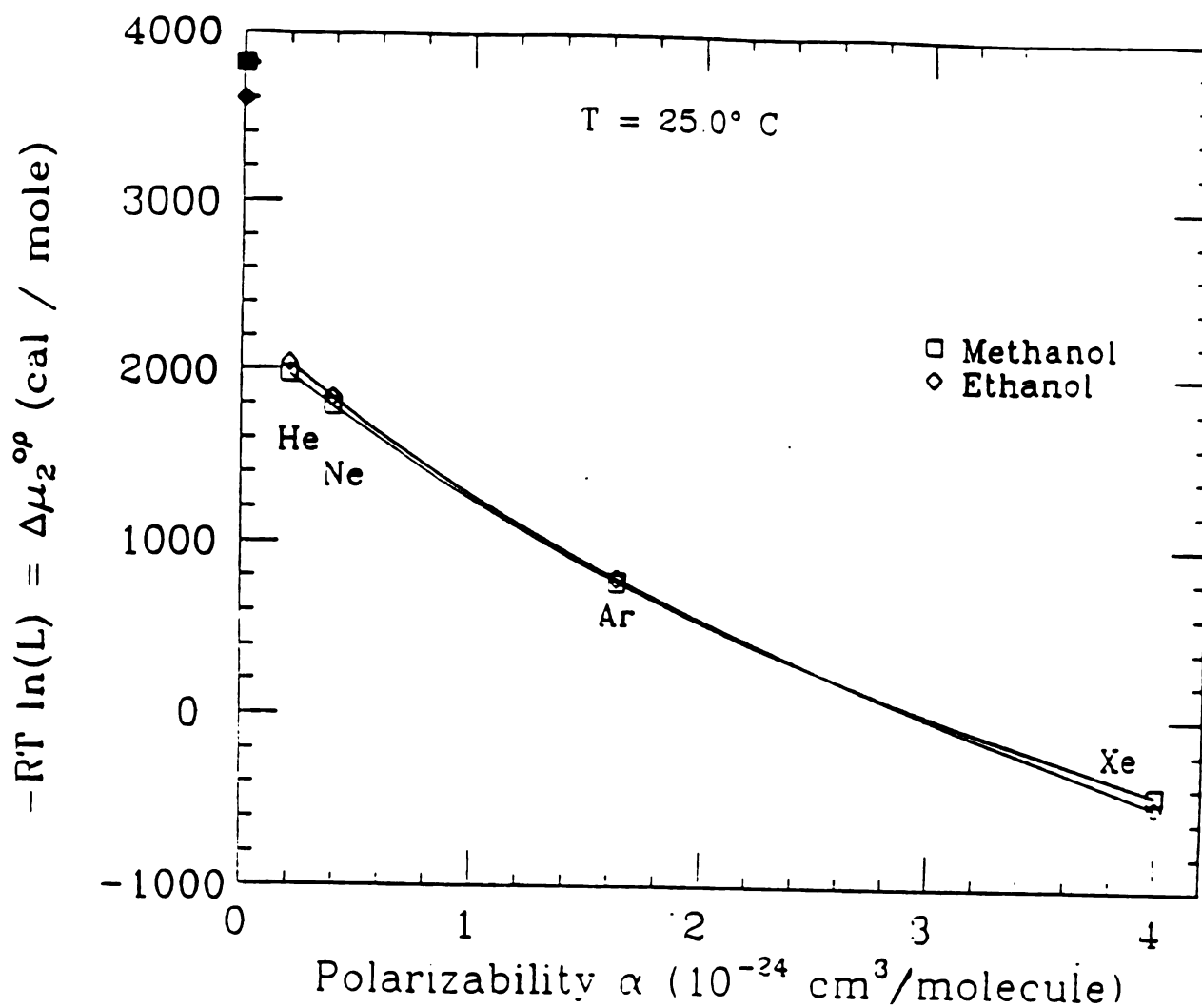


Figure 19. Excess chemical potential vs solute polarizability for noble gases in polar solvents methanol, and ethanol. Filled in points along ordinate are the SPT predicted values for a hard sphere solute of 2.58Å.

intuitively expect the attractive interaction to lower the free energy of solvation and increase the solubility. Figure 16b shows the experimental values of $\Delta\mu_2^*$ for Xe in the alkanes; it is encouraging to note that the SPT has much of the same systematic behavior.

The physical significance of g_{cav} is supported by extrapolation of measured solubilities of inert gases in solvents.^{55,66,67} In this technique the excess chemical potential is plotted versus solute polarizability, α_p , in a single solvent at fixed temperature. It has been shown that extrapolation of this data to zero polarizability is equivalent to finding the free energy required to introduce a hard sphere of diameter 2.58Å into the real solvent.^{55,72} The hard core diameter is determined by extrapolating a plot of solute diameter versus polarizability. Such a curve is shown in Figure 17 for the inert gases He through Xe. Figure 18 shows a plot of $-RT\ln L$ versus α_p for the inert gases in n-hexane. Extrapolating to $\alpha_p=0$ is equivalent to writing:

$$\Delta\mu_2^* (\alpha_p = 0, a_2 = 2.58\text{\AA}, T) = g_{cav} (a_1, a_2 = 2.58\text{\AA}, \rho_1, T) . \quad (6.88)$$

This value can then be compared to the SPT prediction of equation (6.74) for a solute of diameter 2.58Å. As Figure 18 shows, the predicted g_{cav} agrees to within 2% of the extrapolated value. Pierotti has used this test on a wide

variety of non-polar solvents with good results.⁵⁵ We performed this test for some of our solvents in order to see if the SPT was applicable. Even for alkanes as long as $n\text{-C}_{14}\text{H}_{30}$ the calculated g_{cav} agrees with the extrapolated value to within 5% (we couldn't test most of our solvents in this manner due to lack of experimental data). The case is different for the polar solvents. Figures 19a and 19b show the extrapolated and SPT results for methanol and ethanol. Clearly for these solvents there is a discrepancy. This can be traced back to our derivation of the effective hard sphere diameter from the solvent heat of vaporization. We recall that Eq. (6.79):

$$\Delta U_v \approx -2\pi N_A \rho \int_0^{\infty} u(r)g(r)r^2 dr \quad , \quad (6.79)$$

holds for normal liquids in which there are only two -body radial forces. For polar liquids one must account for many-body correlations. This renders equation (6.79), and therefore equation (6.87):

$$\Delta H_v = RT + \alpha_{\ell} RT^2 \left(\frac{(1+2y)^2}{(1-y)^3} \right) \quad , \quad (6.87)$$

invalid. We can also see that for methanol and ethanol the discrepancy between the two results decreases as the solvent chain length increases. Although we can't test it at this time; we are confident that for the longer acids, alkanols,

and alkanals the SPT works much better. It should also be mentioned that for the highly polar solvents the effective hard sphere diameter evaluated from solubility data together with the SPT agrees very well with other experiments; this involves using the SPT relation for g_{cav} to evaluate a_1 from the extrapolated result.^{72,73} In other words we use a plot like Figure 19 to find the free energy to dissolve a hard sphere of 2.58Å. The SPT is then applied to this result to give the effective radius of the solvent a_1 . This has proven to be a powerful method for estimating the molecular diameter of a solvent. Such a technique has even been applied successfully to water, which is a very complex liquid.^{70,73}

From the calculated values of $g_{\text{cav}}(T)$, we obtain the enthalpy of cavity formation by the Gibbs-Helmholtz equation:

$$h_{\text{cav}} = -T^2 \left(\partial(g_{\text{cav}}/T) / \partial T \right)_p \quad (6.89)$$

In this calculation we again neglect the temperature dependence of a_1 .^{54,55} Using our previous expression for $g_{\text{cav}}(T)$, we find:

$$h_{\text{cav}} = RT^2 \alpha_\ell \frac{y}{1-y} \left[\frac{6}{1-y} [A] + \frac{36y}{(1-y)^2} [B] + 1 \right],$$

where we have used the notation,

$$[A] = [2(r_{12}/a_1)^2 - (r_{12}/a_1)] , \text{ and}$$

$$[B] = [(r_{12}/a_1)^2 - (r_{12}/a_1) + 1/4] . \quad (6.90)$$

This expression reduces to equation (6.86) in the limit $a_1 = a_2$ (i.e. $r_{12}/a_1 = 1$). Figure 20a shows $h_{\text{cav}}(25^\circ\text{C})$ versus n_{carbon} for our solvents. For comparison Figure 20b shows the experimental excess enthalpy of solvation $\Delta\bar{h}_2^*$ for these solvents.

One may obtain the entropies of cavity formation, $s_{\text{cav}}(25^\circ\text{C})$, from g_{cav} and h_{cav} by the thermodynamic relation $s_{\text{cav}} = (h_{\text{cav}} - g_{\text{cav}})/T$. The s_{cav} values thus obtained are shown on Figure 21a. However, they appear to be unreliable. They do not have the systematic dependence with series that one might expect, nor do they correlate with our experimental results (Figure 21b). In order to check a possible cause for this we have plotted in Figures 22-24, respectively, the heats of vaporization (ΔH_v), number density (ρ_n), and thermal expansivity (α_2) versus carbon number for our solvents. Of these three input parameters in the SPT only the thermal expansivity seems to vary roughly in some of the homologous series. Perhaps better

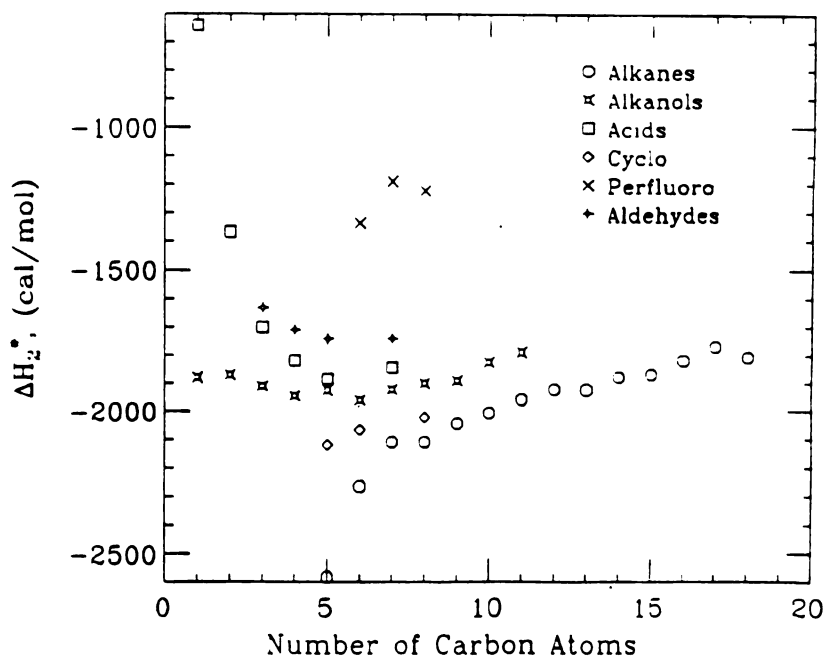
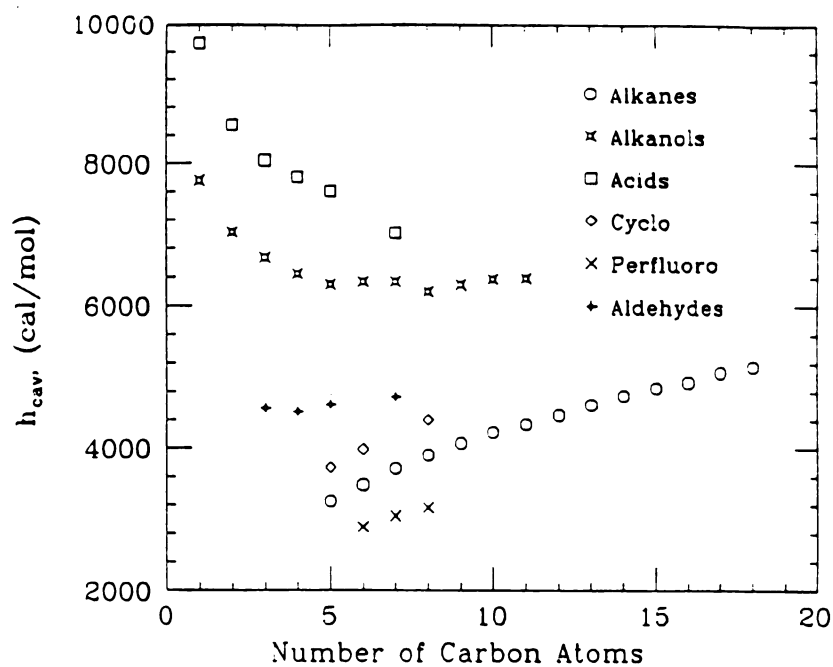


Figure 20. (a) h_{cav} for Xe in 45 organic solvents vs number of carbon atoms. (b) corresponding experimental excess enthalpy, Δh_2^* .

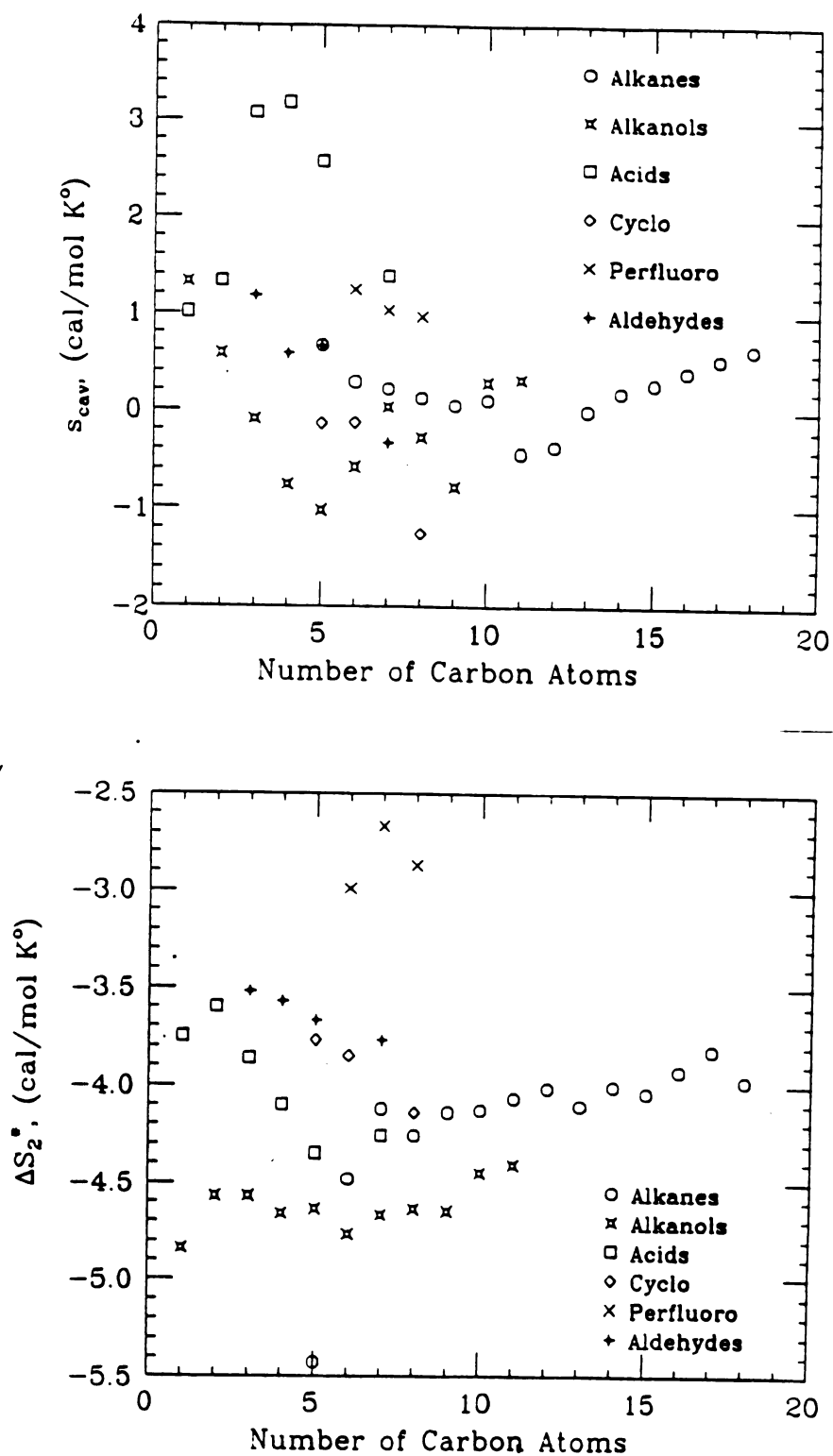


Figure 21. (a) s_{cav} for Xe in 45 organic solvents vs number of carbon atoms. (b) corresponding experimental excess entropy, ΔS_2^* .

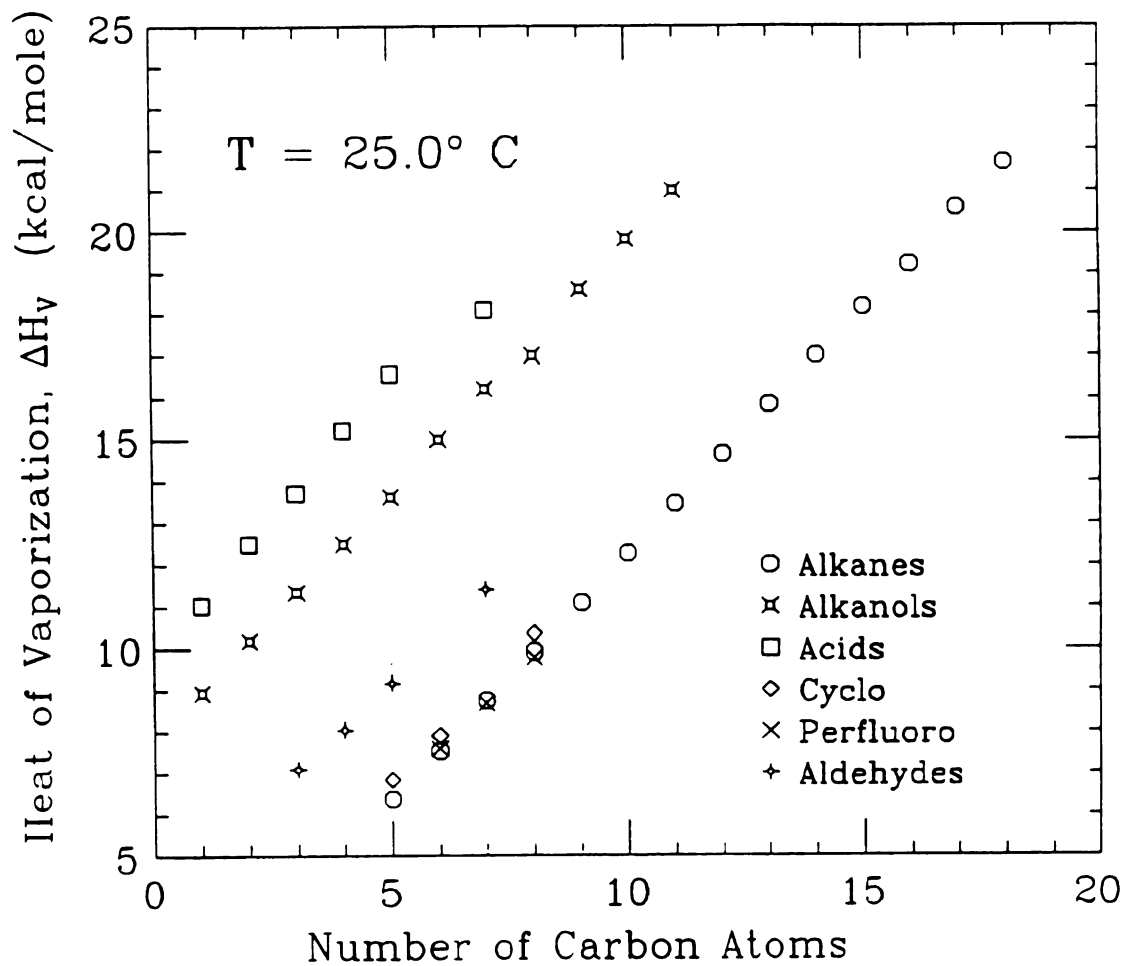


Figure 22. Heat of vaporization for 45 organic solvents at 25°C vs. number of carbon atoms.

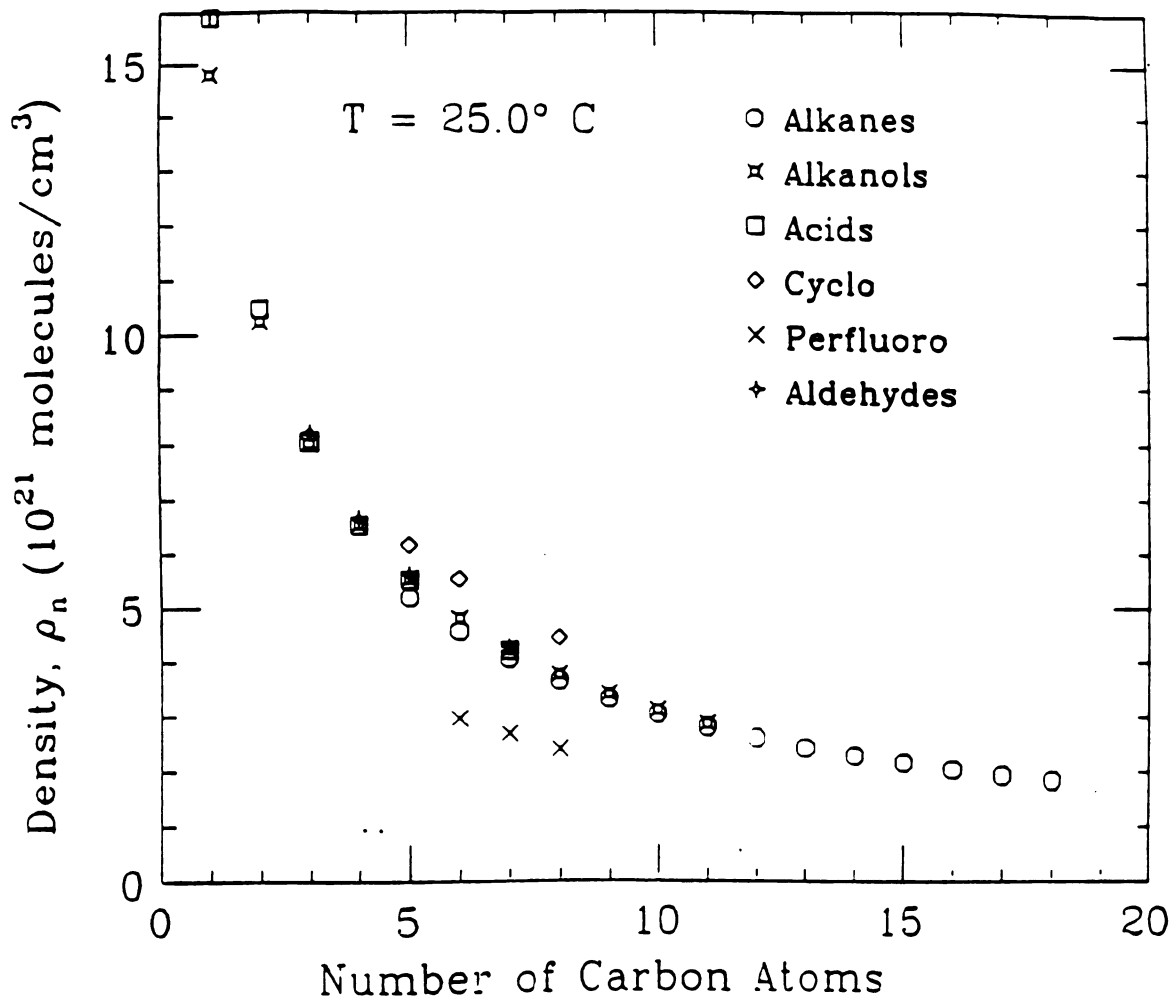


Figure 23. Number Density for 45 organic solvents at 25°C vs number of carbon atoms.

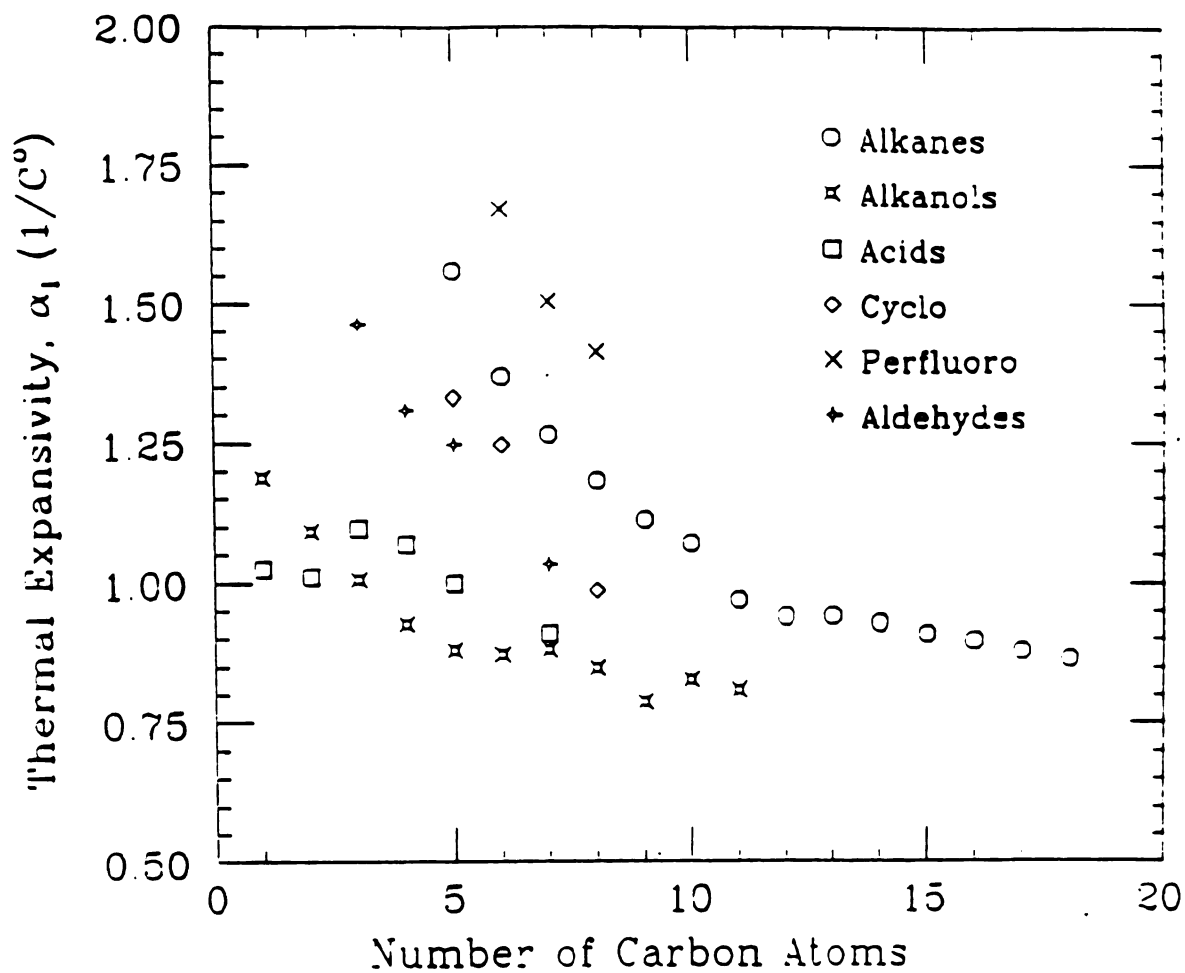


Figure 24. Thermal Expansivity for 45 organic solvents at 25°C vs number of carbon atoms.

Table VI. Cavity enthalpy and entropy.

alkanes

n-C	$h_{cav} \left(\frac{\text{cal}}{\text{mol}} \right)$	$s_{cav} \left(\frac{\text{cal}}{\text{molK}} \right)$
5	3251	0.67
6	3482	0.29
7	3710	0.22
8	3900	0.13
9	4067	0.05
10	4224	0.11
11	4332	-0.44
12	4467	-0.37
13	4613	-0.002
14	4739	0.19
15	4850	0.28
16	4929	0.41
17	5067	0.54
18	5148	0.64

cycloalkanes

n-C	$h_{cav} \left(\frac{\text{cal}}{\text{mol}} \right)$	$s_{cav} \left(\frac{\text{cal}}{\text{molK}} \right)$
5	3725	-0.14
6	3980	-0.13
8	4398	-1.26

Table VI cont....

alkanols

n-C	$h_{cav} \left(\frac{\text{cal}}{\text{mol}} \right)$	$s_{cav} \left(\frac{\text{cal}}{\text{molK}} \right)$
1	7760	1.32
2	7027	0.58
3	6675	-0.10
4	6440	-0.76
5	6291	-1.02
6	6336	-0.58
7	6335	0.03
8	6190	-0.28
9	6289	-0.78
10	6366	0.29
11	6385	0.32

carboxylic acids

n-C	$h_{cav} \left(\frac{\text{cal}}{\text{mol}} \right)$	$s_{cav} \left(\frac{\text{cal}}{\text{molK}} \right)$
1	9730	1.01
2	8538	1.33
3	8046	3.07
4	7820	3.18
5	7620	2.57
7	7017	1.39

Table VI cont.....

alkanals (aldehydes)

n-C	$h_{cav} \left(\frac{\text{cal}}{\text{mol}} \right)$	$s_{cav} \left(\frac{\text{cal}}{\text{molK}} \right)$
3	4563	1.18
4	4510	0.58
5	4611	0.66
7	4722	-0.33

perfluoroalkanes

n-C	$h_{cav} \left(\frac{\text{cal}}{\text{mol}} \right)$	$s_{cav} \left(\frac{\text{cal}}{\text{molK}} \right)$
6	2893	1.25
7	3046	1.03
8	3166	0.97

measurements of these are required. In any case it appears as though the s_{cav} 's are approximately centered on zero, whereas the total excess entropy, Δs_2^* , is about -4 cal/mol K. We conclude that the SPT alone does not adequately predict the solvation entropies. This is in sharp contrast to previous workers, who used the mole fraction scale to analyze their results.^{55,67,70,71,74}

A surprising result of these SPT calculations is that the cavity formation process is almost completely enthalpic (energetic). Table VI clearly shows that the entropic term is less than 10% of the enthalpic term (this is even more enthalpic than our experimental data; recall $\Delta \bar{h}_2^*/T\Delta \bar{s}_2^* \approx 1.8$). This is in strong contrast to a real hard sphere fluid which is completely controlled by entropic considerations. The key difference between these two situations can be seen in equation (6.90):

$$h_{cav} = RT^2 \alpha_L \frac{y}{1-y} \left[\frac{6}{1-y} [A] + \frac{36y}{(1-y)^2} [B] + 1 \right] \quad (6.90)$$

If the fluid were truly hard spheres then the thermal expansivity and hence the cavity enthalpy would be zero. By putting in the real solvent behavior we are accounting for the full interaction between solvent molecules. At first this may seem improper, but if we write out explicitly the expression for the excess chemical potential due to repulsive interactions $\Delta \mu_h^*$ from equations (6.52) and (6.53)

we find:

$$\Delta\mu_h^* = -kT \ln \left[\frac{\int d\vec{r}^N \exp[-\beta U(\vec{r}^N) - \beta B_h]}{\int d\vec{r}^N \exp[-\beta U(\vec{r}^N)]} \right] .$$

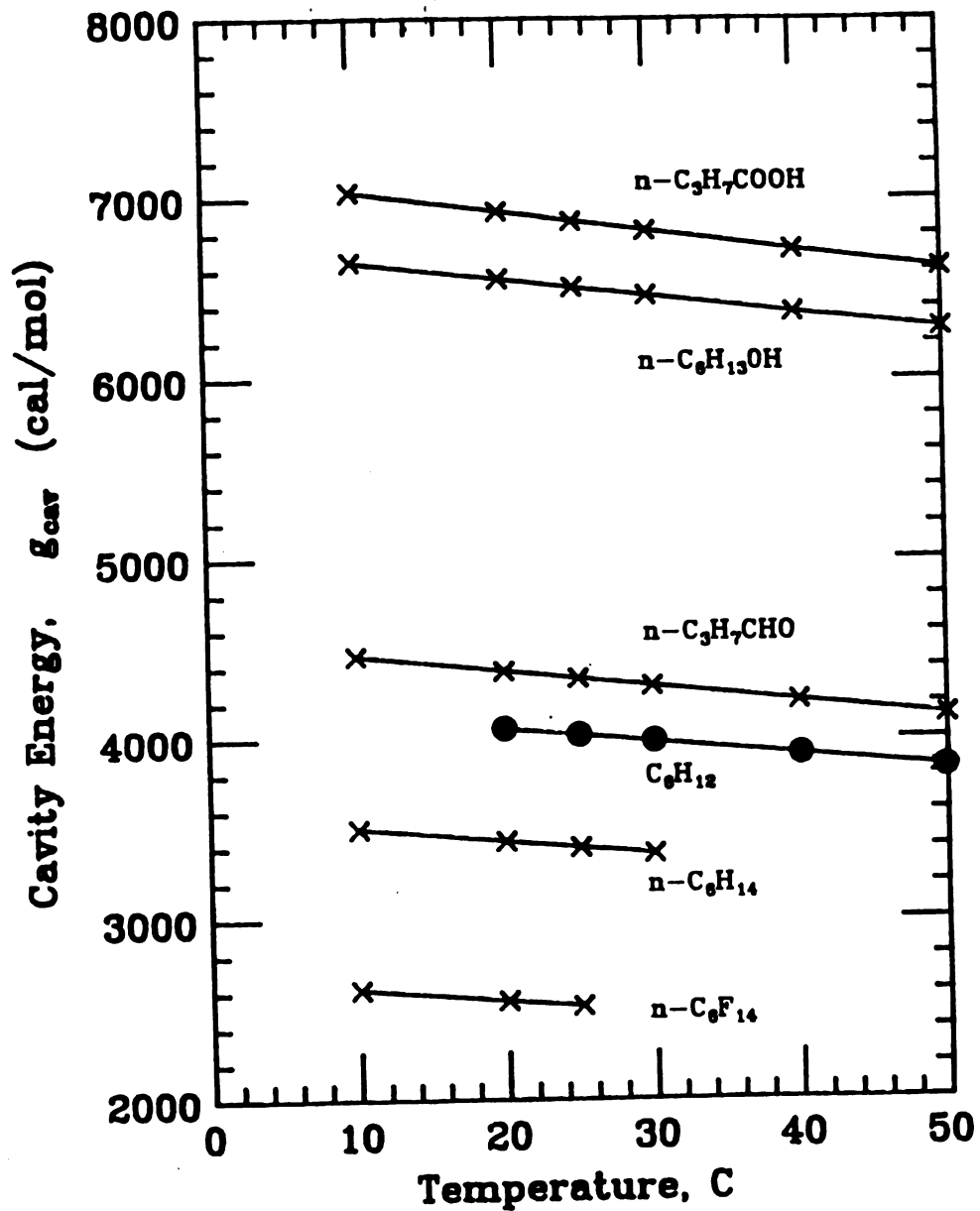
It is clear that in evaluating g_{cav} we should include the full solvent-solvent interaction. It is only the solute-solvent interaction which is broken up. Whether the SPT properly accounts for this by using the real expansivity requires further testing.

To complete our present discussion Figure 25 shows the calculated values of $g_{cav}(T)$ for six typical solvents, one from each homologous series. These results were obtained by applying equations (6.74) and (6.87) at each temperature for which the calculation is made; i.e., $a_1(T)$ values were obtained from equation (6.87) for each temperature. The $\Delta H_{vap}(T)$ data for these calculations were obtained from Watson's relation and critical temperature (T_c) data³³:

$$\Delta H_v(T_2) = \Delta H_v(T_1) \left[\frac{(1 - T_2/T_c)}{(1 - T_1/T_c)} \right]^{0.38} \quad (6.91)$$

The calculated temperature dependence of $g_{cav}(T)$ on Figure 25 is in the opposite direction from the observed values on Figure 9. However the slopes of the lines on Figure 25 are not the entropies of cavity formation.

Figure 25. Cavity free energy, g_{cav} , vs. T for Xe in 6 representative organic solvents.



6.8 The Interaction Term

After the cavity is formed in the hard sphere solvent, one introduces a solute molecule into the cavity and lets it interact with the solvent molecules; the free energy associated with this step is g_{int} . The natural next step is to calculate g_{int} for Xe in our solvents.

This proves to be very difficult even for our simplest solvents. Since g_{int} is a Gibbs free energy one may write it in terms of enthalpic and entropic contributions as:

$$g_{int} = h_{int} - Ts_{int} \approx u_{int} - Ts_{int} \quad (6.92)$$

This means that the two principal quantities which determine g_{int} are the potential energy of interaction, u_{int} , and the entropy of interaction, s_{int} . Both of these are difficult to calculate.

Solvent reordering, caused by the solute-solvent interaction, is probably the origin of most of the entropy of interaction and one therefore expects that $s_{int} < 0$.⁵⁴ Neff and McQuarrie⁷⁵ include a term in their expression for g_{int} which may account for this entropy; it gives the contribution to the free energy due to changes in solvent-solvent structure when a solute is introduced. This term [equation (27) of Ref. 74] depends on a derivative of the solvent-solvent distribution function, $g_{11}(r)$, which is hard to calculate.

Other workers^{55,71} neglect s_{int} and make the

approximation that $g_{int} \approx u_{int}$. I believe that s_{int} cannot be neglected, but rather may be commensurate with the entropy of solvation Δs_2^* . This contention is supported by consideration of the entropy of interaction in pure solvents for which it can sometimes be estimated. For example, Reiss et al.⁵⁴ have calculated the heat of vaporization for liquid Ar at its boiling point using the SPT and thermodynamics. From their results [equations (4.3)-(4.11) and Table II of Ref. 54] one finds $s_{int} = -4.6$ cal/mol K.

We have made a similiar calculation for other pure liquids and find $s_{int} = -10$ cal/mol K for CCl_4 at $25^\circ C$, and $s_{int} = -12$ cal/mol K for $n-C_6H_{14}$ at $25^\circ C$. The entropy of interaction is found by combining equations (2.5), (6.54), (6.84), and (6.92):

$$\begin{aligned} \Delta\mu^* &= -RT\ln(\rho_\ell/\rho_g) = g_{cav} + u_{int} - Ts_{int} \\ &= g_{cav} + 2(RT - \Delta H_v) - Ts_{int} \\ s_{int} &= \left[RT\ln(\rho_\ell/\rho_g) + g_{cav} + 2(RT - \Delta H_v) \right] / T. \end{aligned} \quad (6.93)$$

These s_{int} 's must properly be compared to the solvation entropies for the pure solvent, Δs^* , which one finds as follows: for the pure solvent we plot the excess chemical potential, $\Delta\mu^*$, versus T along the gas-liquid coexistence line. The temperature derivative is then written as:

$$\left(\frac{d\Delta\mu^*}{dT} \right)_c = \left(\frac{\partial\Delta\mu^*}{\partial T} \right)_p + \left(\frac{\partial\Delta\mu^*}{\partial P} \right)_T \left(\frac{dP}{dT} \right)_c, \quad (6.94)$$

where the subscript c means the derivative along the coexistence line. We then utilize the thermodynamic identity; $v_i = (\partial\mu_i/\partial P)_T$, and equation (6.94) reduces to:

$$(d\Delta\mu^*/dT)_c = -\Delta s^* + \Delta v^*(dP/dT)_c \quad (6.95)$$

In Eq. (6.95) Δv^* is the molar volume of solvation, which is approximately equal to the molar volume of the pure liquid.¹⁶ Values we obtained for the corresponding entropy defined by equation (6.95) are $\Delta s^*(\text{CCl}_4) = -9.1$ cal/mol K, and $\Delta s^*(n\text{-C}_6\text{H}_{14}) = -10.6$ cal/mol K., both at 25°C. For these two solvents we calculated s_{cav} 's of about 2 cal/mol K. Thus for pure solvents it appears that s_{int} makes an important contribution to the total entropy.

The interaction energy for a single solute molecule with the solvent may be written as:

$$u_{\text{int}} = \rho_1 \int g_{12}(\vec{r}) u_{12}(\vec{r}) d\vec{r} \quad (6.96)$$

where the terms are as defined previously. Evaluation of equation (6.96) is difficult for nonspherical solvents. An approximate method which assumes spherical symmetry has been used by Pierotti and others.^{55,71} In this technique a Lennard-Jones interaction potential $u_{12}(r)$ is assumed for $u_{12}(\vec{r})$ and the solvent distribution is taken to be uniform, i.e., $g_{12}=1$, outside the cavity radius r_{12} . The integration is over the solute volume, i.e., from r_{12} to infinity. This

is equivalent to an effective Lennard Jones potential with a hard sphere cutoff at $\sigma_{12} = (\sigma_1 + \sigma_2)/2$, as illustrated in Figure 26 (this is a more reasonable cutoff than r_0 because the actual potential is much steeper for $r < \sigma_{12}$ and is thus a better approximation to a hard sphere. Such a perturbation scheme was first suggested by Barker and Henderson⁷⁶). Lennard-Jones potential parameters are usually chosen to fit either solubility data or gas phase properties of the pure solvent and pure solute. However the potentials associated with the solvent are not consistent with the properties of bulk solvent liquids.

I shall now outline a model which is more consistent with our present goal of estimating solubility from knowledge of bulk properties of the solute and solvent. This model is presently designed for non-polar solvents, and will be used to analyze the Xe \rightarrow alkane system. The procedure is as follows:

- 1) We treat the molecules effectively as spheres with a radial Lennard-Jones interaction between molecular centers and a hard sphere cutoff. (For polar solvents we would have to include dipole terms in the interaction).

- 2) The solvent structure is determined solely by the hard sphere packing (van der Waals picture). Therefore we

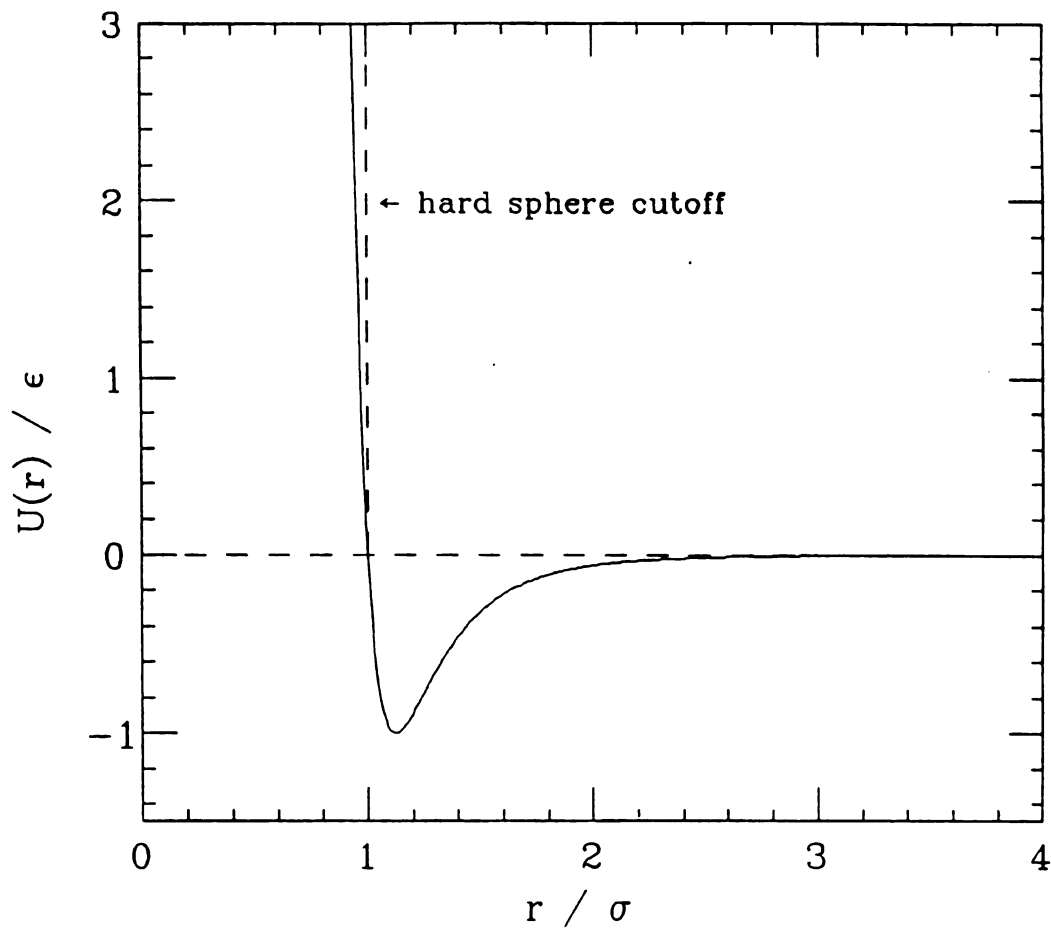


Figure 26. Lennard-Jones potential with hard sphere cutoff.

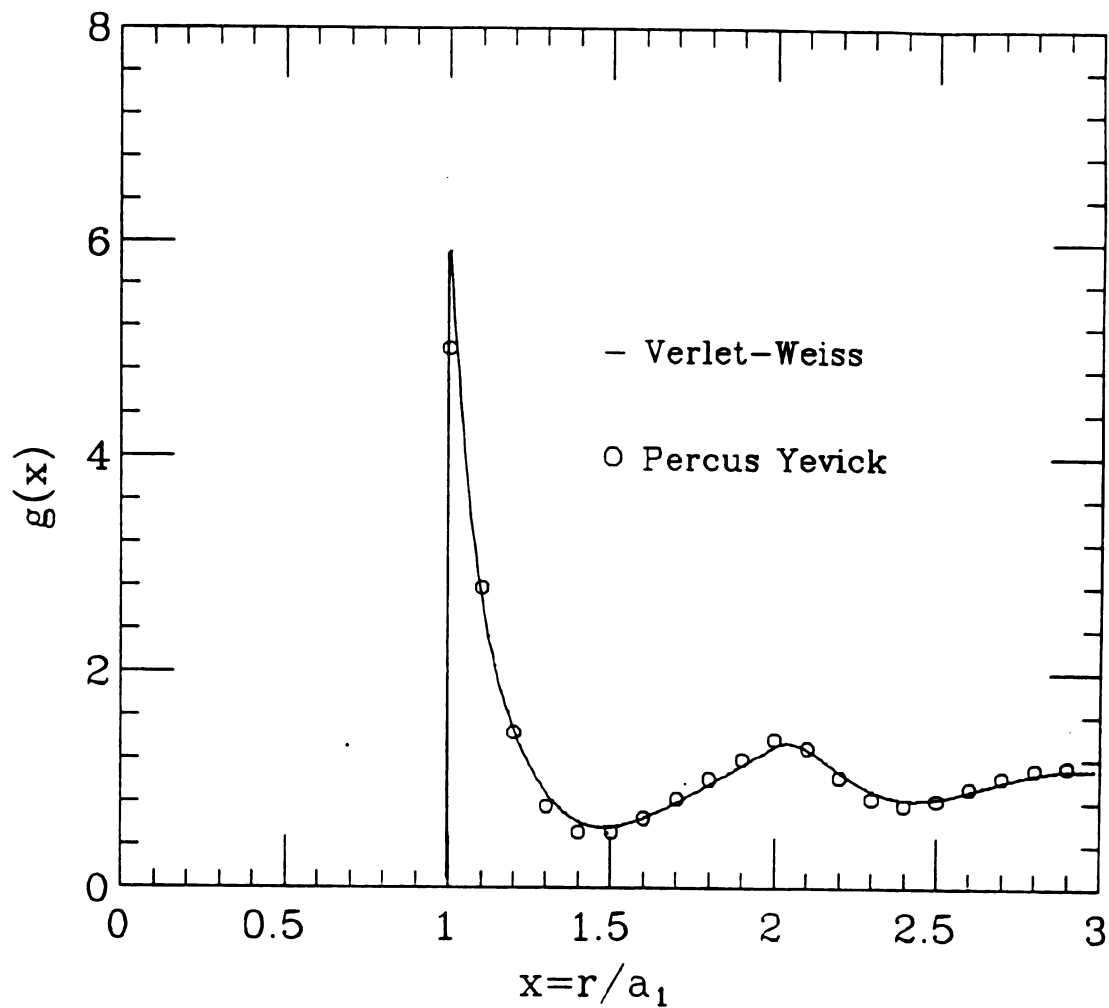


Figure 27. Verlet-Weiss and Percus Yevick pair distribution functions for hard sphere fluid. Packing fraction = 0.5.

write equation (6.96) as:

$$u_{int} = 4\pi\rho_1 \int_{r_0}^{\infty} g_{12}^{hs}(r) u_{12}(r) r^2 dr \quad , \quad (6.97)$$

where g_{12}^{hs} is the radial distribution for a hard sphere reference system, r_0 is the cavity radius $(a_1 + a_2)/2$.

3) Use the SPT to determine the effective hard core diameter of the solvent.

4) Use known Lennard-Jones potential parameters for the solute.^{77,78,79}

5) Apply standard mixing rules for the solute-solvent interaction:³⁵

$$\begin{aligned} u_{12} &= 4\epsilon_{12} \left[(\sigma_{12}/r)^{12} - (\sigma_{12}/r)^6 \right] \\ \epsilon_{12} &= (\epsilon_1 \epsilon_2)^{1/2} \\ \sigma_{12} &= (\sigma_1 + \sigma_2) / 2 = (a_1^{SPT} + a_2) / 2 \quad . \end{aligned} \quad (6.98)$$

6) To determine the Lennard-Jones energy parameter for the solvent, ϵ_1 , we apply this model to the pure solvent and use equation (6.33):

$$\begin{aligned} u_{int} &= 2RT - 2\Delta H_v = 4\pi\rho_1 \int_{r_0}^{\infty} g_{11}^{hs}(r) u_{11}(r) r^2 dr \\ u_{11}(r) &= 4\epsilon_1 \left[(\sigma_1/r)^{12} - (\sigma_1/r)^6 \right] \\ r_0 &= \sigma_1 = a_1^{SPT} \quad . \end{aligned} \quad (6.99)$$

The primary difference between this model and previous models is that we use the actual hard sphere distribution function (Pierotti assumed $g_{12} = 1$), and we evaluate the Lennard-Jones energy parameter for the solvent, ϵ_1 , from heat of vaporization data (as opposed to using solubility data to determine ϵ_1).

The hard sphere distribution function for a 1-component system of hard spheres is well known from computer simulations and is uniquely determined by the density and diameter of the fluid molecules (when applying this to real fluids temperature only enters indirectly in that the density is temperature dependent). We shall employ the Verlet and Weiss⁸¹ expression for $g(r)$. This is a semi-empirical modification of the Percus-Yevick analytic solution for $g(r)$ which reproduces numerical results very accurately.^{80,81} All of their results are in terms of the dimensionless variable x defined by; $x=(r/a)$. Figure 27 shows the Verlet-Weiss pair distribution functions for a hard sphere fluid with a packing fraction of 0.5. Near $x=1$ there is significant local structure, i.e., $g_{vw}(1) \approx 5.8$. Since the potential drops off rapidly (r^{-6}) it is very important to properly account for nearest neighbor effects. This is why the assumption of a uniform fluid distribution outside the cavity will probably greatly underestimate the interaction energy. It is also clear from Figure 27 that the fluid correlations fall off rapidly and by the time one reaches $x=3$ the fluid is essentially randomized (no long

range order). We shall therefore adopt the following convention for $g(x)$, i.e.:

$$\begin{aligned} g(x) &= 0 & x < 1 \\ g(x) &= g_{\text{verlet-weiss}}(x) & 1 \leq x < 3 \\ g(x) &= 1 & x \geq 3 \end{aligned} \quad (6.100)$$

The interaction energy for the pure solvent can then be written as:

$$\begin{aligned} u_{\text{int}} = 16\pi\epsilon_1\rho_1a_1^3 & \left[\int_{x=1}^3 g_{\text{vw}}(x) \left((1/x)^{10} - (1/x)^4 \right) dx \right. \\ & \left. + \int_{x=3}^{\infty} \left((1/x)^{10} - (1/x)^4 \right) dx \right] \quad (6.101) \end{aligned}$$

Evaluating the second integral we find:

$$u_{\text{int}}(\text{alkanes}) = 16\pi\epsilon_1\rho_1a_1^3 \left[(\text{INT1}) - (1/81) \right] \quad (6.102)$$

where INT1 is the first bracketed term in (6.101). A computer program was written to evaluate INT1 (listing in appendix #) using the standard trapezoidal rule.⁸² We generally found good convergence in the integral by using 500 or more steps. Table VII lists the values of INT1 for the alkanes. We used the bulk number densities and SPT packing fractions from Tables IV and V. Having evaluated the integral we can apply equations (6.99) and (6.102) to

find the Lennard-Jones energy parameter, ϵ_1 , for the pure solvent:

$$\epsilon_1 = (2RT - 2\Delta H_v) / \left(16\pi\rho_1 a_1^3 (\text{INT1} - 1/81) \right) . \quad (6.103)$$

These are tabulated in column 4 of Table VII; column 4 lists the values of ϵ_1 one would obtain by assuming $g = 1$. We can now use these values to determine the interaction energy for Xe-alkanes. The Lennard Jones potential parameters for Xe are ⁷⁷; $\epsilon_2/k = 221^\circ\text{K}$, and $\sigma_2 = a_2 = 3.973\text{\AA}$. To evaluate the solute-solvent pair correlation function, g_{12}^{hs} , we use the single fluid approximation³⁵ which states that for a multicomponent system $g_{\mu\nu}$ scales with $a_{\mu\nu}$, i.e.:

$$g_{\mu\nu}(r/a_{\mu\nu}) = g_x(r/a_x) \quad , \quad (6.104)$$

for all μ, ν . For our case this reduces to the statement:

$$g_{12}(x_{12}) = g(x) \quad , \quad (6.105)$$

where $x_{12} = r/a_{12}$. Therefore we may write equation (6.97) as:

Table VII. Parameters to evaluate interaction energy. Second column is the hard sphere cutoff. Third column is the energy integral using the Verlet-Weiss distribution function. Fourth column is the resulting Lennard-Jones energy parameter for the pure organic solvent.

alkanes

n-C	a_{12} (Å)	INT1	ϵ_1/k
5	4.7245	0.2731	477
6	4.9250	0.2722	526
7	5.0995	0.2703	585
8	5.2580	0.2677	648
9	5.4055	0.2648	708
10	5.6795	0.2620	773
11	5.6795	0.2576	834
12	5.7980	0.2546	921
13	5.9045	0.2524	973
14	6.0085	0.2498	1044
15	6.1120	0.2470	1115
16	6.2045	0.2448	1177

Table VIII. Predicted enthalpy of solvation for ^{136}Xe in n-alkanes at 25.0°C.

alkanes

n-C	u_{int}	h_{cav}	h_{pred}
5	-5069	3251	-1818
6	-5300	3482	-1818
7	-5503	3710	-1793
8	-5654	3900	-1754
9	-5800	4067	-1733
10	-5919	4224	-1695
11	-6023	4332	-1691
12	-6185	4467	-1718
13	-6214	4613	-1601
14	-6296	4739	-1557
15	-6373	4850	-1523
16	-6422	4929	-1493

$$u_{int}(Xe \rightarrow \text{alkanes}) = 16\pi\epsilon_{12}\rho_1 a_{12}^3 \left[(\text{INT1}) - (1/81) \right],$$

where the bracketed terms are exactly the same as for the pure fluid, $\epsilon_{12} = (\epsilon_1\epsilon_2)^{1/2}$, and $a_{12} = (a_1 + a_2)/2$. Combining this result with equation (6.102) and (6.99) we find:

$$u_{int}(Xe \rightarrow \text{alkanes}) = (\epsilon_1/\epsilon_2)^{0.5} (a_{12}/a_1)^3 (2RT - 2\Delta H_v). \quad (6.106)$$

Table VIII shows the values of u_{int} for Xe in the alkanes.

6.9 Comparison with Experimental Data

We may now combine our calculated values for h_{cav} and u_{int} to find the total enthalpy (energy) of solvation. Figure 28 shows a plot of the combined theoretical term, $h_s = h_{cav} + u_{int}$, and the experimentally determined enthalpy, $\Delta \bar{h}_2^*$, versus number of carbons, for Xe in alkanes ranging from hexane (C_6) to hexadecane (C_{16}). The theoretical and experimental data both have the same systematic tendency; i.e. the enthalpy becomes less negative for the longer chain alkanes. According to our model this means that the solvent size dependence, a_1 , in the cavity term slightly dominates over the solvent energy dependence, ϵ_1 , in the interaction term. The general agreement between the two sets of data is within 20%. This points out one of the biggest problems in calculations of this sort, viz; to describe the total solvation process we usually calculate

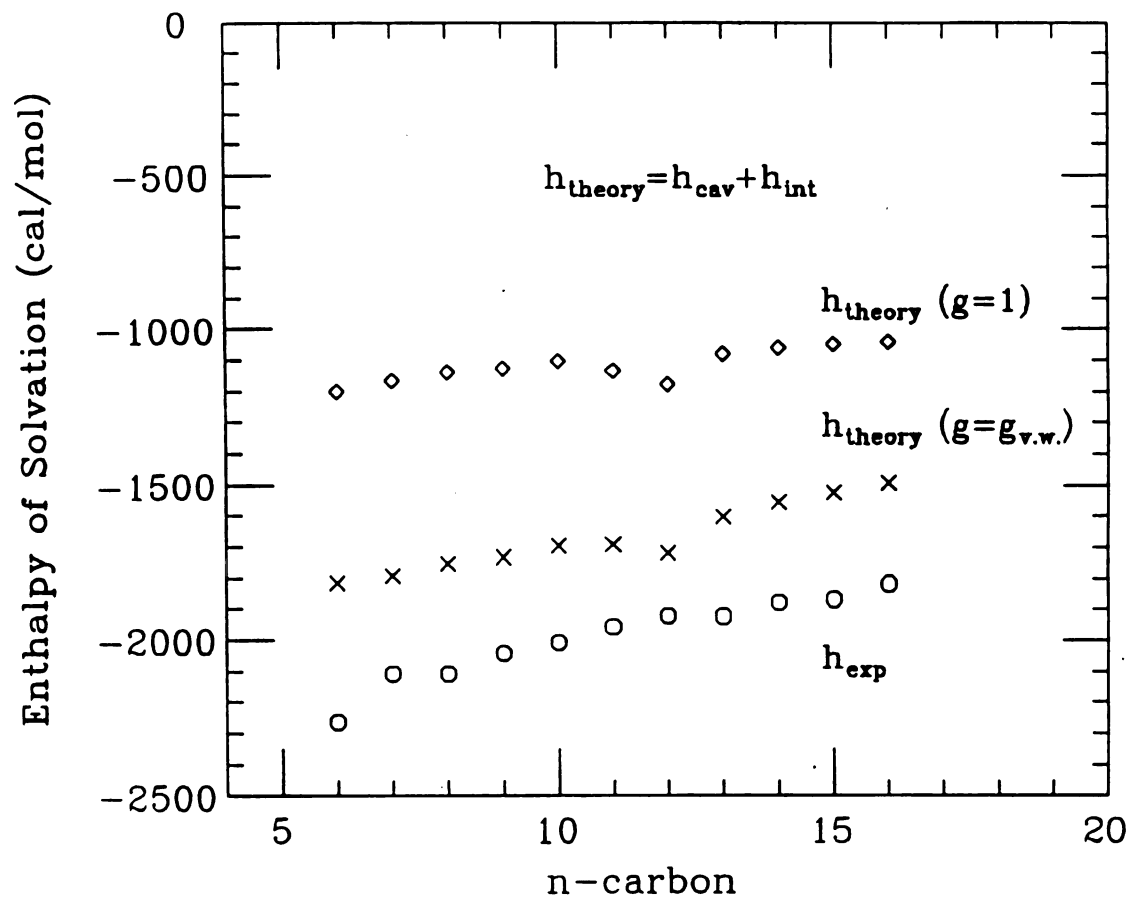


Figure 28. Calculated and experimental excess enthalpies of solvation for Xe in alkanes.

two separate processes which each have characteristic energies that are opposite in sign and of larger magnitude than their sum. This puts an extra burden of accuracy in the calculation of each term. For example the discrepancy between h_s and $\Delta \bar{h}_2^*$ for decane is about 16% of the experimental value which in turn is only 7% of h_{cav} or 5% of u_{int} . To claim that a model as simple as ours could do better than this would be an exaggeration. For completeness Figure 28 also includes the theoretical predictions that one would obtain by using a random fluid distribution, $g_{11} = g_{12} = 1$, throughout the entire calculation of u_{int} . Agreement obtained in this case is not as good as that obtained with the hard sphere distribution of Verlet and Weiss.⁸¹

We expect that equation (6.106) should not just be applicable to Xe, but should hold for any non-polar solute with a well defined diameter, a_2 . In order to test this hypothesis we have looked at solubility data for the inert gases He, Ne, Ar, and Kr in several alkanes. Solubility data was obtained from reference (24). The original data were quoted on the mole fraction scale. In order to convert data to the number density (Ostwald solubility) scale we inverted equation (3.20):

$$L(T) = RT / \left[P v_1(T) \left[(1/x_2(T)) - 1 \right] \right] , \quad (6.107)$$

where v_1 is the molar volume of the solvent and P is the pressure of the gas (all measurements were at 1 atm). Once

the temperature dependent solubilities were calculated, we could easily find the excess chemical potential, enthalpy, and entropy using standard thermodynamics. Table IX gives the values of $\Delta\mu_2^*$, $\Delta\bar{h}_2^*$, and $\Delta\bar{s}_2^*$ for the inert gases in the solvents hexane, octane, nonane, decane, dodecane, and tetradecane. Figures 29a and b show the predicted and experimental enthalpies versus ϵ_{solute} for the inert gases in octane and tetradecane, respectively. The solute parameters are shown below.^{77,78,79}

solute	ϵ_2/k ($^{\circ}\text{K}$)	$\sigma_2 = a_2$ (\AA)
He	6.03	2.63
Ne	34.9	2.78
Ar	119.3	3.448
Kr	172.7	3.59

Table X lists all the relevant theoretical quantities that we can calculate for the alkanes; i.e. g_{cav} , h_{cav} , s_{cav} , and u_{int} .

Once again our simple theory seems to capture some of the general systematics but is not sufficiently accurate to make reliable predictions. A particular flaw can be seen in the predicted values of enthalpy for the less polarizable solutes like Ar, Ne, and He. Experimental data indicates that for these solutes the enthalpy increases with solvent size, however the theory predicts just the opposite. This

Table IX. Excess chemical potential, enthalpy and entropy for He, Ne, Ar, and Kr in the alkanes, including: hexane, octane, nonane, dodecane, and tetradecane.

Helium (20 C)

n-C	$\Delta\mu_2^*$ ($\frac{\text{cal}}{\text{mol}}$)	Δh_2^* ($\frac{\text{cal}}{\text{mol}}$)	Δs_2^* ($\frac{\text{cal}}{\text{molK}}$)
6	1801	2271	1.602
8	1975	2312	1.150
9	2048	2715	2.274
10	2102	2260	0.537
12	2214	2153	-0.2076
14	2279	1840	-1.496

Neon (20 C)

n-C	$\Delta\mu_2^*$ ($\frac{\text{cal}}{\text{mol}}$)	Δh_2^* ($\frac{\text{cal}}{\text{mol}}$)	Δs_2^* ($\frac{\text{cal}}{\text{molK}}$)
6	1587	1699	0.383
8	1732	2046	1.070
9	1816	1902	0.295
10	1857	1941	0.288
12	2014	2096	0.283
14	2048	1838	-0.715

Table IX. cont.....

Argon (20 C)

n-C	$\Delta\mu_2^*$ ($\frac{\text{cal}}{\text{mol}}$)	Δh_2^* ($\frac{\text{cal}}{\text{mol}}$)	Δs_2^* ($\frac{\text{cal}}{\text{molK}}$)
6	436	-297	-2.501
8	594	301	-0.999
9	631	43.9	-2.002
10	676	53.4	-2.123
12	756	276	-1.636
14	811	79.0	-2.495

Krypton (20 C)

n-C	$\Delta\mu_2^*$ ($\frac{\text{cal}}{\text{mol}}$)	Δh_2^* ($\frac{\text{cal}}{\text{mol}}$)	Δs_2^* ($\frac{\text{cal}}{\text{molK}}$)
6	-168	-787	-2.11
8	-49.3	-816	-2.62
9	2.86	-718	-2.46
10	44.5	-767	-2.77
12	110	-594	-2.40
14	148	-850	-3.41

Table X. g_{cav} , h_{cav} , s_{cav} , and u_{int} for He, Ne, Ar, and Kr in the alkanes, including pentane through hexadecane

Helium (25 C)

n-C	$g_{cav} (\frac{cal}{mol})$	$h_{cav} (\frac{cal}{mol})$	$s_{cav} (\frac{cal}{molK})$	$u_{int} (\frac{cal}{mol})$
5	1766	1744	-0.07	-529
6	1965	1857	-0.36	-564
7	2109	1971	-0.47	-595
8	2235	2065	-0.57	-620
9	2345	2147	-0.66	-644
10	2428	2227	-0.67	-664
11	2580	2273	-1.03	-682
12	2647	2340	-1.03	-706
13	2672	2417	-0.78	-714
14	2715	2482	-0.78	-729
15	2765	2538	-0.76	-742
16	2791	2579	-0.71	-752

Table X. cont.....

Neon (25 C)

n-C	$g_{cav} \left(\frac{\text{cal}}{\text{mol}} \right)$	$h_{cav} \left(\frac{\text{cal}}{\text{mol}} \right)$	$s_{cav} \left(\frac{\text{cal}}{\text{molK}} \right)$	$u_{int} \left(\frac{\text{cal}}{\text{mol}} \right)$
5	1891	1888	-0.01	-1344
6	2103	2011	-0.31	-1430
7	2258	2136	-0.41	-1506
8	2392	2239	-0.51	-1566
9	2510	2330	-0.61	-1622
10	2598	2416	-0.61	-1671
11	2762	2469	-0.98	-1716
12	2834	2542	-0.98	-1774
13	2860	2625	-0.79	-1794
14	2905	2696	-0.70	-1828
15	2958	2757	-0.67	-1861
16	2986	2802	-0.62	-1885

Table X. cont....

Argon (25 C)

n-C	$g_{cav} \left(\frac{\text{cal}}{\text{mol}} \right)$	$h_{cav} \left(\frac{\text{cal}}{\text{mol}} \right)$	$s_{cav} \left(\frac{\text{cal}}{\text{molK}} \right)$	$u_{int} \left(\frac{\text{cal}}{\text{mol}} \right)$
5	2504	2603	0.33	-3137
6	2786	2782	-1.05	-3304
7	2990	2961	-0.10	-3450
8	3167	3110	-0.19	-3563
9	3323	3240	-0.28	-3670
10	3439	3363	-0.25	-3760
11	3659	3445	-0.72	-3840
12	3753	3550	-0.68	-3955
13	3784	3666	-0.40	-3983
14	3842	3766	-0.26	-4046
15	3911	3853	-0.19	-4105
16	3945	3915	-0.10	-4144

Table X. cont.....

Krypton (25 C)

n-C	$g_{cav} \left(\frac{\text{cal}}{\text{mol}} \right)$	$h_{cav} \left(\frac{\text{cal}}{\text{mol}} \right)$	$s_{cav} \left(\frac{\text{cal}}{\text{molK}} \right)$	$u_{int} \left(\frac{\text{cal}}{\text{mol}} \right)$
5	2646	2771	0.42	-3958
6	2945	2964	0.06	-4160
7	3161	3154	-0.02	-4337
8	3347	3314	-0.11	-4472
9	3512	3454	-0.20	-4601
10	3634	3586	-0.16	-4708
11	3868	3674	-0.65	-4803
12	3967	3787	-0.60	-4943
13	4000	3911	-0.30	-4976
14	4060	4017	-0.14	-5050
15	4133	4111	-0.07	-5121
16	4169	4177	-0.03	-5167

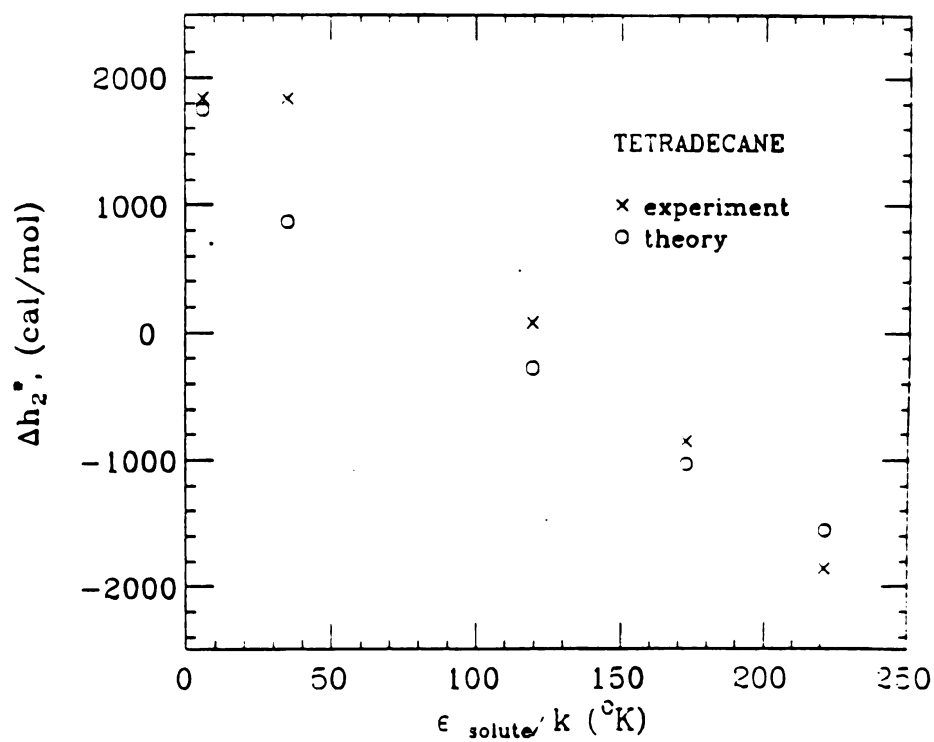
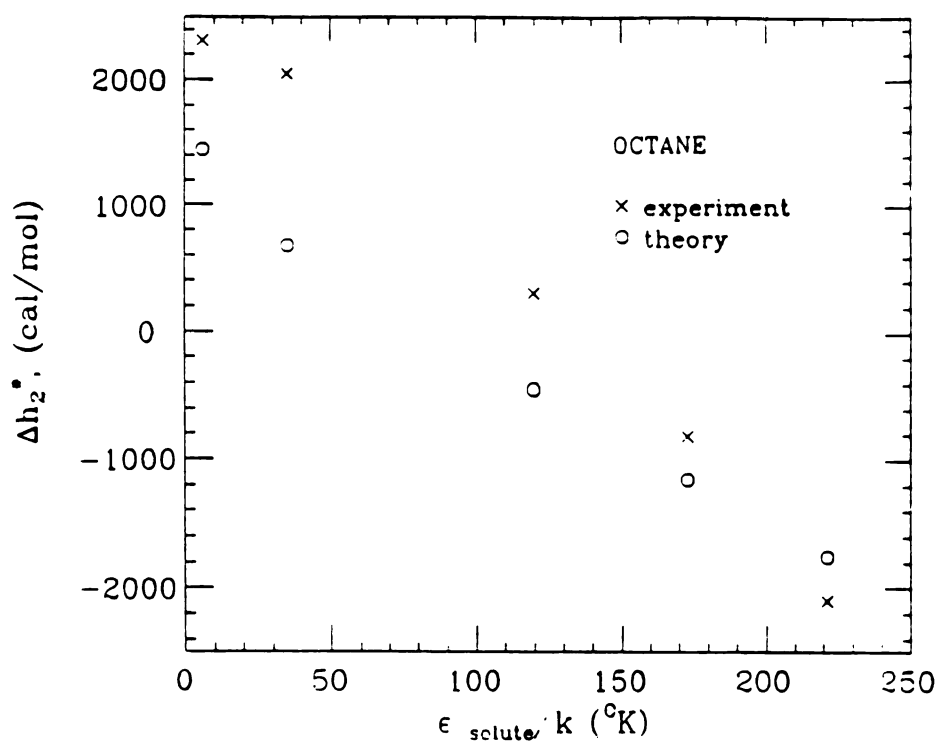


Figure 29. Calculated and experimental excess enthalpies of solvation for He, Ne, Ar, Kr, and Xe in (a) octane, (b) tetradecane.

seems to indicate that for these solutes we are overemphasizing the attractive contribution to h_s . A possible explanation for this lies in our use of the single fluid approximation for g_{12} ; i.e. $g_{11}(r/a) = g_{12}(r/a_{12})$. It has been shown that this approximation gets worse as the solute and solvent become more disparate in size. The most prominent effect is that the main peak in the correlation function tends to become smaller as the ratio of solute to solvent size decreases.⁸³ An interesting feature in Figure 29 is that the enthalpy increases as the solute becomes less polarizable, and crosses over to a positive value at argon. If we recall equation (5.4):

$$\frac{dL}{dT} = L \frac{\Delta \bar{h}_2^*}{R T^2}, \quad (5.4)$$

we see that for the less polarizable gases the Ostwald solubility actually increases with temperature. This is opposite to our usual experience (when you heat a liquid you drive it towards the vapor phase!), but is easily understood from our model, i.e. as the solute becomes less polarizable it behaves more like a hard sphere, and the SPT shows that it always takes a positive energy to make a cavity. This positive energy then leads to our observed temperature dependence via (5.4).

This seems about as far as we can take a simple model for explaining gas solubility. The usual recourse at this point is to introduce solubility parameters that are

characteristic of the solute-solvent combination.^{33,84}

Although this leads to very accurate predictions over a wide range of temperature and solute concentration we shall leave it to the chemical engineers.

7. Empirical Analysis and Predictions

Although analytic techniques give only limited understanding of these solubility data, as discussed in the previous section, empirical techniques may be applied usefully to them as we demonstrate now.

The idea underlying our empirical analysis is to construct the thermodynamic quantities $\Delta\mu_2^*$, $\Delta\bar{h}_2^*$, and $\Delta\bar{s}_2^*$ for each solvent as the sum of contributions from the functional groups which make up the solvent molecules. For our 45 solvents we shall attempt to decompose $\Delta\mu_2^*$ into Xe interactions with the functional groups: CH_2 (in linear molecules), CH_3 , OH, COOH, CHO, and CH_2 (in cyclomolecules).

Figure 30 is a plot of the excess chemical for 40 solvents verses number of CH_2 groups at 25°C. At first glance this does not look like a promising candidate for separation into functional group contributions. One might hope that the addition of a CH_2 to any molecule might bring about the same change in excess chemical potential in each homologous series, but this is clearly not the case since the slopes for each series are so different. In fact for the polar molecules $\Delta\mu_2^*$ turns upward as we approach zero CH_2 groups, while for the nonpolar alkanes and cycloalkanes the chemical potential becomes more negative (this holds for the

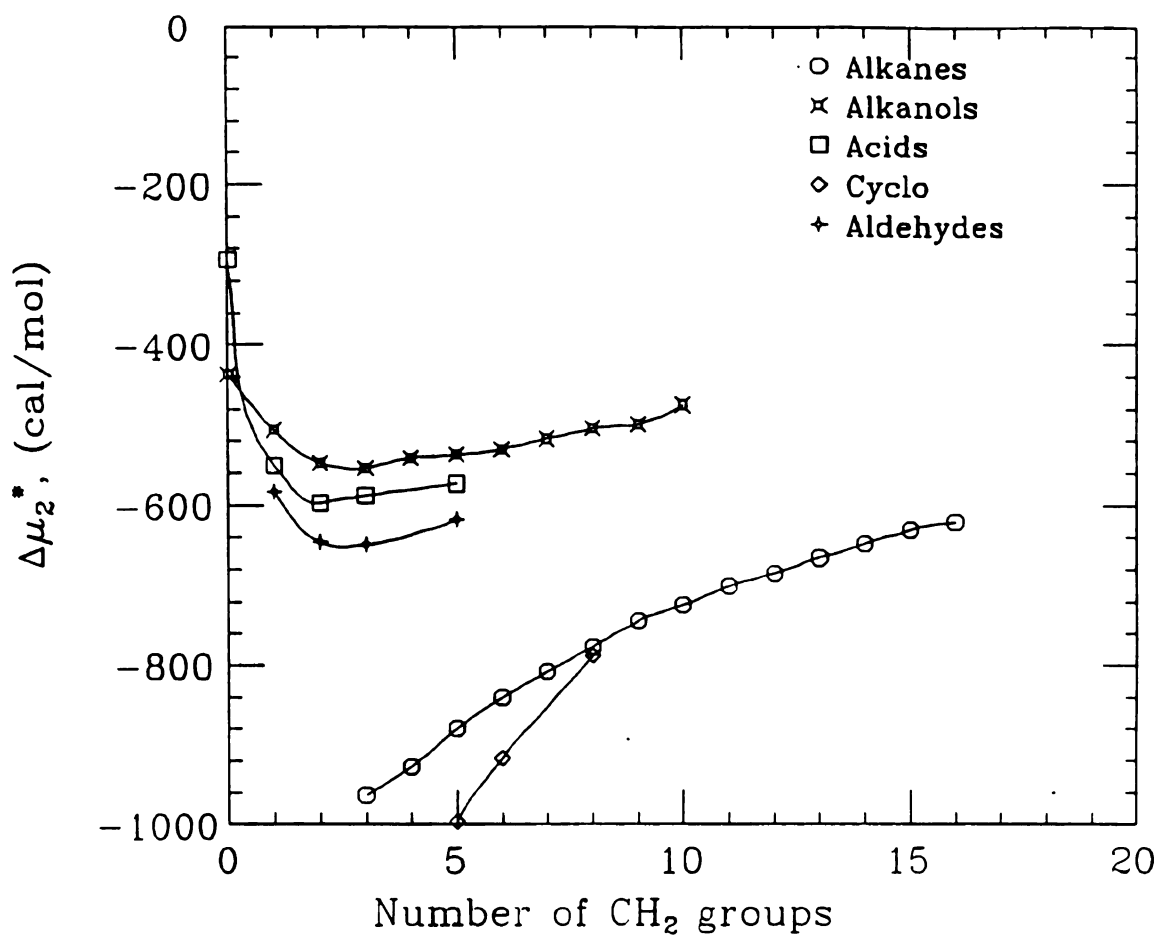


Figure 30. Excess chemical potential $\Delta\mu_2^* = -RT \ln L$ vs number of CH_2 groups at 25°C .

perfluoroalkanes as well). In order to get some insight into what is happening we must look at our expression for $\Delta\mu_2^*$; i.e. equation (6.35):

$$\Delta\mu_2^* = \int_0^1 \int_0^\infty 4\pi\rho_1 g_{12}(r,\lambda) u_{12}(r) r^2 dr d\lambda \quad . \quad (6.35)$$

As one increases the number of CH_2 groups there are several parts of Eq. (6.35) that vary; the solvent number density, ρ_1 (as illustrated on Table IV and Figure 23), the pair correlation function g_{12} , and the intermolecular potential $u_{12}(r)$. There is a great deal of evidence from computer simulations that the pair potential can be broken into group contributions. If we assume this is true and that the correlation function changes slowly, we may be able to appropriately scale our data.

Figure 31 is a plot of the data, for 37 solvents, from which one may obtain group contributions for $\Delta\mu_2^*$. The ordinate is $\Delta\mu_2^*/\rho_1$ at 25°C and the abscissa is the number of CH_2 groups in the solvent molecule.

The four sets of points on Figure 31 which give data for alkanes, alkanols, carboxylic acids, and alkanals, can be fitted to straight lines which have approximately the same slopes. This makes empirical analysis possible. One therefore takes the weighted average slope of these four lines to be the contribution to $\Delta\mu_2^*/\rho_1$ of each CH_2 group in a linear molecule. The analysis omits solvents which have one or zero CH_2 groups, but the data for these are included

on Figure 31. This quantity, called ϵ_{μ} (cal/mol)/(mol/liter), is given at the upper left of Table IX. In like manner the average slope of the curve for cycloalkanes on Figure 31 gives the corresponding ϵ_{μ} for an additional CH_2 group in a cyclomolecule. The perfluoroalkanes' data are not good enough to be analyzed this way because the samples were mixed isomers. If one extrapolates on Figure 31 the points for alkanes to the limit of zero CH_2 groups one gets as intercept the contributions to $\Delta\mu_2^*/\rho_1$ of the two CH_3 groups; i.e. $2\epsilon_{\mu}(\text{CH}_3)$, at the ends of these molecules. The intercept on the ordinate axis obtained by extrapolation of the alkanol data is $\epsilon_{\mu}(\text{CH}_3) + \epsilon_{\mu}(\text{OH})$, from which one may obtain $\epsilon_{\mu}(\text{OH})$ by subtracting off $\epsilon_{\mu}(\text{CH}_3)$ previously obtained. In similiar fashion we obtained $\epsilon_{\mu}(\text{COOH})$ and $\epsilon_{\mu}(\text{CHO})$. Values for all six of these ϵ_{μ} 's are shown in Table XI. The formula by which one reconstructs an estimated $\Delta\mu_2^*$ at 25°C is, say, for an alkanol with, say, m CH_2 groups:

$$\Delta\mu_2^*(\text{est}) = \rho_1 \left[\epsilon_{\mu}(\text{CH}_3) + m\epsilon_{\mu}(\text{CH}_2, \text{lin}) + \epsilon_{\mu}(\text{OH}) \right], \quad (7.1)$$

from which $L(25^\circ\text{C})$ may be obtained from $\Delta\mu_2^*(\text{est}) = -RT \ln L$.

Figure 32 shows values for average enthalpy obtained from our solubility measurements. The ordinate is $\Delta\bar{h}_2^*/\rho_1$ and the abscissa is, as in Figure 31, the number of CH_2

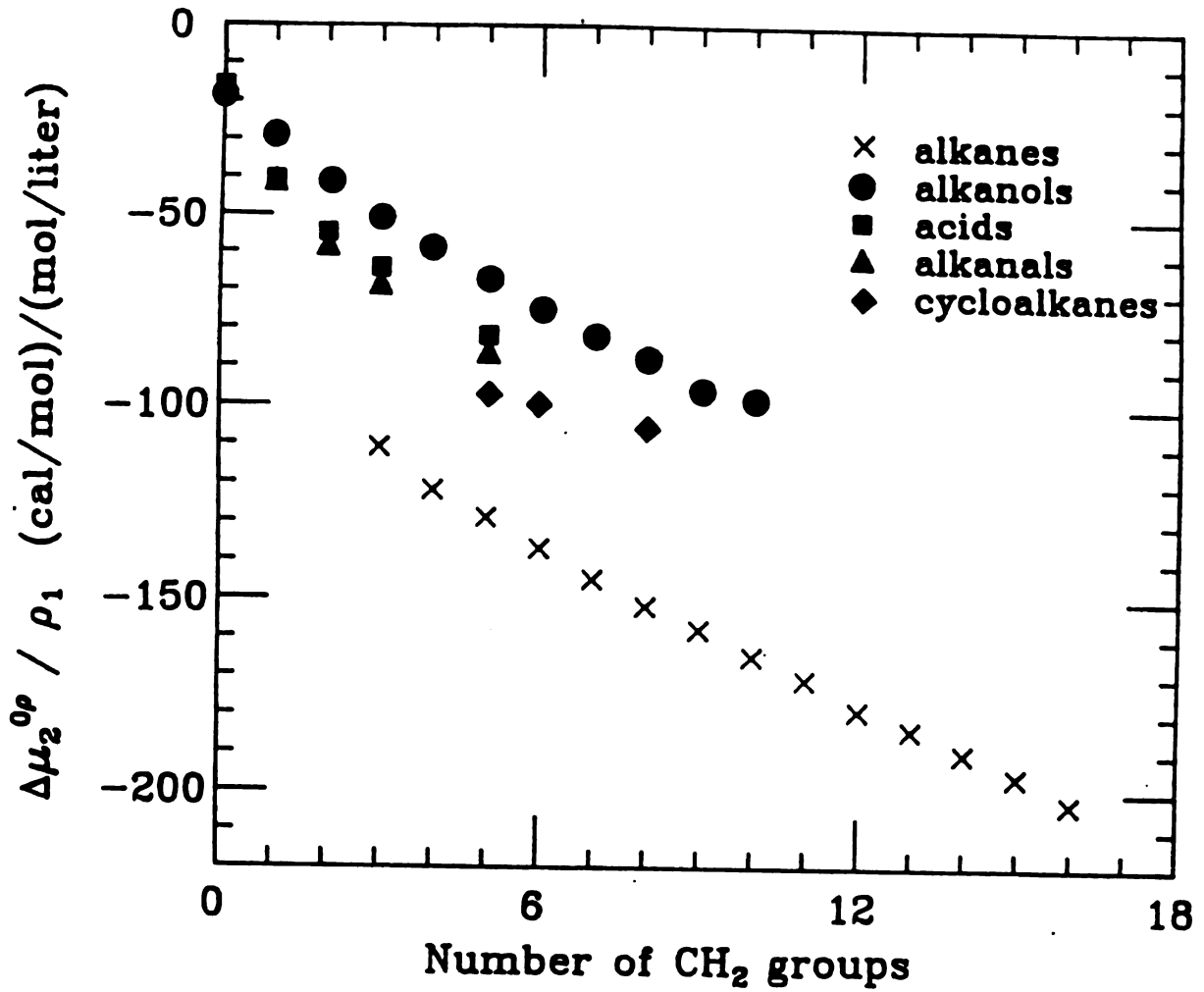


Figure 31. Experimental data for Xe in 37 solvents. Excess chemical potential divided by solvent number density vs number of CH₂ groups at 25°C.

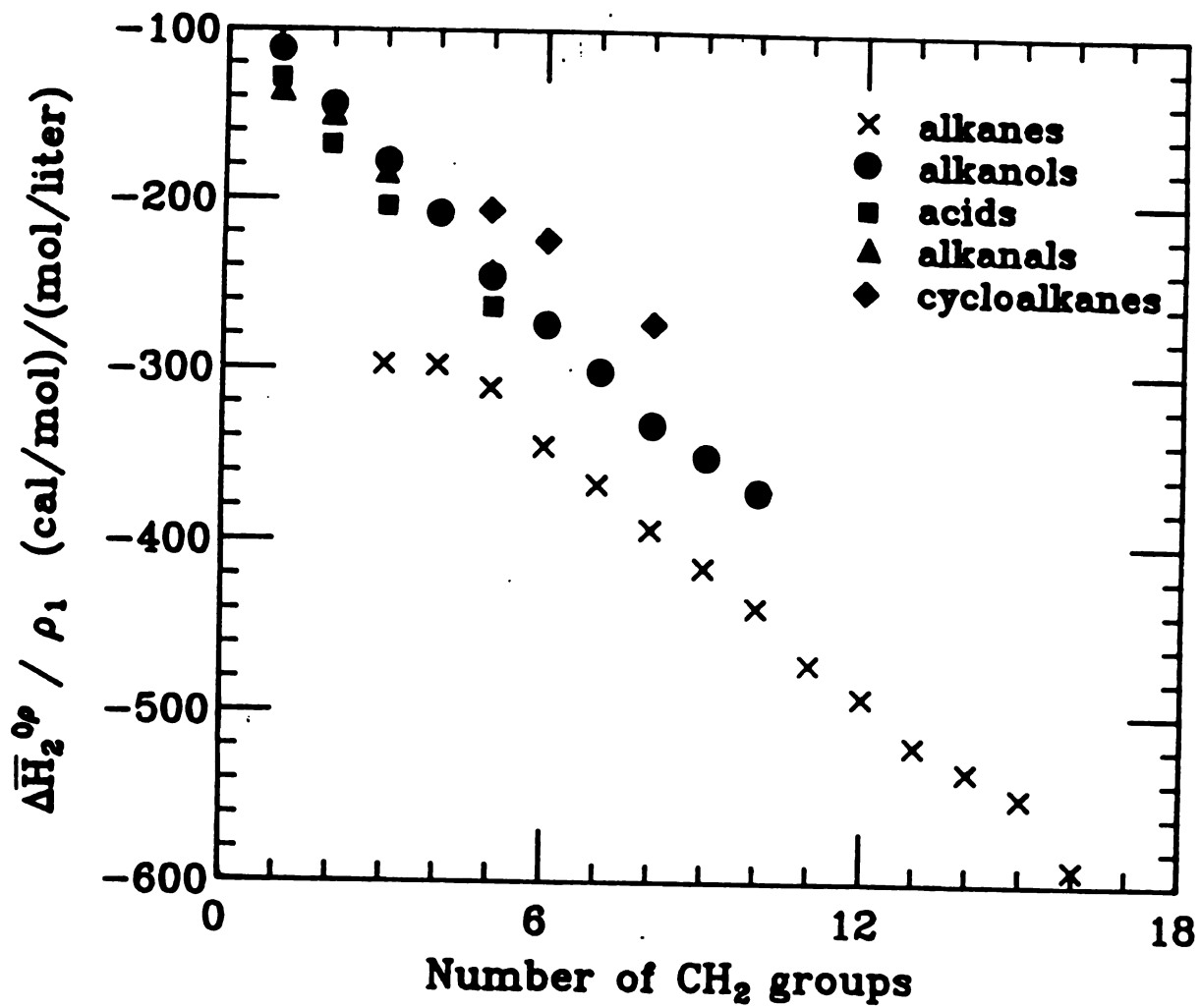


Figure 32. Experimental data for Xe in 37 solvents. Excess enthalpy divided by solvent number density vs number of CH₂ groups .

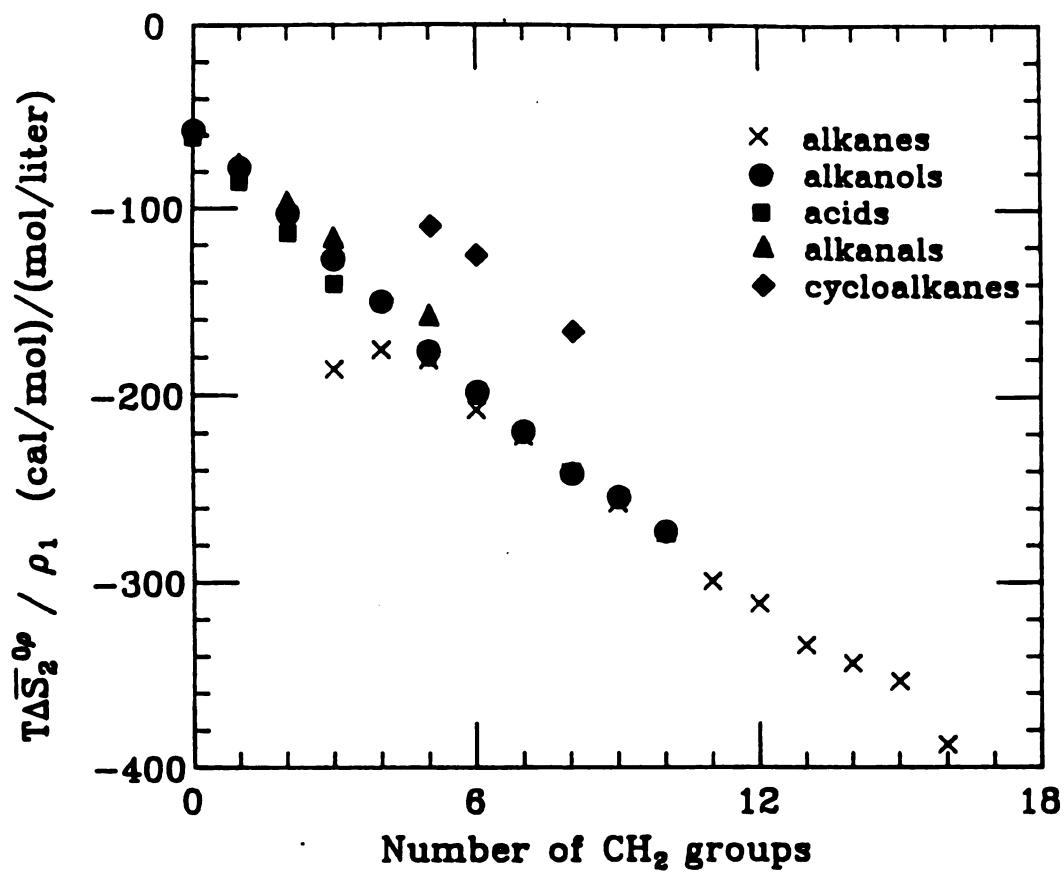


Figure 33. Experimental data for Xe in 37 solvents. $T\Delta\bar{S}_2^*$ divided by solvent number density vs. number of CH₂ groups.

Table XI. Empirical Energy parameters for Xe solubility in 37 organic solvents.

Group	Energy contribution (25°C) (cal/mol)/(mol/liter)		
	ϵ_{μ}	ϵ_H	ϵ_{TS}
CH ₂ (lin)	-7.45	-28.02	-20.36
CH ₃	-47.67	-99.01	-50.21
OH	+18.41	+ 4.64	-14.89
COOH	+10.16	- 9.57	-20.86
CHO	+ 7.22	+ 3.02	- 5.32
CH ₂ (cycl)	- 2.98	-22.09	-19.11

Table XII. Predicted vs. experimental values of Ostwald solubility for ¹³³Xe in selected organic solvents at 25.0°C.

Solvent	Predicted L (25°C)	Experimental L (25°C)
n-C ₁₂ H ₂₆	3.50	3.39
n-C ₇ H ₁₃ OH	2.42	2.44
n-C ₄ H ₉ COOH	2.52	2.70
n-C ₄ H ₉ CHO	2.69	2.99

groups in the solvent molecule. For these quantities, as on Figure 31, the curve for alkanes, alkanols, carboxylic acids, and alkanals, are approximately parallel straight lines. One obtains the enthalpic contribution ϵ_h for each of the six component functional groups by a similiar analysis as for ϵ_μ . The values of ϵ_h obtained in this way are given in the middle column of Table XI. The formula by which one constructs $\Delta\bar{h}_2^*$ is, say for the same alkanol as in equation (7.1):

$$\Delta\bar{h}_2^*(\text{est}) = \rho_1 \left[\epsilon_h(\text{CH}_3) + m\epsilon_h(\text{CH}_2, \text{lin}) + \epsilon_h(\text{OH}) \right] . \quad (7.2)$$

The $\Delta\bar{h}_2^*$ values predicted by equation (7.2) are averages over the experimental temperature intervals; nominally they correspond to about 25°C.

Figure 33 shows values for the average entropy obtained from our solubility measurements. The ordinate is $T\Delta\bar{s}_2^*/\rho_1$. It has been multiplied by the average temperature $T=298.15$ K so that the ordinate's dimensions will be (cal/mol)/(mol/liter) the same as on Figures 31 and 32. The componental entropy contributions ϵ_{TS} are shown on table V for the six functional groups. Values of ϵ_{TS} were obtained by applying to the data on Figure 33 the same technique as before. The formula by which one constructs $\Delta\bar{s}_2^*$ from these componental contributions is:

$$\Delta\bar{s}_2^*(\text{est}) = \rho_1 / T_{298} \left[\epsilon_{TS}(\text{CH}_3) + m\epsilon_{TS}(\text{CH}_2, \text{lin}) + \epsilon_{TS}(\text{OH}) \right] , \quad (7.3)$$

for the same solvent as in equations (7.1) and (7.2).

Finally, one may estimate the temperature dependence of $\Delta\mu_2^*$, over the temperature intervals near those for which the original data apply, from:

$$\Delta\mu_2^*(T, \text{est.}) = \Delta\bar{h}_2^*(\text{est.}) - T\Delta\bar{s}_2^*(\text{est.}) \quad (7.4)$$

In applying this equation, one uses equations (7.2) and (7.3) along with ϵ_h and ϵ_{TS} values in Table XI, and one obtains an estimate of solubility $L(T)$ for Xe in whichever solvent that has been reconstructed.

As a test of the ability of equations like (7.1) to predict Ostwald solubility, we show on Table XII a comparison between predicted and experimental values for five solvents, each chosen from about the middle of its series. The predictions are obtained from $L(25^\circ\text{C}) = \exp[-\Delta\mu_2^*(\text{est.}/RT_{298})]$. The predicted values of $L(25^\circ\text{C})$ are within 12% of the experimental values for all of our solvents with two or more CH_2 groups. The probable explanation for deviations at low carbon number is that the solvents are becoming more ordered and the correlation function begins to change rapidly at short chain length.

The above test is largely one of consistency rather than predictability. But if suitable data were available, one could test whether our ϵ_μ values could be used to predict Xe solubility in, say, dicarboxylic acids, polyalcohols, and

other solvents.

Finally, Figure 34 shows a plot of $(\Delta\mu_2^* - g_{cav})/\rho_1 = g_{int}/\rho_1$ verses number of CH_2 groups. An extrapolation of the cycloalkane data to zero CH_2 groups gives $g_{int} = 0$, as one would expect. We note for completeness that the straight line fits are somewhat better than those in Figure 31.

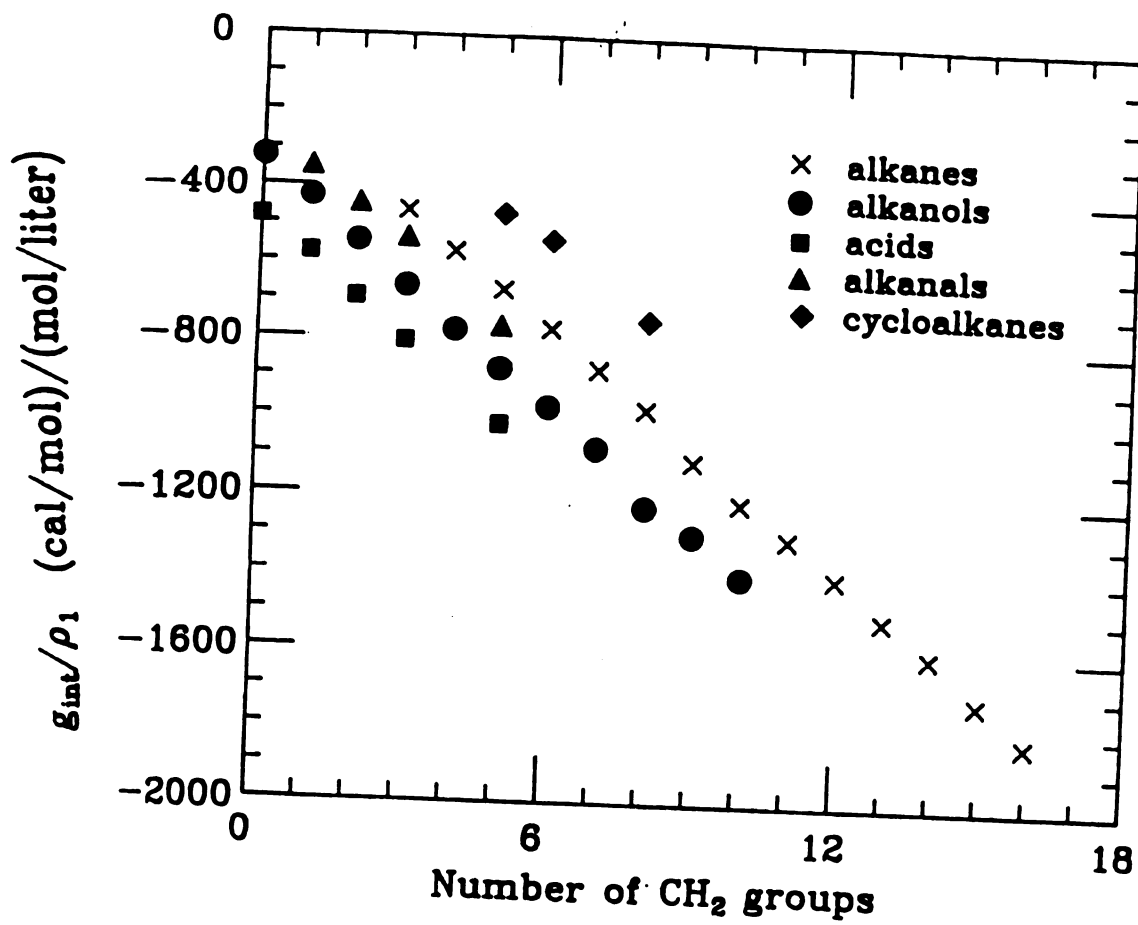


Figure 34. g_{int}/ρ_1 vs number of CH₂ groups for Xe in 37 solvents.

8. Conclusions

In conclusion we discuss briefly how this work can be used to predict and understand solubility data and what further experimental and theoretical work would be useful towards these ends.

The empirical results associated with Table XI and Figures 31,32,33 are suggestive but need testing on other systems before they can be relied on for predictions. Some other C-, H-, and O-containing solvent functional groups for which the values of ϵ_{μ} , ϵ_h , and ϵ_{TS} would be interesting are, e.g. phenyl and its derivatives, carbonyl,alkoxy, etc. If solubility predictions from these prove to be robust one could extend the technique to find contributions of groups containing other elements, say halogens, N, S, etc.

A parallel direction for empirical development is solubility of other inert gases and, beyond that, gases that are isoelectronic, or nearly so, to inert gases, etc. We anticipate that the ϵ_{μ} 's, ϵ_h 's, and ϵ_{TS} 's empirically found for different gases with respect to a single solvent functional group would be simply related to the Lennard-Jones potential parameters of the solutes.⁷¹

Finally there is some indication that the mixed experimental-theoretical term $(-RT\ln L - g_{cav})/\rho_1$, which according to equation (6.54) equals g_{int}/ρ_1 , is meaningful for empirical and analytic purposes. As more data become

available, its use for quantitative predictions can be explored.

There are several interesting reasons why analytical approaches to these data are difficult. In the following paragraphs I would like to summarize some of our observations on this topic.

The quantities which currently lend themselves to theoretical analysis are the free energy of cavity formation, g_{cav} , and its associated enthalpy, h_{cav} , and entropy, s_{cav} , and the energy of interaction u_{int} .

Scaled particle theory provides a formal procedure by which one may calculate g_{cav} . There are several alternative theories which predict cavity free energies most notable of which is the surface tension theory of Sinanoglu.⁸⁵ This approach requires a calculation of the surface energy associated with cavity formation in a solvent. The surface tension's contribution is modified to take into account the microscopic cavity size. Recent reviews have shown that this theory tends to predict cavity energies which are too high, and is inconsistent with pure liquid heat of vaporization data.⁷² In earlier papers we tested it on the perfluoralkanes and found cavity energies to be 2.5 times higher than the SPT prediction.⁶⁵ The general consensus is that Sinanoglu's theory can be used to get rough approximations of the cavity terms but SPT is much preferred when the parameters necessary to apply the later are known or can be evaluated.⁷²

Boublik et al. have developed a version of the SPT for nonspherical hard molecules; such as spherocylinders (cylinders with spherical endcaps) and other convex bodies.⁸⁶ At first this may seem like a better alternative to describing solubility in alkanes, unfortunately, this theory cannot yet account for mixtures of particles of different shapes.¹⁴ More work in this direction may prove to be useful.

Although scaled particle theory may be well suited to predict cavity energies there are restrictions to its application. The solute should be as hard and spherical as possible and must not have strong directional interactions with the solvent molecules. An example of an inappropriate (but important) solute would be a protein, for which a cavity would be an ill defined quantity. The solvent can be any real liquid. However, the effective solvent diameter, a_1 , must be determined with great accuracy. For nonpolar solvents one can evaluate a_1 from heat of vaporization data through equation (6.87). For polar solvents this equation is invalid and one usually has to use solubility data to evaluate a_1 .⁷¹

The fact that the SPT works at all is actually quite amazing and is probably the result of many errors that cancel each other out. This means that we should be cautious when looking at higher order terms; i.e., the enthalpy and the entropy. We have demonstrated that the SPT does not predict the entropy of solvation. This is contrary

to previous thought. The reason this has gone unnoticed in the past is because most workers choose the mole fraction scale.^{55,74} The chemical potential on the mole fraction scale is determined from [equation (8) from ref.55]:

$$\Delta\mu_2 = -RT\ln x_2 = \Delta\mu_2^* + RT\ln(RT/v_1) \quad , \quad (8.1)$$

where v_1 is the molar volume of the solvent. To find the corresponding entropy we take the derivative with respect to temperature:

$$\Delta s_2 = \Delta \bar{s}_2^* - R + RT\alpha_\ell - R\ln(RT/v_1) \quad . \quad (8.2)$$

The extra terms in equation (8.2) are usually much larger than $\Delta \bar{s}_2^*$ but they have no physical interpretation. For example, for Xe in hexane we have $\Delta \bar{s}_2^* = -4.4$ cal/mol K, but $\Delta s_2 = -15.8$ cal/mol K. This excess pseudo-entropy serves to mask the deficiencies in s_{cav} ; i.e., instead of predicting $\Delta s = s_{SPT} = 0.29$ cal/mol K, we would say $\Delta s = s_{SPT} + s_{pseudo} = -11.1$ cal/mol K, which doesn't look so bad when compared to Δs_2 . This does not necessarily mean that the SPT is wrong; it is possible that the rest of the entropy could be in the interaction term, g_{int} .

To settle these many questions one must turn to computer simulations. Using equation (6.36) we obtain :

$$-RT\ln L = \int_0^1 U(\xi) d\xi \quad , \quad (8.3)$$

Swope and Andersen⁴¹ have used molecular dynamics to evaluate (8.3) for inert gases in water. The idea is to run your simulation and gradually couple a solute particle into the solvent. This is done by turning on the solute-solvent potential in a stepwise manner as suggested by Eq. (8.3) and calculating the coupling energy, $U(\xi)$, at each value of ξ until the particle is fully coupled. One can then integrate the smoothed results to obtain the excess chemical potential. Once the particle is fully coupled it is possible to calculate the entropic contribution to the free energy by simply subtracting off the energetic part; i.e.

$$\Delta\mu_2^* = \int_0^1 U(\xi) d\xi \approx U(\xi=1) - T\Delta\bar{s}_2^* . \quad (8.4)$$

Jorgensen¹ has developed interaction site potentials which predict the properties of pure alkanes and pure alkanols. These are potentials in which the molecule is represented by a set of discreet interaction sites that are commonly, but not invariably, located at the sites of the atomic nuclei. For the alkane potentials Jorgensen has used the various functional groups as the interaction sites. These have also been used to predict the solubility of various alkanes and alkanols in water.⁸⁷ While this data is certainly valuable one must note that solubility in water is a much more complicated process than in nonpolar solvents due to the complex structure of liquid water. In principle

it is possible to do the same calculation for inert gases in alkanes and alkanols and maybe other solvents.

By carefully choosing the way the solute - solvent potential is coupled it may be possible to gain insight into how repulsive and attractive interactions affect the solvation entropy. This in turn would clarify the deficiencies in analytic models and help us to correct them.

To complete our experiment it would be interesting to look at Xe solubility in the lighter alkanes, i.e.; ethane, propane, butane and methane (despite the fact that methane's boiling point is lower than xenon's at 1 atm. The trick is that by using a tracer the solute gas is so dilute that it will not condense until a significantly lower temperature⁷⁷). These are simpler solvents and thus may help bridge the gap in our understanding of solubility. Also, our experimental technique offers a unique advantage over other cryogenic experiments in that we can easily measure solubility in the limit of infinite dilution.^{89,90} This makes the subsequent analysis much easier since one can neglect solute-solute interactions.

Our technique may also prove to be useful in analyzing solubility near the solvent's critical point (we again have an advantage over other methods since we can ignore solvent vapor pressure effects). A great deal of recent work has been along the lines of gas solubility near the critical temperature of water⁹¹; performing complementary experiments on non-polar and polar systems such as ours could prove to

be very enlightening.

9. Introduction: Solubility of Nonpolar Gases in Water at Elevated Pressure.

This section of my thesis reports solubility measurements of the gases nitrogen, argon, krypton, and xenon in water. For each of these gases we measured, at 25.0°C, the dependence of gas solubility on partial pressure of the solute. The pressure ranges studied were approximately: 44-116 atm for N₂, 22-101 atm for Ar, 33-81 atm for Kr, and 5-48 atm for Xe. The data are analyzed in terms of molecular theories based on thermodynamics, and statistical mechanics. These experiments are an extension of previous work on Xe solubility in organic liquids and aqueous solutions.^{17,92}

The study of gas solubility in liquids is an old and well developed subject in chemistry and physics. For dilute solutions at sufficiently low pressure, the mole fraction solubility, x_2 , is well described by Henry's Law⁹³:

$$P_2 = k_H x_2 \quad (9.1)$$

where P_2 is the partial pressure of the solute gas and k_H is a constant of proportionality. The so called Henry's constant, k_H , is characteristic of the solute-solvent system

at a given temperature. At higher pressures Eq.(9.1) must be modified to account for nonideality of the vapor. Lewis⁹⁴ introduced a new form of Henry's Law in which the solute partial pressure is replaced by its corresponding fugacity; $f_2 = k_H x_2$. At still higher pressures the measured solubility fails to obey this relation as well. It shall be shown that by measuring deviations from Henry's Law one can obtain information on the solvation process.

The importance of understanding the effects of pressure on gas solubility comes from its many applications. At an industrial level, extraction and separation processes are often performed at elevated pressure. In biology and medicine, interactions of inert gases with living organisms are also important. For example, the gas mixtures breathed at high pressure in deep sea diving consist mainly of inert gases. Interactions between these gases and the diver are responsible for decompression sickness and inert gas narcosis.^{10,95} Solubility limited phenomena are also relevant in marine biology. Several species of deep water fish have swim bladders in which partial pressures of nitrogen up to 10 atmospheres have been observed.⁹⁶ In order to determine the mechanisms used by the fish to inflate its swim bladder, it is important to know the concentrations of dissolved gases available at a given depth. Such variation is generally determined by the hydrostatic pressure.

Another motivation for this research is to look at the

role of hydrophobic effects on gas solubility. Hydrophobic interactions are important for understanding the stability of biologically important macromolecular structures. Hydrophobic effects are thought to play a key role in protein conformation and enzyme specificity.^{97,98} Several experimental studies have investigated the behavior of simple polar and nonpolar organic solutes in water.^{99,100} Inert gases would in some sense be the prototypical hydrophobic solutes because their interactions with water are very weak compared to those of water with itself.

The inert gas elements have been studied extensively as prototype solids,^{77,78} liquids, and gases, so many of their interactions are well known. The low pressure solubility of these gases in water have also been determined accurately.^{6,32} With the advent of improved analytic^{73,101} and computational^{41,102} techniques it has become possible to predict these solubilities with good accuracy. By providing data in different ranges of temperature and pressure one can test the robustness of these theoretical predictions and make appropriate refinements.

10. Experimental

The two most common units of gas solubility are the Ostwald (L) and mole-fraction (x_2) solubilities. They are defined as:

$$L = \frac{\rho_2^l}{\rho_2^g} \quad \text{and} \quad x_2 = \frac{n_2}{n_1+n_2} \quad . \quad (10.1)$$

Ostwald solubility is the ratio, at equilibrium, of the concentration of dissolved gas molecules in the liquid solvent to their concentration in the gas phase. The mole-fraction solubility is the equilibrium fraction of solute molecules in the solvent. In recent literature measurements in terms of the Ostwald solubility are characterized as being on the 'number density scale'.¹⁴

Figure 35 shows a schematic of the experimental apparatus. The Figure is divided into two parts to show each step in the measurement process. First the liquid is saturated with the solute gas at high pressure as depicted in 35a. Once equilibrium is attained the liquid is isolated and the sample cell is transferred to the analysis system, 35b, where the amount of dissolved solute in the pressurized liquid is determined. Together, this

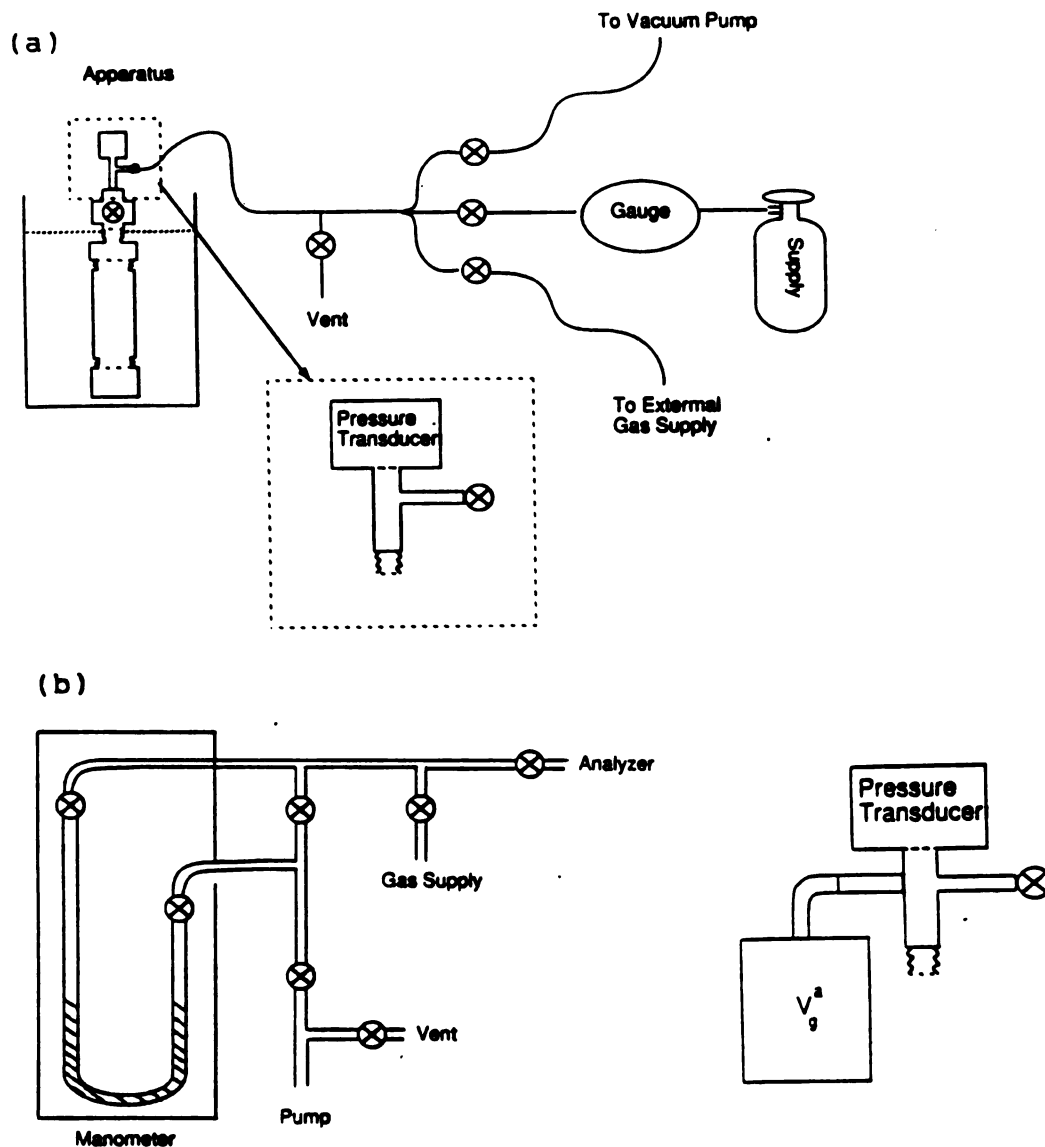


Figure 35. Schematic of experimental setup
 (a) high pressure equilibration system (b)
 analysis system.

constitutes a modified Van Slyke method¹⁰³ in which the sample volume is the entire liquid volume. Our technique is different from Van Slyke's in that it allows us to measure directly the mole -fraction solubility, Ostwald solubility, and partial molar volume.

We briefly outline some experimental details below. The sample cell is a 100cm³ stainless steel volume with a ball valve to isolate the liquid and allow for easy transfer between the equilibration and analysis stages of the experiment. The solute gases we used were obtained commercially. Their purities were: N₂(99.99%), Ar(99.998%), Kr(99.997%), and Xe(99.996%), (N₂, Kr, Xe from Linde Gas Products, Ar from Matheson Gas Products).

At the beginning of the experiment we load the sample cell with twice distilled water which has been degassed using standard methods. The water is loaded under vacuum to prevent air pockets from forming. The cell is weighed and the mass of the water, after making proper buoyancy corrections for the weight of displaced air, is denoted m_0 . To help prevent gas spaces from developing in the cell upon liquid compression we add some extra water above the ball valve. The mass of the additional water is Δm^+ . The cell is then connected to gas volume V_g and pressurized. Mixing is achieved with a specially designed magnetic stirrer. Gas pressure is monitored with an accurate capacitive transducer (Setra Systems), and a pressure gauge (Heise Inc.) for calibration. The sample cell and gas volume are submerged

throughout the entire experiment in a constant temperature water bath at $25.0 \pm 0.1^\circ\text{C}$.

After some time, typically 2-3 days depending on stirring speed and solubility, the pressure readings reach a steady state. To be sure that equilibrium is attained we monitor the pressure for an extra 8-12 hours. At this point we record the final pressure of the solute gas, P_{eq} , and the ball valve on the sample cell is closed. The gas volume is then slowly depressurized. Excess liquid above the ball valve is collected and weighed. This mass is denoted Δm^- . The water remaining in the sample cell is now:

$$m_{\text{H}_2\text{O}} = m_0 + \Delta m^+ - \Delta m^- \quad . \quad (10.3)$$

The analysis system as illustrated in Fig. 35b consists of a detachable gas volume, V_g^a , with a pressure transducer and mercury manometer. The gas volume is variable in the sense that different sized cells can be attached to the side arm of the analyzer. We choose the gas volume such that the pressure of the evolved solute will be within the optimum range of our sensing devices. This pressure can be estimated via Henry's Law with well known low pressure solubility data.^{6,32} For the solute gases and pressure ranges in this experiment we used two analyzer volumes, namely: $\approx 180\text{cc}$ (N_2 and Xe) and $\approx 360\text{cc}$ (Ar, Kr, and Xe). To measure the amount of solute in the saturated liquid we connect the sample cell to the analyzer and evacuate the

upper volume. The main valve is then opened thus releasing the dissolved gas into V_g^a shown in Fig. 35b. With stirring a steady value of pressure is usually reached within 2-6 hours. The final pressure of the solute gas in the analyzer, P_a , is found after correcting for the vapor pressure of the water.⁷⁹

To calculate the mole-fraction and Ostwald solubilities we first must find the density of the solute gas, $\rho_2^g(P)$, at P_a and P_{eq} . Accurate virial expansions were used in the appropriate pressure ranges for N_2 ,¹⁰⁴ Ar,¹⁰⁵ Kr,¹⁰⁶ and Xe.¹⁰⁷ One can then find the number of moles of gaseous solute in the analyzer to be:

$$n_2 = \rho_2^g(P_a) [V_g^a + V_g^{(2)}] , \quad (10.4)$$

where $V_g^{(2)}$ is the extra gas volume that arises from the decompression and outgassing of the pressurized liquid. Assuming the low pressure liquid density is that of pure water we have:

$$V_g^{(2)} = V_{cell} - m_{H_2O} / \rho_{H_2O}(25.0^\circ C) , \quad (10.5)$$

where V_{cell} is the volume of the sample cell and m_{H_2O} is defined in Eq.(10.3). To find the total number of moles of solute we must also account for any remaining in the liquid. Adding this correction we find for the total amount of solute in the sample cell at P_{eq} :

$$n_{2,\text{total}} = \rho_2^g(P_a) \left[[V_g^a + V_g^{(2)}] + L^o(m_{H_2O}/\rho_{H_2O}) \right] , \quad (10.6)$$

where L^o is the low pressure limit of the Ostwald solubility at 25.0°C.^{6,32} The number of moles of water in the sample cell, n_1 , is the mass of the water divided by the molecular weight, i.e., $n_1 = m_{H_2O}(g)/18.01534(g/mol)$. One can then easily calculate the mole fraction solubility from Eq.(10.2). At the equilibrium pressure P_{eq} the liquid volume is fixed to be that of the sample cell, therefore the number density of solute molecules in the liquid is $\rho_2^l = n_{2,\text{total}}/V_{\text{cell}}$. Dividing this quantity by the gas number density at P_{eq} one obtains the Ostwald solubility, L , as given in Eq.(10.2). One may also use this technique to obtain a rough estimate of the solute molar volume by:

$$\bar{v}_2 \approx \left[V_{\text{cell}} - [m_{H_2O}/\rho_{H_2O}(25\text{ C}^\circ, 1\text{ atm})] \exp(-x(P_{eq} - P_a)) \right] / n_2 , \quad (10.7)$$

where x is the isothermal compressibility of pure water,¹⁰⁸ $x = 4.57 \cdot 10^{-5} \text{ atm}^{-1}$, and n_2 is given by Eq.(4). Essentially this expression means that if we take V_{cell} , the known volume of the pressurized liquid, and subtract off a term due to liquid compression then the remaining volume, which is in the square brackets of Eq.(10.7) is due to the solute molar expansion. Dividing this by the amount of solute in the liquid gives the molar expansion produced per mole of

solute added, i.e., \bar{v}_2 . Since our solutions are very dilute, typically $x_2 \approx 10^{-4}$, we assume in this development that the density is the same as for pure water. This assumption is also supported by the fact that our results agree fairly well with literature values.^{109,110}

We stress that the strength of this technique is that by fixing both the sample volume and mass, one may easily find the Ostwald solubility and the molar volume. Other methods usually sample only a known mass of saturated liquid and therefore are limited in that they measure only mole fraction directly. Separate measurements are then needed to calculate the solubility on the number density (Ostwald) scale. It has been argued that the number density scale has certain advantages over the mole fraction scale in analyzing results from a statistical mechanics perspective.⁹⁹ The primary weakness of our current technique is that the measurement takes a relatively long time. A better alternative would be to use small samples of fixed volume from a large reservoir of equilibrated liquid.^{111,103} This is a more traditional approach with the important addition that we know the sample volume at P_{eq} .

11. Results

The experimental results we obtained are shown in Table XIII. The first column gives the pressure at which the measurement was made, the second column gives the corresponding fugacity. The third and fourth columns tabulate solubilities on the mole fraction and number density (Ostwald) scale respectively. We also include the average value obtained for partial molar volume of the solute. The fifth and sixth columns give the data in terms of a new solubility parameter which will be discussed below. Judging from reproducibility and by comparison with other data^{6,112} a conservative estimate of our fractional uncertainty in solubility is about 1-1.5%. The primary sources of error are pressure measurement (± 2.0 psi for high pressure, ± 0.5 Torr for low pressure), volume measurement ($\pm 0.1\%$ reproducibility), and microbubble formation in the pressurized liquid. The first two terms lead to an uncertainty of less than 0.2% so it seems that the last term is the main contributor.

Fugacities were calculated from volumetric properties of the real gas via²⁰:

$$f = p \exp \left[\frac{1}{RT} \int^p \left[v(p') - \frac{RT}{p'} \right] dp' \right] \quad (11.1)$$

The integral in Eq. (11.1) measures the cumulative deviation of the real gas volume, $v(p')$, from that of the corresponding ideal gas at pressure p' . To obtain $v(p')$ we used the virial expansions referred to in the previous section.¹⁰⁴⁻¹⁰⁷ The fugacity is related to the chemical potential per mole of the gas by¹²⁶:

$$\mu_2^g = RT \ln \left(\frac{f_2 \Lambda^3}{k T} \right) , \quad (11.2)$$

where f_2 is in atmospheres and $k = R/N_A = \text{cm}^3\text{-atm/molecule-}^\circ\text{K}$ and $\Lambda = h/(2\pi mkT)^{1/2}$ is the thermal wavelength of the solute.¹⁶

Figure 36 shows a plot of the equilibrium fugacity versus mole-fraction solubility for our data. Also included is data for N_2 in water at 25.0°C from Ref.(112). As one can see, the agreement with our measurements is good. The curves in Fig. 36 have the common feature that the mole-fraction solubility increases approximately linearly with fugacity. Table XIII shows that the Ostwald solubility tends to decrease with f_2 . If the system was in complete accord with Henry's Law we would expect the quantity $k_H = f/x_2$ to be constant for each gas. Figures 37(a-d) show such plots with respect to solute concentration. For N_2 , Ar, and Kr there is a clear increase in k_H by as much as 7-10% in the concentration range studied. For xenon there appears to be very little variation in k_H . A problem that we encountered with xenon was that above a pressure of 17

atmospheres the solubility decreased rapidly and the molar volume increased to about $125\text{cm}^3/\text{mole}$. The data point from Table XIII at 23.33 atm seems to be anomalous in the sense that the solubility has decreased sharply, compared with lower pressures, but we did not see a large molar expansion. We associate this effect with the onset of clathrate formation.¹¹³ This speculation was confirmed in separate experiments with xenon-water mixtures at $P_{\text{eq}} > 30$ atm. Instead of subjecting the equilibrated sample to analysis we quickly depressurized the cell and pour the liquid into a beaker. Several ice-like crystals, as large as 5mm in diameter, were observed. These melted away within minutes. We have included on Table XIII the solubility measured during the clathrate phase but we are not sure that the results are reliable since it is known that this is a glassy state which may require very long equilibration times.¹¹³ It might be worthwhile to repeat our low pressure xenon measurements because the pressure ranges we explored were at the lower end of our sensing accuracy. Our technique using radioactive tracers which would be useful toward this end.¹⁸

Table XIII. Experimental results for solubility of N_2 , Ar, Kr, and Xe in water at 25.0°C. The second column is the solute partial pressure. The third column is the solute fugacity. The fourth and fifth columns are the mole-fraction and Ostwald solubilities respectively. The sixth column is the new solubility parameter γ . The seventh column is the excess chemical potential of the solute in the liquid. The eighth column is the experimental average value of partial molar volume.

Solute	P(atm)	f_2 (atm)	x_2 ($\times 10^4$)	L	γ	τ_{21}^E (cal)	\bar{v}_2 (cm ³ /mol)
N_2	44.55	44.25	4.902	0.01485	0.01501	2488	
	50.46	50.10	5.482	0.01468	0.01484	2495	
	63.68	63.17	6.809	0.01448	0.01463	2503	
	77.28	76.63	8.100	0.01423	0.014355	2514	31 \pm 2
	93.30	92.54	9.562	0.01397	0.014045	2527	
	102.19	101.38	10.32	0.01380	0.01383	2536	
	115.80	114.99	11.46	0.01360	0.01356	2548	
	Ar	22.505	22.190	5.428	0.0322	0.0331	2019
	25.50	25.01	6.136	0.0321	0.0331	2019	
	38.12	37.24	8.993	0.0313	0.0327	2026	
	44.38	43.20	10.36	0.0309	0.0325	2030	
	55.95	54.11	12.81	0.0301	0.0321	2038	33 \pm 1
	68.88	66.15	15.41	0.0292	0.0316	2047	
	71.67	68.73	16.08	0.0293	0.0317	2044	
	79.19	75.65	17.43	0.0287	0.0313	2053	
	87.90	83.61	19.06	0.0282	0.0309	2059	
	101.27	95.70	21.59	0.0276	0.0306	2065	
Kr	33.30	31.01	13.45	0.0508	0.0588	1679	
	40.64	37.26	15.91	0.0485	0.0579	1688	
	41.16	37.69	16.22	0.0481	0.0583	1683	
	52.14	46.64	20.03	0.0463	0.0582	1685	30 \pm 2
	58.88	51.93	21.53	0.04345	0.05625	1705	
	69.73	60.08	25.13	0.0417	0.0567	1700	
	80.58	67.91	27.87	0.0391	0.0556	1712	
	80.68	67.99	27.79	0.0389	0.0554	1714	
Xe	4.791	4.669	3.592	0.0994	0.1041	1340	
	6.344	6.103	4.716	0.0982	0.1046	1338	
	8.151	7.800	5.979	0.0950	0.1038	1342	
	9.415	8.947	6.930	0.0950	0.1048	1336	47 \pm 2
	11.25	10.58	8.089	0.0917	0.1034	1345	
	12.10	11.33	8.750	0.0915	0.1045	1338	
	14.69	13.55	10.36	0.0880	0.1034	1345	
	15.74	14.44	11.035	0.0869	0.1034	1345	
	Xe	23.33	20.48	13.60	0.068	0.090	1428
	32.78	27.19	17.48	0.057	0.0864	1451	117
	33.29	27.52	17.62	0.057	0.0859	1454	125
	47.89	35.99	21.17	0.040	0.079	1506	131

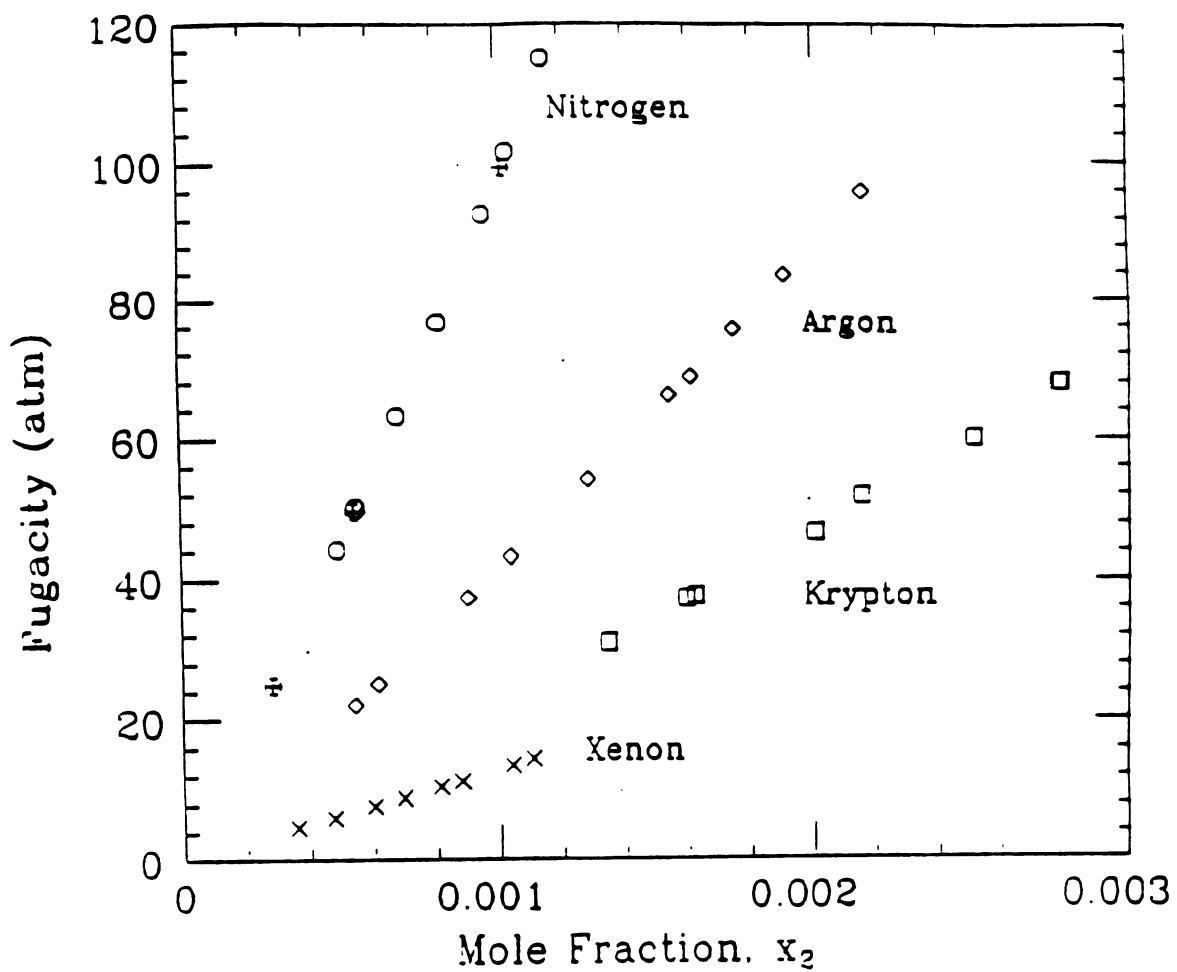


Figure 36. Solute fugacity vs mole-fraction solubility at 25°C.

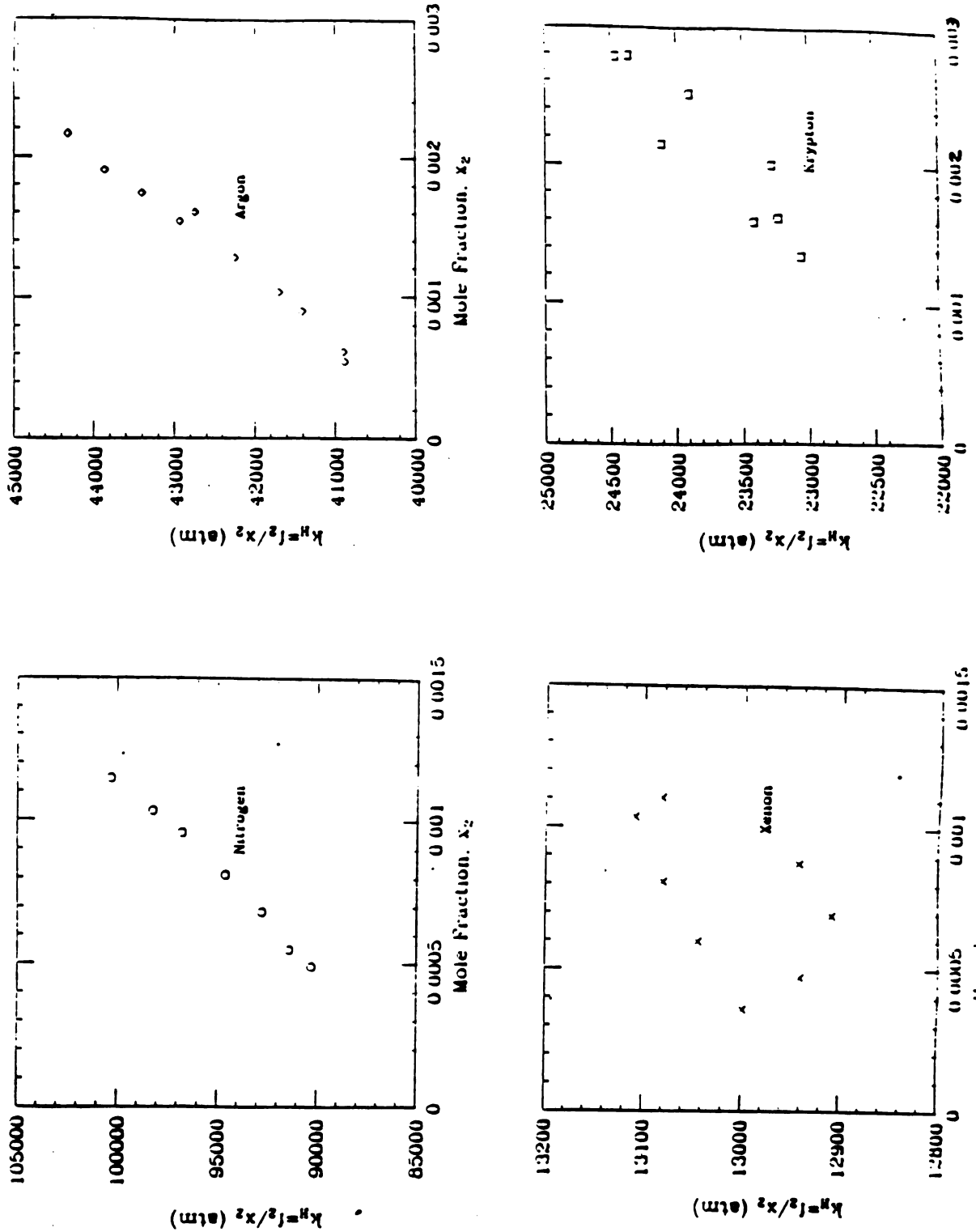


Figure 37. Henry's constant vs mole-fraction solubility at 25°C.

12. Pressure and Concentration Dependence

Deviations in Henry's Law, such as those shown by our data, are best analyzed in terms of the solute chemical potential. In our experiments the vapor pressure of the solvent, $P(\text{H}_2\text{O}, 25^\circ\text{C}) \approx 23.76$ torr, was small compared to the solute gas pressures and can be ignored. The chemical potential per mole of gaseous solute can then be written as:

$$\mu_2^g(T, P) = \mu_2^\phi(T) + RT \ln \left[\frac{f_2(T, P)}{P^\phi} \right] , \quad (12.1)$$

where $\mu_2^\phi(T)$ is the standard chemical potential of the gas at temperature T and pressure P^ϕ . The choice of reference pressure is such that the gas behave ideally at P^ϕ . We shall follow the usual convention and set P^ϕ equal to 1 atm.^{20,22} This expression for μ_2^g is identical to Eq.(12.1) but will prove to be easier to work with in subsequent discussions.

The chemical potential of the solute in the liquid, μ_2^l , is completely described by the variables T, P , and x_2 . At constant T one may express the differential change in μ_2^l as

114.

$$(d\mu_2^1)_T = \left(\frac{\partial \mu_2^1}{\partial x_2} \right)_{P,T} dx_2 + \left(\frac{\partial \mu_2^1}{\partial P} \right)_{x_2,T} dP . \quad (12.2)$$

To understand how μ_2^1 depends on solute concentration we use the Kirkwood-Buff (KB) solution theory.¹¹⁵ This is an exact formal treatment in which the solution properties are obtained from integrals over pair correlation functions. For two components the KB integral is defined as:

$$G_{ij} = \int_0^\infty [g_{ij}(r) - 1] 4\pi r^2 dr , \quad (12.3)$$

where $g_{ij}(r)$ is the orientationally averaged pair correlation function between species i and j , and depends only on intermolecular separation r . To relate these quantities to $\mu_2^1(T, P, x_2)$ we use Eq. (22) of Ref. (115):

$$\frac{1}{RT} \left(\frac{\partial \mu_2^1}{\partial x_2} \right)_{P,T} = \frac{1}{x_2} + \frac{\rho_1 (2G_{12} - G_{11} - G_{22})}{1 + \rho_1 x_2 (G_{11} + G_{22} - 2G_{12})} , \quad (12.4)$$

where ρ_1 is the molar concentration of the solvent. For dilute solutions Eq. (12.4) can be expressed in terms of the infinite dilution limits of the molar volumes and solvent isothermal compressibility, κ_1 ²⁶:

$$\frac{1}{RT} \left(\frac{\partial \mu_2^1}{\partial x_2} \right)_{P,T} = \frac{1}{x_2} + \frac{1}{v_1^0} \left(-G_{22} + v_1^0 - 2v_2^0 + RTx_1^0 \right) + O(x_2)^2 . \quad (12.5)$$

Throughout this thesis we use the superscript 0 to refer to the infinite dilution limit. Integrating Eq. (12.5) and keeping terms to first order in x_2 yields ¹¹⁶:

$$\mu_2^1(x_2, T, P) = \mu_2^0(T, P) + RT \ln x_2 + x_2 \xi(T) + O(x_2)^2 , \quad (12.6)$$

where

$$\xi(T) = RT(-G_{22} + v_1^0 - 2v_2^0 + RTx_1^0)/v_1^0 , \quad (12.6a)$$

and $\mu_2^0(T, P)$ is a constant of integration.

The KB integral, G_{22} , plays an important role in determining the concentration dependence of the chemical potential. It is a measure of correlations among solute particles in solution. This can be illustrated by multiplying G_{22} by the solute concentration ρ_2 :

$$\rho_2 G_{22} = \int_0^\infty \rho_2 [g_{22}(r) - 1] 4\pi r^2 dr . \quad (12.7)$$

This quantity reflects the total average excess (or deficiency) of solute molecules surrounding a fixed solute

with respect to a uniform distribution.⁹⁹ For example, if G_{22} is positive the solute molecules are more correlated than if they were distributed randomly. This sort of solvent induced clustering in aqueous solutions is commonly referred to as a hydrophobic interaction.⁹⁷ An exaggerated example of such a situation would be micelle formation in detergent solutions.¹¹⁷ A driving force in this example is the fact that the detergent has both polar and nonpolar regions which compete to minimize the free energy. The resulting conformation is that solute molecules cluster together with polar regions in contact with the water and the nonpolar regions in contact with each other. This sort of mechanism plays a vital role in biological process such as membrane formation and protein conformation.¹¹⁸ It is not obvious that such mechanisms should come in to play for nonpolar gases, particularly those we have studied, since these solutes have little structure, i.e., the solutes are mono- or di- atomic and cannot be divided into polar and nonpolar regions. It has been shown however that solvent induced interactions can lead to clustering in hard sphere mixtures where there are no attractive interactions at all.¹¹⁹

A more familiar occurrence of G_{22} is through its relation to the osmotic pressure of a solution. By analogy to the virial expansion for real gases one can show that the osmotic pressure (Π) of a two component solution obeys an equation of the form²²:

$$\Pi/RT = \rho_2 + B_2^* \rho_2^2 + B_3^* \rho_2^3 + \dots \quad (12.8)$$

The second osmotic virial coefficient of the dissolved solute is ¹²⁶:

$$B_2^* = - \frac{1}{2} G_{22} \quad (12.9)$$

The value of B_2^* is frequently used in statistical theories of polymer configurations as a measure of the interactions between segments along the polymer chain. ¹²⁰

The pressure dependence of the chemical potential is described by the well known thermodynamic relation ²⁰:

$$\left(\frac{\partial \mu_2^1}{\partial P} \right)_{n_1, T} = v_2 \quad (12.10)$$

where v_2 is the molar volume of the solute in the solvent. Applying this to Eq. (12.6) allows us to evaluate μ_2^\ominus as:

$$\mu_2^\ominus = \int_0^P v_2(P') dP' + C(T) \quad (12.11)$$

where C is an integration constant which depends only on temperature. If the solution is well below the critical temperature of the solvent, the molar volume is weakly dependent on pressure and can be taken outside the

integral.¹²¹ We then substitute its value at infinite dilution, v_2^0 . Putting this result in Eq. (12.6) gives:

$$\mu_2^1 = C(T) + v_2^0 P + RT \ln x_2 + x_2 \xi(T) + O(x_2^2) \quad (12.12)$$

The equilibrium condition between the vapor and the liquid is $\mu_2^g = \mu_2^l$. Using Eq.(12.1) for μ_2^g and Eq.(12.12) for μ_2^l gives:

$$\mu_2^\phi(T) + RT \ln \left[\frac{f_2(T,P)}{x_2 P^\phi} \right] = C(T) + P v_2^0 + x_2 \xi(T) + O(x_2^2). \quad (12.13)$$

In the limit of low pressure and infinite dilution the bracketed term on the left hand side of Eq.(12.13) reduces to Henry's constant k_H^0 , so that one may evaluate $C(T) - \mu_2^\phi(T) = RT \ln(k_H^0)$. This leads to the desired result:

$$RT \ln \left[\frac{f_2(T,P)}{x_2 P^\phi} \right] = RT \ln(k_H^0) + P v_2^0 + x_2 \xi(T) + O(x_2^2) \quad (12.14)$$

This expression was previously derived in Ref. (116), but we have filled in some of the steps. The observed deviations from a constant k_H^0 in (f/x_2) can be attributed to increased Pv work in the liquid, and possible solute-solute

interactions. In the limit $x_2\xi(T)\rightarrow 0$ we obtain a well known result in chemical engineering:

$$\ln(f_2/x_2P^\phi) = \ln(k_H^\circ) + \frac{v_2^\circ P}{RT} \quad (12.15)$$

Equation (12.15) is known as the Krichevsky-Kasarnovsky equation.^{112,121} For the gas-liquid systems in this paper (Pv_1°) is typically 20-100 times greater than (x_2RT) . Therefore, by Eq. (12.14), we will only be sensitive to $\xi(T)$ if G_{22} is significantly larger than the molar volumes, i.e., $\xi(T) \approx x_2RT (C - G_{22}/v_1^\circ)$, where C is of order (-3) for typical solute molar volumes and solvent compressibilities.

13. Data Analysis

Equation (12.14) can be used to obtain information on the pressure and concentration dependence of gas solubility. Figure 38 shows a plot of the quantity $[\ln(f_2/x_2 P^\phi) - Pv_2^\circ/RT]$ versus x_2 for each of our solutes. A linear regression fit to the data gives for the ordinate axis intercept the value of $\ln(k_H^\circ)$ and the slope determines $\xi(T)/RT$. From $\xi(T)$ and Eq. (12.6a) one may then find G_{22} .

The calculated slope was very sensitive to the choice of molar volume so that reliable values of G_{22} are difficult to determine. To illustrate this point, Table XIV lists values of G_{22} and $\ln(k_H^\circ)$ obtained for each solute at for different assumed values of v_2° . The values of v_2° are taken from Ref. 109, in which standard literature values are compiled, along with the authors' own direct measurements. The values of v_2° given in Table XIV represent the range of generally acceptable data. A common way to obtain the partial molar volume of gases in liquids is to use solubility data in conjunction with Eq.(12.15). This obviously is not appropriate to our analysis, which relies on Eq.(12.14), since the resulting molar volume would give zero for $\xi(T)$. When possible we have used values of v_2° which were determined directly, and have indicated when otherwise. For

xenon the only direct measurement of molar volume is by Biggerstaff et al. at elevated pressure.¹¹⁰ The data on Figure 38 were fitted using the following intermediate values of molar volume; $\bar{v}_2^{\circ}(\text{N}_2) = 34.2\text{cm}^3/\text{mol}$,¹²² $\bar{v}_2^{\circ}(\text{Ar}) = 32\text{cm}^3/\text{mol}$, $\bar{v}_2^{\circ}(\text{Kr}) = 32\text{cm}^3/\text{mol}$, and $\bar{v}_2^{\circ}(\text{Xe}, P < 17\text{atm}) = 43.5\text{cm}^3/\text{mol}$ (the average nitrogen value corresponds to a measured value in Ref 122). The corresponding values of $\xi(T)/RT$ are 5.198, -11.817, -5.071, and -15.812 respectively.

On Figure 38 we have shown on the ordinate axis using filled symbols the experimental values of $\ln(k_H^{\circ})$ for each solute at 25.0°C as given in reference 6, viz., $k_H^{\circ}(\text{N}_2) = 85251$, $k_H^{\circ}(\text{Ar}) = 39746$, $k_H^{\circ}(\text{Kr}) = 22252$, $k_H^{\circ}(\text{Xe}) = 12885$. The intercepts of our graphs are much less dependent on choice of molar volume than the slopes and agree with the known results very well. Thus, the values of k_H° that one obtains from our plot are: $k_H^{\circ}(\text{N}_2) = 84669$, $k_H^{\circ}(\text{Ar}) = 39875$, $k_H^{\circ}(\text{Kr}) = 22261$, and $k_H^{\circ}(\text{Xe}) = 12925$. We also found that the xenon data at higher pressures could be fit to the same curve as the pre-clathrate data, provided we used our experimental value of $v_2^{\circ}(\text{Xe}, P > 20\text{atm}) \approx 125\text{cm}^3$.

It is interesting to note what happens when v_2° is treated as a free parameter which can be varied to obtain the best straight line fits by chi squared minimization.

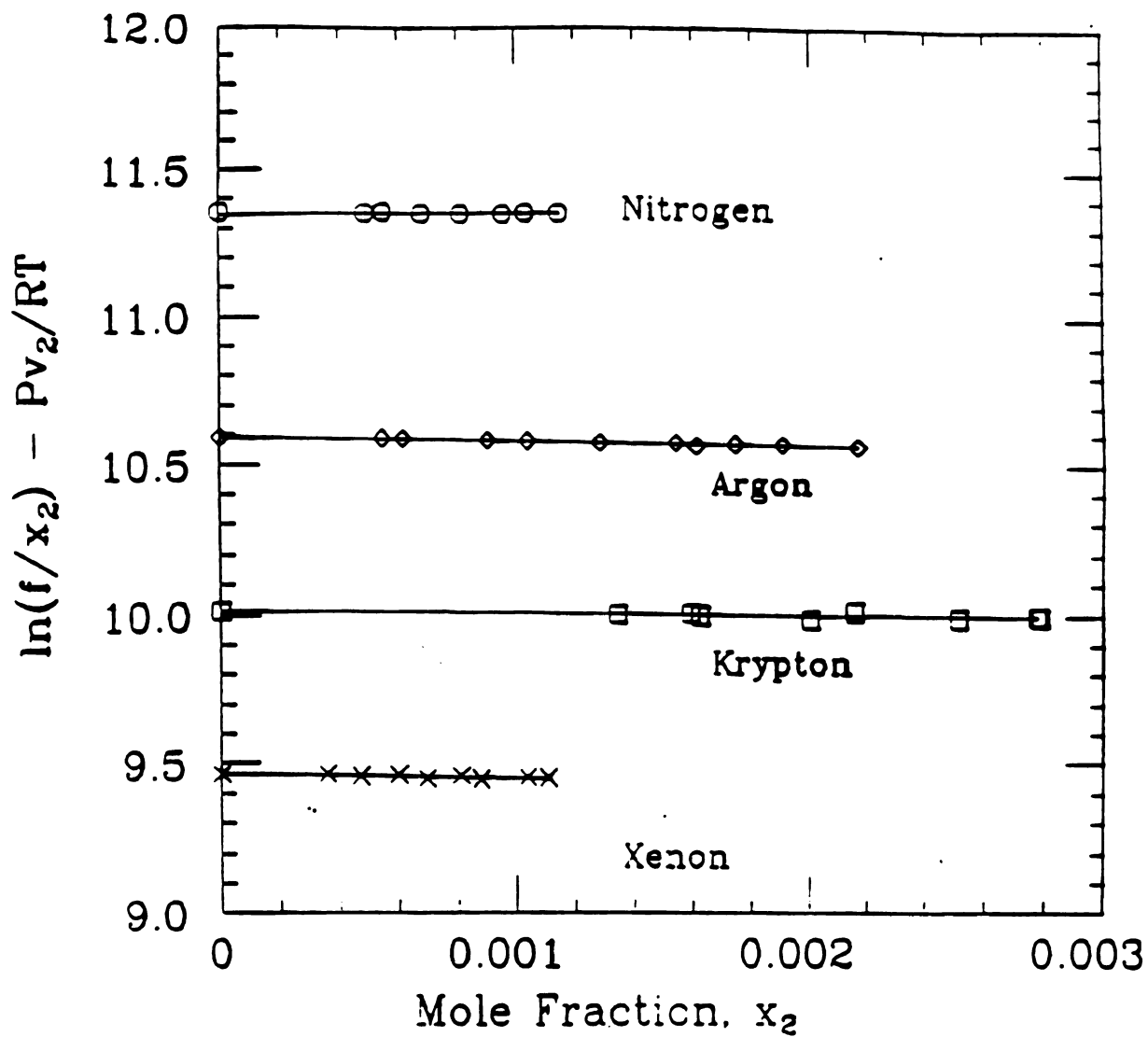


Figure 38. $\ln(f_2/x_2) - Pv_2^0/RT$ vs mole-fraction solubility at 25°C.

Table XIV. Results of Kirkwood-Buff analysis. The third column gives the partial molar volume of the solute used in Eq.(12.14). The fourth and fifth columns give the results for the KB integral G_{22} and the log of the infinite dilution limit of Henry's constant, $\ln(k_H^0)$.

Solute	T(°C)	v_2^0 (cm ³ /mol)	G_{22} (cm ³ /mol)	$\ln(k_H^0)$
N ₂	25.0	33 ¹	-236	11.346
		35.7 ²	-27	11.347
Ar	25.0	32 ^{2,3}	+169	10.5935
Kr	25.0	33 ²	+24	10.010
		31 ²	+69	10.011
Xe	25.0	41 ⁴	+196	9.4668
		46 ³	+240	9.4669
He	0.0	15.5	-157	11.791
		23.7	+927	11.801
		29.7	+1720	11.809
He	25.0	15.5	-22	11.874
		23.7	+998	11.881
		29.7	+1745	11.886
N ₂	25.0	33	-4.5	11.360
		35.7	+345	11.369
N ₂	50.0	33	-92	11.604
		35.7	+330	11.611
H ₂	0.0	20	-18.5	10.953
		25.2	+262	10.958
		26.7	+343	10.960
H ₂	25.0	20	+7.0	11.170
		25.2	+314	11.173
		26.7	+403	11.174
H ₂	50.0	20	+3.0	11.242
		25.2	+305	11.245
		26.7	+392	11.245
CH ₄	25.0	34.5	-13	10.588
		37.4	+223	10.598
C ₂ H ₆	37.8	51	+125	10.595
		53	+870	10.609

In every case the optimum fit leads to $|G_{22}| < 50 \text{cm}^3/\text{mole}$. However the resulting value of the 'effective molar volume', v_2^{eff} , is often not in agreement with experiment, i.e., we obtain by this procedure $v_2^{\text{eff}}(\text{N}_2) = 36 \text{cm}^3/\text{mol}$, $v_2^{\text{eff}}(\text{Ar}) = 26 \text{cm}^3/\text{mol}$, $v_2^{\text{eff}}(\text{Kr}) = 28 \text{cm}^3/\text{mol}$, and $v_2^{\text{eff}}(\text{Xe}) = 10 \text{cm}^3/\text{mol}$. The value for Xe is certainly unphysical since Xe is known to have the largest molar volume of the four gases studied.

Table XIV also shows the results obtained by application of this analysis to data of other worker on high pressure gas solubility in water. These data appear below the double horizontal line on Table XIV. The systems include He(25-1000atm; 0°C, 25°C),¹²³ H_2 (25-1000atm; 0°C, 25°C, 50°C)¹¹², N_2 (25-1000atm; 25°C, 50°C),¹²⁴ CH_4 (0-6000psi; 25°C),¹²⁴ C_2H_6 (0-10,000psi; 37.8°C).¹²⁵ For H_2 and N_2 (50°C) the gas phase fugacities used were those of Demming and Shupe.¹²⁷ For the remaining gases the fugacities were calculated in the manner described earlier; the equation of state data we used to calculate f_2 is taken from references 128, 104, 129, and 130 for He, N_2 , CH_4 , and C_2H_6 , respectively. Although ethane isn't a spherical solute we include it because of its similarity to Xe in aqueous solutions; i.e. both gases have comparable solubilities at 1 atm and both form aqueous clathrates at 25.0°C.^{6,113,131} The analysis uses all the published solubility data except the first point of the methane data (P=341psia) for which x_2 seemed anomalously high. Once again we see that the calculated values of G_{22}

are strongly dependent on the choice of molar volume. Molar volume data are taken from Ref.(109). For He there is no direct measurement of molar volume. Of the three quoted values shown in Table XIV, two are obtained from solubility measurements ($v_2^0 = 15.5\text{cm}^3/\text{mol}$, $v_2^0 = 29.7\text{cm}^3/\text{mol}$)^{132,96} and the other is an estimate from the pure liquid triple point density.¹¹⁶ These data, also, have the general feature that one can choose an effective molar volume which leads to the best fit of the data. The effective molar volumes that one obtains are: $v_2^{\text{eff}}(\text{He}) = 15.5\text{cm}^3/\text{mol}$, $v_2^{\text{eff}}(\text{H}_2) = 20\text{cm}^3/\text{mol}$, $v_2^{\text{eff}}(\text{N}_2) = 33\text{cm}^3/\text{mol}$, $v_2^{\text{eff}}(\text{CH}_4) = 34\text{cm}^3/\text{mol}$, and $v_2^{\text{eff}}(\text{C}_2\text{H}_6) = 50\text{cm}^3/\text{mol}$. All are close to the experimental results with the exception of He and H₂.

Watanabe and Andersen¹¹⁶ have performed molecular dynamics simulations of the Kr-water system. Their results indicated that the Kr solutes tended to undergo 'hydrophobic repulsion' in solution. By integrating the solute-solute correlation function, as evaluated from computer simulations, they found that $G_{22}(\text{Kr}) = -1004\text{\AA}^3/\text{molecule} = -604\text{cm}^3/\text{mol}$. This means the solutes tended to avoid one another in solution. In the appendix of that paper they include an analysis of solubility measurements which is similar to ours. They find a definite correlation between $\ln(k_H^0)$ for a given solute and its corresponding second osmotic virial coefficient, B_2^* of Eq. (12.9). The general tendency was that as $\ln(k_H^0)$ increased, B_2^* decreased. By extrapolating experimental results they postulated that

$G_{22}(\text{Xe}) \approx -775 \text{cm}^3/\text{mol}$, $G_{22}(\text{Kr}) \approx -362 \text{cm}^3/\text{mol}$, $G_{22}(\text{Ar}) \approx +16 \text{cm}^3/\text{mol}$, and $G_{22}(\text{Ne}) \approx +821 \text{cm}^3/\text{mol}$. They assert that the less soluble gases (large k_H^0) are less polarizable and tend to demonstrate hydrophobic clustering. The more polarizable gases such as Kr and Xe are relatively hydrophilic and prefer to be surrounded by water. We see no systematic variation of this type. We believe that the systematic variation observed in reference 116 for He, N_2 , H_2 and CH_4 is attributable to choice of molar volume, and selection of data (for example, they neglect all nitrogen data above $x_2=0.003$ at 25°C and above $x_2=0.004$ at 50°C). Our results do not rule out such behavior, but within the experimental uncertainty of v_2^0 we cannot support such findings. It is necessary to point out that the Kr solutions of Watanabe and Andersen's¹¹⁶ computer simulation were 5-10 times more concentrated than the solutions we made. It is possible that at this higher concentration one starts to see clathrate behavior for krypton such as we observed for xenon. The ice-like cages¹³³ which form around the solute in the clathrate phase could provide a mechanism for 'hydrophobic repulsion' between solutes.

Our results are more consistent with the theoretical calculations of Pratt and Chandler.¹⁰¹ They developed a theory of the hydrophobic effect which is based on an integral equation for the relevant pair correlation functions of the aqueous solution. The theory is more accurate than previous analytic attempts because it utilizes

the experimentally determined oxygen-oxygen correlation function of pure water as an input parameter. Table V of Ref. 101 tabulates the calculated values of second osmotic virial coefficient, B_2^* , for hard spheres in water in and a hard sphere solvent. Although Pratt and Chandler's model predicted some hydrophobic clustering of the solutes, the resulting values of G_{22} only ranged from -15 to 96 (cm^3/mol). Since a hard sphere is in some sense the limiting case of an inert gas solute with zero polarizability it might be reasonable to expect that G_{22}^{hs} would be the largest possible value for the inert gases. Unfortunately no attempt was made by the authors to calculate G_{22} for more polarizable gaseous solutes.

To briefly summarize, we found that the solubility data could be accurately fit by taking account only pressure effects on the solute chemical potential. The contribution of solute-solute interactions expected at high concentrations, is uncertain since the partial molar volumes v_2^0 are not known accurately enough.

There is evidence, however, that solute concentration effects may play a role in some aqueous systems. Figure 39 shows solubility data on the systems He- H_2O and N_2 - H_2O , both at 25.0°C. On Fig. 39 the quantities plotted are the same as those on Fig 38, i.e. $\ln(f_2/x_2 P^\phi) - P v_2^0/RT$ versus x_2 . We show curves representing each value of molar volume listed on Table XIV. Although the best fit for He is obtained with $v_2^0 = 15.5\text{cm}^3$, this seems too low in relation

to other values of the noble gases.¹⁰⁹

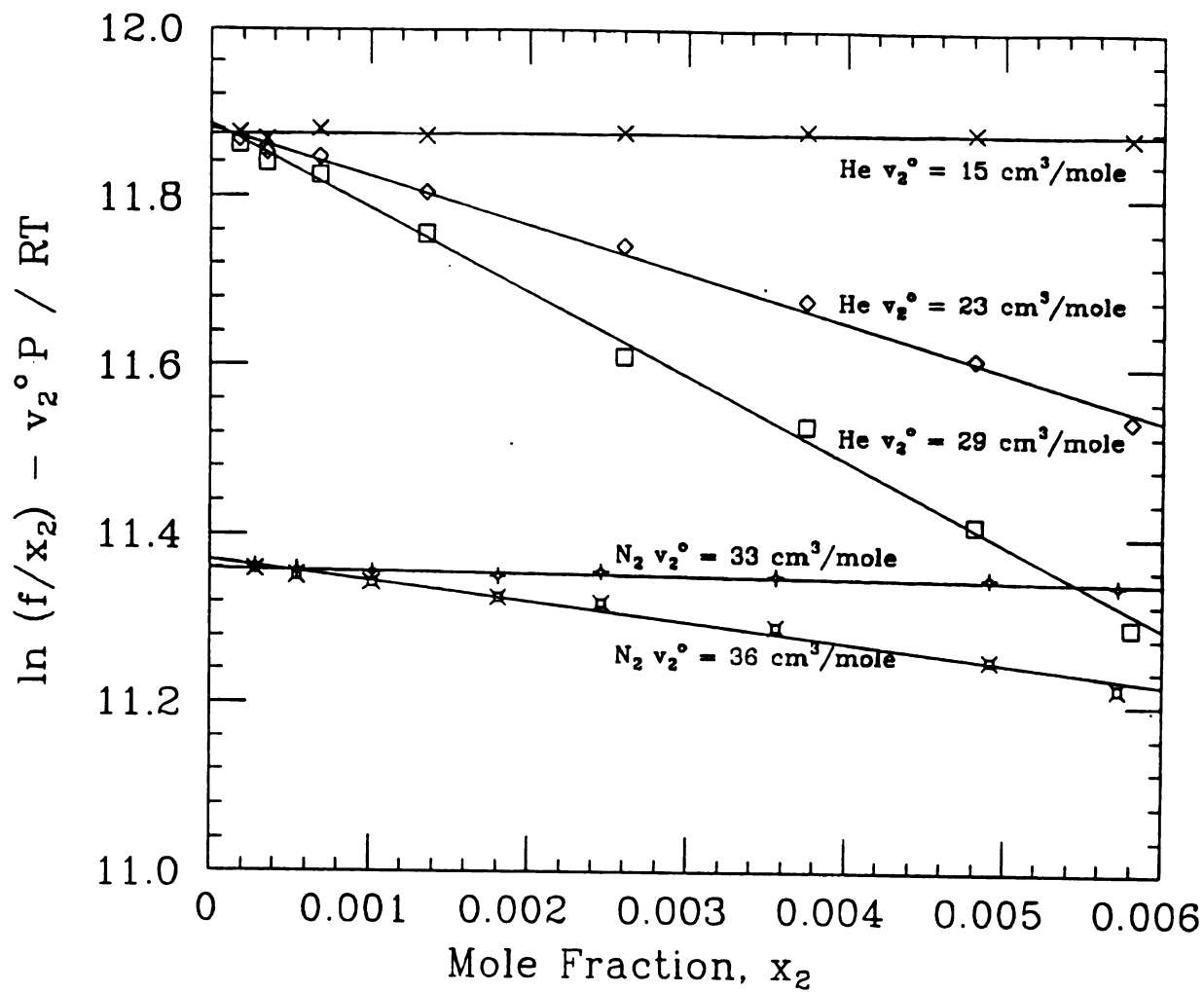


Figure 39. $\ln(f_2/x_2) - Pv_2^0/RT$ vs mole-fraction solubility for He and N_2 at 25°C for various values of v_2^0 .

14. Number Density Scale

So far we have analyzed the high pressure results in terms of the mole fraction scale. In this chapter we consider the thermodynamics of solvation on the number density scale. This scale along with its many advantages has been put forth by Ben-Naim.¹³⁴

To illustrate how this applies to our high pressure solubility data we write the chemical potential (in the T,P,N ensemble) for the solute in the gas and liquid phases:

$$\mu_2^g = RT \ln(\rho_2^g \Lambda^3) + \mu_2^{*g} \quad (14.1a)$$

$$\mu_2^l = RT \ln(\rho_2^l \Lambda^3) + \mu_2^{*l} \quad (14.1b)$$

where $\Lambda = h/(2\pi mkT)^{1/2}$ is the thermal wavelength of the solute particle.¹⁴ The first term on the right hand sides of Eqs.(14.1a) and (14.1b) represents the free energy per mole of an ideal gas at the specified solute density, and temperature. The second term, μ_2^* , represents the excess free energy per mole (over the ideal case) due to intermolecular interactions in the gas and liquid phases. Formally μ_2^* should also include contributions from the internal partition function of the solute. For simple solutes like the inert gases these contributions are mostly electronic and we assume as usual that they do not change

when the solute goes into the solvent. The excess chemical potential in phase i , μ_2^{*i} , ($i=1$ or g) can be interpreted as avagadros number multiplied by the free energy to take an extra solute from infinity and place it at fixed positions in phase i of the assembled system. (see discussion in Chapter 6 for details.) By equating μ_2^1 with μ_2^g we find the equilibrium condition in terms of the Ostwald solubility, L , to be :

$$\Delta\mu_2^* = \mu_2^{*1} - \mu_2^{*g} = -RT\ln L \quad , \quad (14.2)$$

where $L = (\rho_2^1/\rho_2^g)$. The key quantity that one wishes to understand in developing a theory of solvation is the excess chemical potential in the liquid, μ_2^{*1} . When the gas phase is at low density it can be treated as ideal, i.e., $\mu_2^{*g} = 0$. For this case Eq.(14.2) gives a direct measure of μ_2^{*1} (see Eq.(3.11)). When the gas is at a higher density one must account for its nonideality. For the nonideal case we use Eq. (11.2) to find the chemical potential in terms of the solute fugacity. Using the equilibrium condition we now find an expression for μ_2^{*1} :

$$\mu_2^{*1} = -RT\ln\left(\frac{\rho_2^1 RT}{f_2}\right) = -RT\ln(\gamma) \quad . \quad (14.3)$$

This introduces the new dimensionless solubility parameter, $\gamma = (\rho_2^1 RT / f_2)$. In the low pressure limit γ reduces to L . Equation (14.3) also holds when the solvent vapor pressure

isn't negligible, as would apply near the critical temperature of the solvent. In that situation Eq.(11.1) no longer gives the solute fugacity correctly. Rather one must then employ standard mixing rules in the gas phase to find f_2 .^{121,131}

Because our experimental technique allows for direct measurement of ρ_2^1 we can easily evaluate L and γ . Columns 5 and 6 of Table 13 lists the results of our solubility measurements in terms of the parameter γ . Also included are the values of μ_2^{*1} as given by Eq. (14.3).

The statistical mechanics of solute-solvent mixtures starts with a standard partition function^{135,16} from which, as we have shown in chapter VI, one may obtain the excess chemical potential for a single solute molecule in the liquid solvent¹⁴:

$$\mu_2^{*1} = -kT \ln \langle \exp(-B_0/kT) \rangle \quad . \quad (14.4)$$

The key quantity in Eq.(14.4), B_0 , is the binding energy of a single solute to a fixed configuration of the solute solvent system. The ensemble average of the exponential is taken over all configurations. In practice Eq.(14.4) is difficult to evaluate unless one performs some sort of weighted average which neglects improbable configurations.^{102,136} Another way of writing μ_2^{*1} is to use a coupling parameter approach:

$$\mu_2^{*1} = \int_0^1 U(\lambda) d\lambda \quad , \quad (14.5)$$

where the averaged interaction potential between the solute and the liquid is a function of the coupling parameter, λ .^{38,39,40} Normally one ignores solute-solute interactions with this technique. If solute-solute interactions become important the resulting chemical potential will be a function of the solute concentration in the liquid, i.e., $\mu_2^{*1} = F(\rho_2^1)$. The solute density can then be determined through Eq.(14.3).

The pressure and concentration dependence of μ_2^{*1} can be evaluated in a manner analogous to our earlier derivation. Starting from Eq. (22) of Ref (115) one can easily show for dilute solutions:

$$\begin{aligned} -RT \ln(\gamma) = & -RT \ln(L^0) + P v_2^0 + \rho_2^1 RT(-G_{22} - v_2^0 + RT x^0) \\ & + O(\rho_2^1)^2 \end{aligned} \quad (14.6)$$

where L^0 is the infinite dilution limit of the Ostwald solubility, and $-RT \ln(L^0)$ is the excess chemical potential in the same limit.

The number density scale also offers advantages in studying the temperature dependence of the solvation process. The excess molar enthalpy and entropy in the liquid are:

$$s_2^{*1} = - \left(\frac{\partial \mu_2^{*1}}{\partial T} \right)_{P,n} \quad h_2^{*1} = \mu_2^{*1} + Ts_2^{*1} \quad (14.7)$$

where μ_2^{*1} is given by Eq. (14.3).

The excess free energy of solution is commonly described on the mole fraction scale by Henry's constant via; $\mu_2^{ex} = RT \ln(k_H)$, where $k_H = (f_2/x_2)$. In this case the term excess refers to a hypothetical standard state²² and ideal solution.²² Henry's constant is related to the solubility parameter γ by:

$$\gamma = (\rho_1^1 + \rho_2^1)RT/k_H \quad (14.8a)$$

$$\approx \rho_1^1 RT/k_H, \quad \text{when } \rho_2^1 \ll \rho_1^1 \quad (14.8b)$$

The corresponding entropy and enthalpy evaluated on the mole fraction scale includes terms which depend on the thermal expansivity of the liquid. These terms are irrelevant in the description of the solvation process on a statistical mechanical level. A more complete discussion of this topic is found in chapter III and Ref. (134).

In the limit that solute-solute interactions are negligible a useful expression for the solvation entropy at a given pressure P may be obtained by applying Eq.(14.7) to Eq. (14.6). The result is:

$$s_2^{*1}(P) = s_2^{*1(0)} - P \left(\frac{\partial v_2^0}{\partial T} \right)_{P,n}, \quad (14.9)$$

where $s_2^{*1(0)}$ is the entropy associated with the infinitely dilute solution at low pressure. This result seems reasonable since changes in molar volume would be closely tied to solvent ordering around the solute.

An application of the new solubility parameter γ is in the case of gas solubility at temperatures near the solvent critical point. This subject has become a source of great interest because of its applications towards industrial power¹³¹ and the study of geological processes¹³⁷. For dilute solutions approaching the solvent critical temperature the gas pressure is dominated by the solvent vapor. It has been experimentally observed, for water and nonaqueous solvents, that Henry's constant k_H passes through a minimum and then declines as the temperature is raised from the triple point to the critical point.¹³¹ In a recent article Japas and Sengers⁹¹ have noted that for $x_2 \ll 1$ a linear relation exists between the solution density ρ_1 and the quantity $\Delta = T \ln(k_H/f_1^*)$, where f_1^* is the fugacity of the pure solvent vapor at temperature T .⁹¹ For nonpolar gases in water this correlation exists over a range of more than 150 K below the steam critical point of 647 K (see figures 2-6 of ref 91). We can understand this result by using Eq. (14.8b) to convert from Henry's constant to γ . We can then solve for Δ in terms of γ :

$$\Delta = T \ln(k_H/f_1^*) \approx T \ln(\rho_1^1 RT/f_1^* \gamma_2) = T \ln(\gamma_1/\gamma_2), \quad (14.10)$$

where $\gamma_1 = (\rho_1^1 RT/f_1)$ and $\gamma_2 = (\rho_2^1 RT/f_2)$. We have also assumed that for dilute solutions the solvent fugacity f_1 is equal to that of the pure solvent f_1^* . This is probably justified since $x_2 \approx 10^{-4}$. Multiplying Eq. (14.10) by R gives:

$$R\Delta \approx RT \ln(\gamma_1) + RT \ln(\gamma_2) = \mu_1^{*1} - \mu_2^{*1} \quad (14.11)$$

Therefore the quantity Δ is proportional to the difference in excess chemical potentials between the solvent and the solute, both evaluated in the liquid phase. In chapter 6 we derived expressions for the excess chemical potential using a coupling parameter approach. Applying this to the solute and solvent we find:

$$\begin{aligned} \mu_2^{*1} &= 4\pi\rho_1^1 \int_0^1 \int_0^\infty u_{12}(\vec{r}) g_{12}(\vec{r}, \lambda) d^3\vec{r} d\lambda + O(\rho_2^1) \\ &\approx \rho_1^1 [\text{INT-12}] \end{aligned} \quad (14.12a)$$

$$\begin{aligned} \mu_1^{*1} &= 4\pi\rho_1^1 \int_0^1 \int_0^\infty u_{11}(\vec{r}) g_{11}(\vec{r}, \xi) d^3\vec{r} d\xi + O(\rho_2^1) \\ &\approx \rho_1^1 [\text{INT-11}] \end{aligned} \quad (14.12b)$$

where λ and ξ are the solute-solvent and solvent-solvent coupling parameters respectively, and [INT-12] and [INT-11] represents 4π times the integrals appearing in 14.12a and 14.12b. Using this result Eq (14.11) can be written as:

$$\Delta \approx \rho_1^{-1} \left([\text{INT-11}] - [\text{INT-12}] \right) / R \quad . \quad (14.13)$$

For dilute solutions the solvent density ρ_1^{-1} is approximately equal to the total solution density ρ_1 . It is then apparent that the observed linear relation between Δ and ρ_1 is a consequence of Eq (14.13). This tells us that as we approach the critical temperature of the solvent the integrals [INT-11] and [INT-12] either become weakly dependent on the solution density or linearly dependent on the solution density. Why this happens at high temperature is unknown and merits further study.

15. Conclusions

In conclusion we discuss briefly how this work can be used to predict and understand solubility data and what further experiments would be useful towards these ends.

We have found that the solubility of simple nonpolar gases in water can be adequately predicted as a function of pressure using Eq.(12.14). Although solute-solute effects may play some role in the solvation process the change in chemical potential with pressure is primarily due to the increased Pv work to place the solute in the solvent. The possible exceptions to this are He, H₂, and perhaps Xe. The first two cases were discussed earlier. We include Xe in this list because our experimental technique was not as sensitive as we would have liked it to be in the pre-clathrate range. The other reason to study Xe is because it is the most polarizable inert gas (excluding radon). If the solvation properties of He and Xe were known with sufficient accuracy, one could set limits on the range of expected hydrophobic behavior of the inert gases.

It is known that gas solubility in non-aqueous liquids can be dependent on concentration. For example, H₂ solute in NH₃ solvent shows large deviations from Eq. (12.15) at mole fraction concentrations near 10 percent.^{121,138} To

account for these effects one can use thermodynamic arguments based on a two suffix Margules equation¹²¹ (a semi-empirical form of the excess free energy) to show that:

$$\ln(f/x_2 P^\phi) = \ln(k_H^\circ) + \frac{A}{R T} (x_1^2 - 1) + \frac{v_2^\circ P}{R T}, \quad (15.1)$$

where x_1 is the mole fraction concentration of the solvent and A is a constant. This equation is known as the Kritchevsky-Ilinskaya equation.¹³⁹ It is often used in chemical engineering to model solutions of light gases such as He or H_2 in liquid solvents where the solubility is appreciable.¹²¹ It is only valid if the partial molar volume of the solute is independent of pressure and composition over the range studied. If this assumption holds the constant A can be determined by fitting solubility data. Equation (15.1) can be understood at a statistical mechanical level. If the solution is sufficiently dilute we may substitute $(x_1^2 - 1) \approx -2x_2$. By comparison with Eq. (12.14) the coefficient A is identified as $-\frac{1}{2}\xi(T)$. This allows for convenient transformation of data that has been compiled in engineering journals.¹²¹ Further experiments with nonpolar liquids will be useful for comparison with aqueous solutions.

We have also argued that the number density scale provides a better framework to analyze solubility data. For dilute systems like those discussed in this paper it is

fairly straightforward to convert from the mole fraction to the number density scale by Eq. (14.8b). However for more concentrated solutions one would need a separate measurement of the total solution density in order to extract the relevant thermodynamic properties, particularly the enthalpy and entropy. Our experimental technique automatically measures the saturated solution density by sampling a fixed volume of liquid. We feel that present experimental methods^{111,125} could easily be modified to include density measurement. This may be especially valuable in the study of gas-liquid mixtures near the solvent critical point, where the solute molar volumes tend to increase drastically. 110,131,140

APPENDIX

Appendix A: Derivation of Equation (6.78).

For a liquid in equilibrium with its own vapor can rewrite Eq. (6.76) as:

$$RT \ln(P_g/RT) - RT \ln \rho_\ell - g_{cav} - g_{int} = 0, \quad (A.1)$$

where we have assumed the vapor phase to be ideal. We now take the total derivative of A.1 with respect to temperature along the liquid-gas coexistence curve.

$$\begin{aligned} R \ln(P_g/RT) - R \ln \rho_\ell + RT \frac{d}{dT} [\ln P_g]_c - RT \frac{d}{dT} [\ln RT]_c \\ - RT \frac{d}{dT} [\ln \rho_\ell]_c - \frac{d}{dT} [g_{cav} + g_{int}]_c = 0. \end{aligned} \quad (A.2)$$

The subscript c refers to the derivative along the coexistence curve. We note that this along the coexistence curve the chemical potential in the gas and the liquid are always equal, which is why Eq.(A.2) is zero. The total derivative of the chemical potential with respect to temperature can be written as:

$$\left(\frac{d\mu}{dT}\right)_c = \left(\frac{\partial\mu}{\partial T}\right)_P + \left(\frac{\partial\mu}{\partial P}\right)_T \left(\frac{dP}{dT}\right)_c. \quad (A.3)$$

Using standard thermodynamics Eq. (A.3) becomes:

$$\left(\frac{d\mu}{dT}\right)_c = -s + v \left(\frac{dP}{dT}\right)_c . \quad (\text{A.4})$$

Multiplying Eq. (A.2) by T and using identity (A.4) we have:

$$\begin{aligned} & RT \ln(P_g/RT) - RT \ln p_\ell + RT^2 \frac{d}{dT} [\ln P_g]_c - RT^2 \frac{d}{dT} [\ln RT]_c \\ - & RT^2 \frac{d}{dT} [\ln p_\ell]_c + Ts_{cav} + Ts_{int} - T(v_{cav} + v_{int}) \left(\frac{dP}{dT}\right)_c = 0. \end{aligned} \quad (\text{A.5})$$

Subtracting (A.5) from (A.1) yields an expression for the enthalpies h_{cav} and h_{int} :

$$\begin{aligned} h_{cav} + h_{int} - RT^2 \frac{d}{dT} [\ln p_\ell]_c - RT^2 \frac{d}{dT} [\ln RT]_c + RT^2 \frac{d}{dT} [\ln P_g]_c \\ - TPv_\ell \frac{d}{dT} [\ln P_g]_c = 0 , \end{aligned} \quad (\text{A.6})$$

where $v_\ell = v_{cav} + v_{int}$ is the molar volume of the liquid solvent. The Clausius-Clapyeron equation allows us to write the dervatives of the vapor pressure in terms of the heat of vaporization (H_v) via:

$$\frac{d}{dT} [\ln P_g]_c = H_v/RT^2 . \quad (\text{A.7})$$

Putting this result into Eq.(A.6) and evaluating the other temperature derivatives in terms of the gas and liquid

expansivities we find the desired result:

$$h_{cav} + h_{int} - RT + RT^2\alpha_{\ell} + H_v \left[1 + Pv_{\ell}/RT \right] = 0 . \quad (\text{A.8})$$

Appendix B: Computer Program to Evaluate U_{int} .

```

C      THIS PROGRAM CALCULATES THE PAIR CORRELATION
C      FUNCTION FOR A HARD SPHERE FLUID. USING THE
C      SEMI-EMPIRICAL APPROXIMATION BY
C      VERLET ET AL OUTLINED IN
C      'EQUILIBRIUM THEORY OF SIMPLE LIQUIDS
C      PHYS REV A, VOL 5, NUMBER 2, 1972

C      THEIR TECHNIQUE MODIFIES THE PERCUS YEVIK SOLUTION FOR
C      HARD SPHERES, SO THAT IT FITS NUMERICAL SIMULATION DATA.
C      TO DO THIS WE ALSO MUST USE THE PERCUS-YEVICK
C      SOLUTION BASED ON THE TECHNIQUE OUTLINED IN
C      'ANALYTICAL REPRESENTATION OF THE PERCUS YEVIK HARD SPHERE RADIAL
C      DISTRIBUTION FUNCTION' BY W.R. SMITH AND D.HENDERSON
C      MOL PHYS.,1970, VOL19, NO 3, 411-415
C      THIS VERSION ONLY EVALUATE TERMS UP TO X/R=3.0 AFTER WHICH WE
C      TAKE G(X/R)=1.0

C      *****ALSO HAS BEEN MODIFIED TO EVALUATE THE ENERGY OF INTERACTION
C      Uint FROM WHICH WE WILL DETERMINE THE LENNARD-JONES PARAMETERS FOR
C      THE PURE LIQUID

C      *****
C      VARIABLES ARE DESCRIBED IN SMITH'S PAPER
C      IMPLICIT COMPLEX=8 (C)
C      DIMENSION CT(3),CS(3),CS1(3),CS2(3),CS3(3)
C      DIMENSION CL(3),CL1(3)
C      DIMENSION CAO(3),CBO(3),CB1(3)
C      DIMENSION CB2(3),CB3(3)
C      DIMENSION CG(2)
C      REAL N,F,I,THIRD,ALPHA,YP,YM,BETA,VERL
C      REAL Q0,Q1,Q2,Q3,XR,GTOT,KOUNT,FON,GTOTI
C      REAL INTERVAL,NPOINT,UTOT,SUM,UPREV,INTEGRAL

C      FIRST WE EVALUATE THE THREE ZERO'S OF S(b)
C      ONE IS REAL AND THE TWO OTHERS ARE COMPLEX
C       $S(b) = ((1-N)^{2} + b^{3}) + (6 \cdot N \cdot (1-N) \cdot b^{2}) + (18 \cdot N \cdot b) + (12 \cdot N \cdot (1 \cdot 2 \cdot N))$ 

C      TYPE *, 'PACKING FRACTION N='
C      ACCEPT *,N

C      *****
C      CONVERT REAL PACKING FRACTION TO P.Y. EQUIVALENT PACKING FRACTION
C      SEE VERLET pg 481
C       $N=N-(N \cdot N/16)$ 
C      FON IS THE FUNCTION  $\rho/d$  IN VERTLET'S PAPER
C       $FON=.75 \cdot N \cdot N \cdot (1-.7117 \cdot N-.114 \cdot N \cdot N)/(1-N)^{4}$ 
C      *****

C      *****
C      VARIOUS ALGEBRAIC MANIPULATIONS
C      SEE SMITH et al pg 412-413
C       $F=3 \cdot (3 \cdot N)-N \cdot N$ 
C       $THIRD=1.0/3.0$ 
C       $ALPHA=(1+2 \cdot (N \cdot N/F)^{2})^{.5}$ 
C       $YP=(1+ALPHA)^{2} \cdot (THIRD)$ 
C       $YM=1 \cdot (3 \cdot (1-ALPHA)^{2} \cdot (THIRD))$ 
C      TYPE *,N

```

```

TYPE *,F
TYPE *,ALPHA
TYPE *,YP
TYPE *,YM
CJ=CEXP(CMPLX(0.00000,2.09439510))
C CJ=EXP(2*PI*i/3)
TYPE *,CJ
CJO=CMPLX(1,0)
CJ1=CJ
CJ2=CJ*CJ
CJ_1=CEXP(CMPLX(0.00000,-2.09439510))
CJ_2=CEXP(CMPLX(0.00000,-4.18879021))
C CJ_1=(CJ)**-1      CJ_2=(CJ)**-2
TYPE *,CJ2
TYPE *,CJ_2
CX0=(CMPLX(YP,0.0000)*CJO)+(CMPLX(YM,0.0000)*CJO)
CX1=(CMPLX(YP,0.0000)*CJ1)+(CMPLX(YM,0.0000)*CJ_1)
CX2=(CMPLX(YP,0.0000)*CJ2)+(CMPLX(YM,0.0000)*CJ_2)
TYPE *,CX0
TYPE *,CX1
TYPE *,CX2
type *,third
BETA=(2*N*F)**(third)
CT(1)=(-2*N*BETA*CX0)/(1-N)
CT(2)=(-2*N*BETA*CX1)/(1-N)
CT(3)=(-2*N*BETA*CX2)/(1-N)
TYPE *,'t0,      t1,      t2      ='
TYPE *,CT(1),CT(2),CT(3)
C THESE ARE THE THREE ROOTS OF S(t)
C NOW WE SHALL EVALUATE THE OTHER VARIABLES
C WE USE THE SAME NOTATION AS SMITH AND HENDERSON EXCEPT
C ALL OUR VARIABLES ARE PRECEDED BY "C", i.e. THEY ARE COMPLEX
C ALSO CHANGE SUMATIIONS i=0 TO 2 BECOMES K=1 TO 3

C FIRST WE SHALL MAKE SURE THAT OUR ROOTS GIVE S(t)=0
DO 10 K=1,3
Q3=(1.0-N)**2.0
Q2=6.0*N*(1.0-N)
Q1=18.0*N*N
Q0=12.0*N*(1+2.0*N)
CS(K)=Q3*CT(K)*CT(K)*CT(K)+Q2*CT(K)*CT(K)+Q1*CT(K)-Q0
TYPE *,CS(K)
10 CONTINUE

C NOW EVALUATE OTHER CONSTANTS
DO 100 K=1,3
CL(K)=(1.0*(N/2))*CT(K)+(2.0*N)+1.0
CL1(K)=1.0*(N/2)

CS1(K)=3.0*Q3*CT(K)*CT(K)+2.0*Q2*CT(K)+Q1
CS2(K)=6.0*Q3*CT(K)+2.0*Q2
CS3(K)=6.0*Q3

CA0(K)=CT(K)*CL(K)/CS1(K)

CBO(K)=(-12.0*N*CL(K))/(CS1(K)*CS1(K))

```

```

CB1(K)=(1.0-(CT(K)*CS2(K)/CS1(K)))*CL(K)+(2.0*CT(K)*CL1(K))
CB2(K)=CT(K)*CL(K)

100 CONTINUE
C   O.K. NOW WE'VE DEFINED ALL THE FRICKIN' VARIABLES LETS PLUG THEM
C   IN AND EVALUATE Gn(x)  n= 1 TO 2

TYPE *, 'HOW LARGE IS THE INTERVAL BETWEEN POINTS'
ACCEPT *, INTERVAL
TYPE *, 'XR IS EVALUATED STARTING FROM 1.0'
XR=1.0
NPOINTS=2/INTERVAL
TYPE *, 'NPOINTS=', NPOINTS
DO 2000 KOUNT=1, NPOINTS-1
CXG1TOT=0.0
CXG2TOT=0.0

C   OPEN(1, FILE='PERYEV.DAT', STATUS='NEW')

DO 1000 K=1, 3
CXG1=CAO(K)*CEXP(CT(K)*(XR-1))
CXG1TOT=CXG1TOT+CXG1

CXG2=CBO(K)*(CB1(K)+CB2(K)*(XR-2.0))*CEXP(CT(K)*(XR-2.0))
CXG2TOT=CXG2TOT+CXG2

1000 CONTINUE
C   TYPE *, CXG1TOT
C   TYPE *, CXG2TOT

CG(1)=CXG1TOT/XR
CG(2)=CXG2TOT/XR

C   WE ARE ALMOST DONE, NOW ALLS WE GOTTS TA DO IS EVALUATE G(X)
C   SEE EQ (1) IN PAPER

IF (XR.GE.3.0) GTOT=REAL(1.0)
IF (XR.LT.3.0) GTOT=REAL(CG(1)+CG(2))
IF (XR.LT.2.0) GTOT=REAL(CG(1))
IF (XR.LT.1.0) GTOT=REAL(0.0)

IF (XR.EQ.1.0) GTOTI=GTOT
VERL=24.0*FON*(XR-1)/(N*GTOTI)
GTOT=GTOT+(FON/XR)*COS(VERL)*EXP(-VERL)

C   TYPE *, 'GTOT=', GTOT, 'XR=', XR

C   STORE DATA IN FILE FOR TOP DRAWER PERYEV.DAT
C   WRITE(1, *) XR, GTOT

C   *****
C   EVALUATE THE POTENTIAL ENERGY

```

```
UTOT=GTOT*((XR**4)-(XR**10))
IF (MARKER .EQ. 0) THEN
  MARKER=1
  UPREV=UTOT
  GO TO 1999
ELSE
  SUM=SUM+UTOT+UPREV
  UPREV=UTOT
END IF

1999 XR=XR+INTERVAL

2000 CONTINUE

INTEGRAL=INTERVAL*SUM/2
TYPE *, 'INTEGRAL=', INTEGRAL

C   CLOSE(1)

STOP
END
```

References

1. W.L. Jorgensen, J.D. Madura, and C.J. Swenson, *J. Am. Chem. Soc.* 106, 6638 (1984).
2. F.H. Stillinger, *Science*, 209, 451, (1980).
3. M.P. Allen, and D.J. Tildesley, Computer Simulations of Liquids, (Oxford University Press, Oxford, 1987).
4. P.J. Leonard, D. Hendersen, and J.A. Barker, *Trans. Far. Soc.*, 66, 2439, (1970).
5. L.L. Lee, and D. Levesque, *Mol. Phys.*, 26, 1351, (1973).
6. E. Wilhelm, R. Battino, and R.J. Wilcock, *Chem. Rev.*, 77, 219, (1977).
7. P. Seeman, *Pharmacol. Rev.*, 24, 583, (1972).
8. R.M. Featherstone, and C.A. Muehlbacher, *Pharmacol. Rev.*, 15, 97, (1963).
9. L. Pauling, *Science*, 134, 15, (1961).
10. P.B. Bennett and D.H. Elliot, eds., The Physiology and Medicine of Diving and Compressed Air Work, 2nd ed., (Baillière Tindall, London, 1975).
11. C.O. Kunz and C.J. Paperiello, *Science*, 192, 1235, (1976).
12. United States Atomic Energy Commission, Reactor Safety Study, draft WASH-14- U.S. Atomic Energy Commission, (Washington D.C., 1974).
13. T.M.S. Chang and R.P. Geyer, eds., Blood Substitutes, (Marcel Deker Inc., New York, 1989).
14. A. Ben-Naim, Solvation Thermodynamics, (Plenum, New York, 1987).
15. R. Fowler and E.A. Guggenheim, Statistical Thermodynamics, (Cambridge University Press, Cambridge, 1939), sec 823.

16. D. Chandler, Introduction to Modern Statistical Mechanics, (Oxford Press, New York, 1987).
17. G.L. Pollack, R.P. Kennan, J.F. Himm and P.W. Carr, J. Chem Phys. 90, 6569, (1989).
18. G.L. Pollack, J. Chem. Phys., 75, 5975, (1981).
19. G.L. Pollack and J.F. Himm, J. Chem. Phys., 77, 3221 (1982).
20. R.S. Berry, S.A. Rice, J. Ross, Physical Chemistry, (John Wiley & Sons, New York, 1980).
21. A. Ben-Naim, J. Phys. Chem., 82, 792, (1978).
22. D. Eisenberg and D. Crothers, Physical Chemistry with Applications to the Life Sciences, (The Benjamin/Cummings Publishing Co., Menlo Park Ca., 1979).
23. R.C. Richardson and E.N. Smith, eds., Experimental Techniques in Condensed Matter Physics at Low Temperatures, (Addison-Wesley Publishing Co., Redwood City Ca., 1988).
24. R. Battino and H.L. Clever, Chem. Rev., 66, 395, (1966).
25. C.M. Lederer, J.M. Hollander, and I. Perlman, Table of Isotopes, sixth edition, (John Wiley and Sons, New York, 1967).
26. J.F. Himm, Ph.D. Thesis, Department of Physics and Astronomy, Michigan State University, 1986.
27. K. Siegbahn, ed., Alpha-, Beta-, and Gamma-ray Spectroscopy, volume 1, (North Holland, Amsterdam, 1965).
28. H.G. Cuming and C.J. Anson, Mathematics and Statistics for Technologists, (Chemical Publishing Co., New York, 1967).
29. J. Timmermans, Physico Chemical Constants of Pure Organic Compounds, (Elsevier Publishing Co., New York, 1950). Vol.1
30. Beilsteins Handbuch der Organischen Chemie, 4. Auflage, Viertes Erganzungswerk, edited by H.G. Boit (Springer, Berlin, 1972) Vol.1, Part 1.
31. K. Huang, Statistical Mechanics, second edition, (John Wiley and Sons, New York, 1987).
32. B.B. Benson and D Krause Jr., J. Chem. Phys., 64, 689, (1976).

33. R.C.Reid, J.M.Prausnitz and B.E.Poling, The Properties of Gases and Liquids, fourth edition, (McGraw Hill Book Co., New York, 1987).
34. G. Olofsson, A.A. Oshodi, E. Qvarnström and I. Wadsö, J. Chem. Thermodynamics, 16, 1041, (1984).
35. J.P. Hansen and I.R.McDonald, Theory of Simple Liquids, second edition, (Academic Press, London, 1986).
36. T.L. Hill, Statistical Mechanics, (McGraw Hill Book Co., Inc. New York, 1956).
37. L.E. Reichl, A Modern Course in Statistical Physics, University of Texas Press, Austin, 1980).
38. L. Onsager, Chem. Rev., 13, 73, (1933).
39. J.G. Kirkwood, J. Chem. Phys., 3, 300, (1935).
40. T.L. Hill, Statistical Thermodynamics, (Dover Publications, Inc., New York, 1986).
41. W.C. Swope and H.C. Andersen, J. Phys. Chem., J. Phys. Chem., 88, 6548, (1984).
42. N.W. Ashcroft and N.D. Mermin, Solid State Physics, (Holt Rinehart and Winston, New York, 1976).76).
43. D. Chandler, J.D. Weeks and H.C. Andersen, Science, 220, 787, (1983).
44. B.J. Alder and T.E. Wainwright, J. Chem. Phys., 27, 1208, (1957).
45. H.C. Longuet-Higgins and B. Widom, Mol. Phys. 8, 549, (1964).
46. L. Verlet, Phys. Rev., 159, 98, (1967).
47. J.L. Yarnell, M.J. Katz, R.G. Wenzel and S.H. Koenig, Phys. Rev. A., 7, 2130 (1973).
48. D. Chandler, J.D. Weeks, Phys. Rev. Lett., 25, 149, (1970).
49. D. Chandler, Ann. Rev. Phys. Chem., 29, 441, (1978).
50. L. Verlet, Phys. Rev., 163, 201, (1968).
51. H.C. Andersen, D. Chandler, and J.D. Weeks, Adv. Chem. Phys., 34, 105, (1976).

52. H.H. Uhlig, J. Phys. Chem. 41, 1215, (1937).
53. D.D. Eley, Trans. Faraday Soc., 35, 1281, 1421, (1938).
54. H. Reiss, H.L. Frisch, E. Helfand, and J.L. Lebowitz, J. Chem. Phys., 32, 119, (1960).
55. R.A. Pierotti, J. Phys. Chem., 67, 1840, (1963).
56. P.J. Flory, J. Chem. Phys., 9, 660 (1941); 10, 51, (1942).
57. M.L. Huggins, J. Chem. Phys., 9, 440, (1941); Ann. N.Y. Acad. Sci. 43, 1, (1942).
58. H.C. Longuet-Higgins, Discuss. Faraday. Soc., 15, 73, (1953).
59. N.F. Carnahan, K.E. Starling, J. Chem. Phys. 51, 635, (1969).
60. H. Reiss, H.L. Frisch, and J.L. Lebowitz, J. Chem. Phys., 31, 369, (1959).
61. H. Reiss, Advances in Chem. Phys. 9, 1 (1964).
62. R.C. Tolman, The Principles of Statistical Mechanics, (Dover, New York, 1932)
63. J.K. Percus and G.J. Yevick, Phys. Rev., 110, 1, (1958).
64. J.H. Hildebrand, J.M. Prausnitz, and R.L. Scott, Regular and Related Solutions, (Van Nostrand Reinhold Co., New York, 1970).
65. R.P. Kennan and G.L. Pollack, J. Chem. Phys., 89, 517, (1988).
66. Y. Kabatake and B.J. Alder, J. Phys. Chem., 66, 645, (1962).
67. R.A. Pierotti, J. Phys. Chem. 67, 1840, (1963).
68. J.H. Dymond and E.B. Smith, The Virial Coefficients of Pure Gases and Mixtures, (Clarendon, Oxford, 1980).
69. J.O. Hirschfelder, C.F. Curtis, R.B. Bird, Molecular Theory of Gases and Liquids, (Wiley, New York, 1967).
70. R.A. Pierotti, Chem. Rev. 76, 717, (1976).
71. E Wilhelm and R. Battino, J. Chem. Phys., 55, 4012, (1971).

72. N.M. Desrosiers and J.P. Morel, *Can. J. Chem.*, 59, 1, (1981).
73. R.A. Pierotti, *J. Phys. Chem.*, 69, 281, (1965).
74. M. Lucas, *J. Phys. Chem.*, 80, 359, (1976).
75. R.O. Neff and D.A. McQuarrie, *J. Phys. Chem.*, 77, 413, (1973).
76. J.A. Barker and D. Hendersen, *J. Chem. Phys.*, 47, 4714, (1967).
77. G.L. Pollack, *Rev. Mod. Phys.*, 36, 748, (1964).
78. M.L. Klein and J.A. Venables, ed., Rare Gas Solids, (Academic Press, London, 1976-77), Vols I and II.
79. AIP Handbook, 2nd ed., (McGraw-Hill Book Co. New York, 1963).
80. E.W. Grundke and D. Henderson, *Mol. Phys.* 24, 269 (1972).
81. L. Verlet and J.J. Weis, *Mol. Phys.*, 28, 665, (1974).
82. S.E. Koonin, Computational Physics, (The Benjamin/Cummings Publishing Co., Menlo Park Ca., 1986).
83. S.H. Chen, H.T. Davis and D.F. Evans, *J. Chem. Phys.*, 77, 2540, (1982).
84. D. Dimitrelis and J.M. Prausnitz, *Fluid Phase Equilibria*, 31, 1, (1986).
85. O. Sinanoglu, *Theor. Chim. Acta (Berlin)* 33, 279 (1974).
86. T. Boublik, *Mol. Phys.*, 27, 415, (1974); and *J. Chem. Phys.* 63, 4048, (1975).
87. W.L. Jorgensen, J. Gao, and C. Ravimohan, *J. Chem. Phys.*, 82, 3470, (1985).
88. W.L. Jorgensen, *J. Am. Chem Soc.*, 103, 335, (1981).
89. L.A. Weber, *Cryogenics* 25, 338 (1985).
90. A.G. Duncan and M.J. Hiza, *Adv. Cryog. Eng.* 15, 42 (1970).
91. M.L. Japas and J.M.H. Levelt Sengers, *AIChE Journal*, 35, 705 (1989).

92. R.P. Kennan and G.L. Pollack, *J. Chem. Phys.* 88, 6529 (1988).
93. W. Henry, *Philos. Trans.* 93, 29, 274 (1803).
94. G.N. Lewis and M. Randall, revised by K.S. Pitzer and L. Brewer., Thermodynamics, (McGraw Hill Book Co., New York, 1961).
95. J.W. Miller, editor, NOAA Diving Manual, (U.S. Dept. of Commerce, U.S. GPO, Washington D.C., 1979).
96. T. Enns, P.F. Scholander, and E.D. Bradstreet, *J. Phys. Chem.* 69, 389 (1965).
97. W. Kauzmann, *Adv. Protein Chem.* 14, 1 (1959).
98. A. Ben-Naim, Hydrophobic Interactions, (Plenum, New York, 1980).
99. A. Ben-Naim, *J. Chem. Phys.* 67, 4884 (1977).
100. E. Matteoli and L. Lepori, *J. Chem. Phys.* 80, 2856 (1984).
101. L.R. Pratt and D. Chandler, *J. Chem. Phys.* 67, 3683 (1977).
102. T.P. Straatsma, H.J.C. Berendsen and J.P.M. Postma, *J. Chem. Phys.* 85, 6720 (1986).
103. D.D. Van Slyke, *J. Biol. Chem.* 30, 347 (1917).
104. A. Michels, R.J. Lunbeck, and G.J. Wolkers, *Physica* 17, 801, 1951.
105. A. Michels, Hub. Wijker, and Hk. Wijker, *Physica* 15, 627, (1949).
106. J.A. Beattie, J.S. Brierley, and R.J. Barriault, *J. Chem. Phys.* 20, 1613 (1952).
107. A. Michels, T. Wassenaar, and L. Louwerse, *Physica* 20, 99 (1954).
108. Handbook of Chemistry and Physics, 69nd ed., (Chemical Rubber Co., Boca Raton, FL, 1988).
109. J.C. Moore, R. Battino, T.R. Rettlich, Y.P. Handa, and E. Wilhelm, *J. Chem. Eng. Data* 27, 22 (1982).
110. D.R. Biggerstaff and R.H. Wood, *J. Phys. Chem.* 92, 1988, (1988).

111. L.A. Weber, J. Chem. Eng. Data 34, 171 (1989).
112. I.R. Krichevsky and J.S. Kasarnovsky, J. Am. Chem. Soc. 57, (1935).
113. Frost and Deaton, Oil and Gas Jour. 45, 170, (1944).
114. I. Prigogine, The Molecular Theory of Solutions, (North Holland Publishing Co., Amsterdam, 1957).
115. J.G. Kirkwood and F.P. Buff, J.Chem. Phys. 19, 774 (1951).
116. K. Watanabe and H.C. Andersen, J. Phys. Chem. 90, 795 (1986).
117. A. W. Adamson, Physical Chemistry of Surfaces, 4th ed., (John Wiley & Sons, New York, 1982).
118. L. Stryer, Biochemistry, (W.H. Freeman & Co., San Fransisco, 1975).
119. A. Ben-Naim, J. Chem. Phys. 90, 7412 (1989).
120. P.J. Flory, Statistical Mechanics of Chain Molecules, (Interscience, New York, 1969).
121. J.M.Prausnitz, R.N.Lichtenthaler, and E.G. de Azevedo, Molecular Thermodynamics of Fluid Phase Equilibria, 2nd ed., (Prentice-Hall Inc., Englewood, N.J., 1986).
122. N. Bignell, J. Phys. Chem. 88, 5409 (1984).
123. R. Wiebe and V.L. Gaddy, J. Am. Chem. Soc. 57, 847 (1935).
124. O.L. Culberson and J.J. McKetta Jr., Trans. Am. Inst. Min. Metall. Pet. Eng. 192, 223 (1951).
125. O.L. Culberson and J.J. McKetta Jr., Trans. Am. Inst. Min. Metall. Pet. Eng. 189, 319 (1950).
126. W. McMillen Jr. and J.E. Meyer, J. Chem. Phys. 13, 276 (1945).
127. W.E. Demming and L. Shupe, Phys. Rev. 37, 638 (1931); Phys Rev 40, 848 (1932).
128. R. Weibe, V.L. Gaddy, and C. Heins Jr. J. Am. Chem. Soc. 53, 1721 (1931).
129. D.R. Douslin, R.H. Harrison, R.T. Moore, and J.P. McCullough, J. Chem. Eng. Data 9, 358 (1964).

130. H.H. Reamer, R.H. Olds, B.H. Sage, and W.N. Lacy, *Ind. Eng. Chem. Ind. Edn.* 36, 956 (1944).
131. R. Crovetto, R. Fernández-Prini, and M.L. Japas, *J. Chem. Phys.* 76, 1077 (1982).
132. D.D. Eley, *Trans. Faraday Soc.* 40, 184 (1944).
133. F. Franks, editor, *Water: A Comprehensive Treatise*, vol. 7, (Plenum Press, New York, 1973).
134. A. Ben-Naim, *J. Phys. Chem.* 82, 792 (1978).
135. R. Fowler and E.A. Guggenheim, *Statistical Thermodynamics*, (Cambridge University Press, Cambridge, 1939), Sec. 823.
136. W.L. Jorgensen, J.F. Blake, J.K. Buckner, *J. Chem. Phys.* 129, 193 (1989).
137. R.W. Potter and M.A. Clyne, *J. Sol. Chem.* 7, 837 (1978).
138. R. Wiebe and V.L. Gaddy, *J. Am. Chem. Soc.* 59, 1984 (1937).
139. I.R. Krichevsky and A.A. Ilinskaya, *Zh. Fiz. Khim. USSR* 19, 621 (1945).
140. R. Fernández-Prini and M.L. Japas, *J. Phys. Chem.* 93, 3802 (1989).